AN INEXPENSIVE AUTONOMOUS COLONY SEPARATOR WITH SUB MICROMETER REPEATABILITY

A THESIS SUBMITTED TO THE GRADUATE DEVISION OF THE UNIVERSITY OF HAWAI'I AT MANOA IN PARTIAL FULFILLMENT OF THE REQUIREMENTS FOR THE DEGREE OF

Master of Science

in

Mechanical Engineering

October 2018

By

Grant Roy Takara

Thesis Committee:

A Zachary Trimble, Chairperson

Scott Miller

Bardia Konh

Keywords: Precision machine design, automation, microbes, bacteria, unculturable, Arduino, optics

Contents

0.1 Abstract

Recent advances in methods used to domesticate large numbers of unculturable microbes have opened new doors for drug discovery (Nichols, et al., 2010; Ling, et al., 2015). However, there remain challenges in handling these newly cultured samples. Many samples are so small that they can only be viewed via microscopy and are difficult to manipulate. This limits the number of downstream analysis that can be performed. One of which is the domestication of unculturable microbes in vitro. The ability to communicate with other cells has been implicated as a significant factor in the domestication of unculturable microbes (Donofrio, et al., 2010). To summarize, the easier it is for cells to communicate, the more robust they appear to become. What if these colonies recovered in diffusion chambers could be separated into parts that still enable bacteria to easily communicate with each other? The current state of the art to separate bacteria colonies from a diffusion chamber either increases the distance between cells and destroys extracellular structures that facilitate communication or is expensive and lacks automation for high throughput potential.

Thus there exists a need to separate these colonies while preserving extracellular structures inexpensively and autonomously to study this microbial population.

An inexpensive autonomous system with sub micrometer repeatability is realized in this thesis. The material cost to replicate the system is estimated at 4,000 USD in comparison to 150,000 USD commercially available solutions (Leica, 2018). The system has the ability to position itself with sub micrometer repeatability, reducing the amount of damage in theory to specimens during separation in the event of repeat cuts. Lastly, the system has the ability to position over multiple samples, identify the most likely bacteria colony candidate using machine vision, and generate a toolpath. Further work is needed to determine an effective machining method to separate the bacteria colonies from the agar.

0.2 Acknowledgements

I would like to extend my gratitude for my advisor Dr. Zachary Trimble for expanding my understanding of machine design which has grown with viral potency. His passion for teaching and enthusiasm as well as his continual effort to educate has benefitted me greatly and has served as a standard of excellence that I strive for. During my time as a master's student my three big takeaways from his instruction have completely changed the way that I think. The first is that everything is a spring, the first lesson from his precision machine design class. This has changed how I view materials, view the structural loops of machines, and from all scales, how the 3D world can be manipulated and observed. The second is to question if a claim is defendable. This has made my thought process and outcomes more robust and has caused me to think more critically about the information that I am receiving and to urge myself to understand a concept from its fundamentals (instead of just plugging and chugging into an equation). The third is exact constraint design and its use in designing deterministic and reliable systems. Through his heuristic learning approach (which has been challenging but beneficial) I have learned through experience good practices, bad practices, and why the outcome that I have discovered is so.

I would also like to extend my gratitude for individuals including Peter Tsukamoto for his tips on machining that have aided in the fabrication of my thesis, Dr. Ng for introducing me to the field of biotech and drug discovery and for funding me initially and using his lab for exploring the Ichip technology, Dr. Mora for giving me the opportunity to play with electronics that has provided me with further knowledge that was applied to my machine design, Dr. Donachie for thoroughly answering my initial questions on cultures, Dr. Epstein for answering my questions about his research which served as the foundation for this thesis motivation, and finally Mr. Bryan Silver who throughout my time in high school introduced me to the world of engineering that has resulted in my love for learning and empowered me to develop solutions that make the world a better place.

Finally, I would also like to extend my gratitude for my parents, friends, and family, for being perpetually supportive in my educational endeavors. Not many individuals (let alone college students) can say they have a CNC machine shop at home. So, thank you mom and dad for putting up with my small "pop up" and permanent labs at home and not charging me rent so that I can buy and house all this equipment, and for listening to my speeches at home of research and business ideas that I have.

0.2.1 Variable Nomenclature

Nomenclature

α	Angular acceleration
α_{303}	Coefficient of linear thermal expansion for 316 stainless steel
α_{440}	Coefficient of linear thermal expansion for 440 stainless steel
α_{6061}	Coefficient of linear thermal expansion for 6061 aluminum
α_{bi}	Direction cosine vector component for X
$\alpha_{bk206POM}$	Coefficient of linear thermal expansion for bk206POM acetal
$\bar{X}$	Mean
β_{bi}	Direction cosine vector component for Y
ΔT	Change in temperature
δ	Displacement
γ_{bi}	Direction cosine vector component for Z
λ	Wavelength
ω_0	Initial angular velocity
ω_f	Final angular velocity
ω_n	Natural frequency

${}^{i}T_{i+1}$	Homogeneous transformation matrix
ρ	Density
σ	Standard deviation
τ	Torque
Θ	Direction cosine vector
θ_i	Rotation in radians about an axis
φ	Angle of twist in radians
A	Amperes
a	Acceleration
c	Specific heat capacity
cof_x	Center of friction
D	Diameter
dL_i	Change in length
E_{303}	Elastic modulus of 303 stainless steel
E_{6061}	Elastic modulus of 6061 aluminum
F	Focal length
f	Frequency
F_{bi}	Force on a bearing
F_{mg}	Force due to gravity
F_T	Tension force

F_x	Force in the X axis
F_y	Force in the Y axis
F_z	Force in the Z axis
FOS	Factor of Safety
FOV	Field of view
G_{303}	Shear modulus of 303 stainless steel
h	Height
I	Moment of inertia
J_T	Torsion constant
k	Spring constant
l	Length
L_i	Length
m	Mass
N	Newtons
P_{bi}	Position vector of a bearing
q	Thermal energy
r	Radius
rps	evolutions per second
t	time
T_{INC}	Microstepping torque

um	Micrometers
V	Volume
v_x	Velocity in the X axis
w	Width
X	X axis or X coordinate system
Y	Y axis or Y coordinate system
Z	Z axis or Z coordinate system

List of Figures

0.3 Introduction

0.3.1 General

Recent developments in increasing the rate of domestication for unculturable microbes has opened new doors for drug discovery. However, there remain challenges in processing these newly cultured samples. Many samples are so small that they can only be viewed via microscopy. This limits the number of downstream analysis that can be performed such as genome sequencing and in vitro domestication. What is needed is a method to separate samples into approximately equal portions enabling researchers to perform multiple downstream analysis such as genome sequencing, domestication, and screening for bioactivity (Epstein, 2016; Schatz, Bugle, & Waksman, 1944). The current state of the art for separating samples is either suspension in solution which destroys extracellular structures such as biofilm and laser microdissection (Niyaz, & Sägmüller, 2005) which is time consuming and expensive. What is proposed is the development of an inexpensive machine that utilizes a near ultraviolet light laser to autonomously separate samples from diffusion chambers, or Ichips (Nichols, et al., 2010), into approximately equal portions.

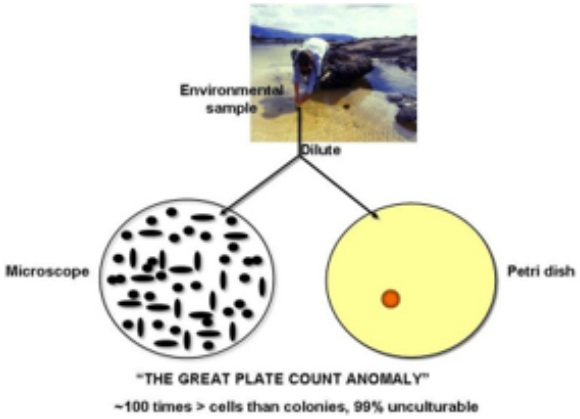

Figure 1: Great Plate Count Anomaly

0.3.2 The Great Plate Count Anomaly

Bacteria while ubiquitous in nature, are notoriously difficult to culture in vitro. This phenomenon is known as the Great Plate Count Anomaly (Staley, 1985). To illustrate, if 100 bacteria cells were collected from the environment and then cultured in vitro only 1 percent would grow.

In 2010 an isolution chip, or Ichip, was shown to culture 60 percent of the initial microbial population in situ. The way that it works is a single cell on average is placed per diffusion chamber and then incubated in situ. The diameter of the porous membrane encapsulating the diffusion chamber is on the order of $0.02\mu m$ in diameter, too small for bacteria to diffuse but large enough for small molecules and nutrients to pass through. After incubation (and sometimes compound subcultures and incubations) the agar plug that contains the sample is placed into a syringe, then squeezed out using a 25 gauge needle, and streaked onto growth media in petri dishes. The current in vitro domestication yield using this method is around 10-15 percent. This is currently at least an order of magnitude greater than what is achieved using conventional methods which is to plate a serial dilution directly onto a petri dish.

To summarize the phenomenon of unculturability a series of claims from literature will be described. The intro environment is a hostile environment since they are

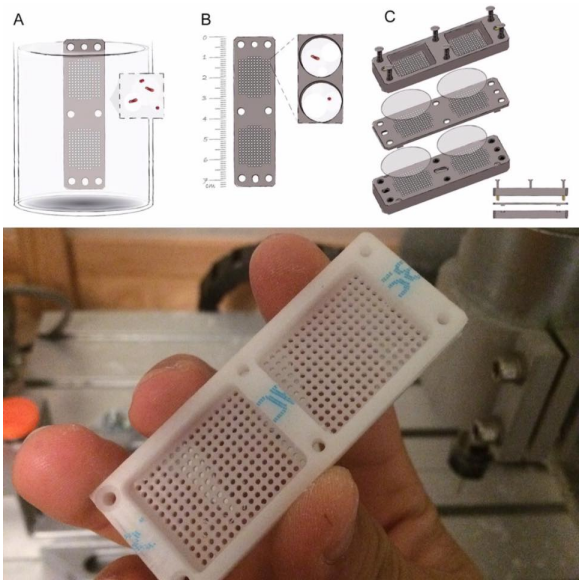

Figure 2: A graphic depicting the assembly of Ichip and an Ichip manufactured in my bedroom. (A) Ichip diagram from (Nichols, et al., 2010). The Ichip is dipped into a beaker filled with molten agar that contains a suspension of cells with a concentration that will fill one chamber on average. (B) One cell on average occupying each chamber. (C) The assembly of the Ichip showing the semi permeable membranes sandwiching the agar filled chambers. (Bottom) A sample Ichip machined with a CNC router.

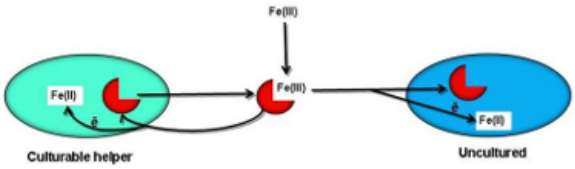

Figure 3: A cartoon of culturable helper excreting siderophores that diffuse toward an unculturable species.

so dissimilar from the natural environment (Epstein, 2009).In addition, it was found that bacteria like to communicate with each other. It was shown in (Donofrio, et al., 2010) that a culturable bacteria sending out siderophores induced growth in invitro for an uncuturable bacteria species.

Biofilm formation such as those on catheters more bacteria cultures more robust to hostile environments such as those with antibiotics (Patel, 2005). Subsequent in situ cultivation leads to a higher rate of domestication. This may be due to the larger quorum size resulting in a behavioral change that can occur for biofilms that form on catheters. It can take months for a unculturable colony to reach a size large enough for domestication. Lastly, the theory of dormancy or microbial scout model could explain the resistance for bacteria to grow in vitro. The idea is that a bacteria cell in a population can exit suspended animation randomly, taste the environment, and determine if the environmental conditions are favorable to enter the growth phase. If the conditions are unfavorable the bacteria may enter suspended animation and go back to sleep (Epstein, 2009).

0.3.3 Drug Discovery

The implications of this newly accessible undiscovered microbial population are immense, particularly in the form of biotechnology and drug discovery. At Novobiotic, a biotech company that utilizes Ichip to culture and screen uncultivated microbes, the rate of new bioactive molecule discovery is 1 in 2,500 isolates (Novobiotic, 2016). Their best antibiotic drug candidate, Teixobactin is currently undergoing pre-clinical

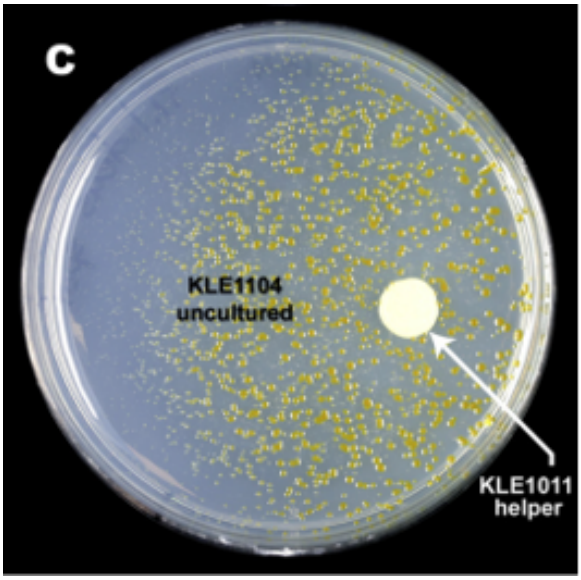

Figure 4: A culturable bacteria helper excreting siderophores and causing an unculturable bacteria species to enter the growth phase. As the concentration of siderophores decreases under the driving force of diffusion, the growth of the unculturable bacteria species also decreases.

trials. The significance of this discovery is two-fold. The first being that it was estimated that a new compound would be discovered 1 in every 10,000,000 strains (Baltz, 2007) for culturable microbes. The second is that Teixobactin displayed efficacy without detectable resistance, thus potentially opening up a new mechanism of action beyond the common 3 that current antibiotics target. A mine of useful chemicals presents itself in this untapped resource.

0.3.4 Automation and Domestication

To further expedite drug discovery, the processes at Novobiotic and in research labs around the world could be optimized. One of the challenges is that samples cultured in situ in diffusion chambers like Ichip are slow growing and microscopic. Thus once they are extracted, they typically have a singular destination of whole genome sequencing which is a destructive process. In addition, the formation of biofilm which is ubiquitous in nature (Epstein, 2009) changes the behavior of cells and can increase their virulence and robustness to hostile environments such as a petri dish. The ability to separate samples into approximately equal portions in terms of cell count while preserving biofilm could enable researchers to domesticate more unculturable microbes in vitro and enable greater access to downstream analysis. Automation is needed due to the large number of samples that are incubated. Each Ichip contains 392 chambers and a technician can load 20 of these a day. This equates to 7840 chambers. Processing such a vast amount of chambers may prove too tedious a task. In addition, if colonies tend to have similar visual characteristics they could prove an easy task for machine vision algorithms to identify and process.

0.3.5 Research Question

The research question is the following: Can an autonomous system be designed and fabricated to separate bacteria colonies from a diffusion chamber into approximately equal sized portions in terms of cell count while preserving extracellular structures

such as exopolymer matrices at an initial cost of a magnitude or less than current state of the art systems? There are two immediate applications that could benefit from such a separation process. Such a separation process would increase access for researchers to study biofilms, especially in difficult to culture pathogenic strains where colony growth may be slow or resist culture in vitro. Such a process would also enable greater accessibility to study of the role of extracellular structures in the domestication of unculturable microbes in vitro.

0.3.6 Objective of Study

The objective of the study is to design and realize a system that can separate samples of microscopic bacteria colonies from a diffusion chamber autonomously and with sub micrometer repeatability.

0.3.7 Organization of the Report

This report is is organized first with an introduction to the background of the application and the motivation to pursue the research question. Following is the literature review of current separation methods and additional text that supports the engineering decisions selected in the design of the presented solution. Next is a detailed description of the machine design starting with the requirements. Summarizing the machine design is a system level architecture diagram. Each subsystem and the decisions that went into the design of each sub system is then described starting with the mechanical subsystem, followed by the electrical subsystem, and the software subsystem. A brief overview describing the manufacturing process is then presented. The material cost to reproduce the system is then presented. The experimental process covers the characterization of the performance of the machine with respect to the engineering requirements. The results of the process with respect to the original intended application is then described. The realized machine and performance is then reviewed in the conclusion. Lastly future works based on what was learned and

research opportunities are presented.

0.4 Literature Review

0.4.1 Current Separation Methods

The current separation methods relevant to uncultured microbes or precision microscopy can be summarized in 3 different methods.

0.4.2 Laser Capture Microdissection

Laser capture microdissection and laser microdissection is a system found in well funded research and diagnostic laboratories.

The drawbacks to this technology are the high cost and lack of automation. In addition, laser microdissection requires a skilled user. Lastly sample preparation requires freezing and cutting with a microtome (Niyaz, & Sägmüller, 2005; Leica, 2000; Zeiss), this would cause stress to microbial specimens that could jeopardize its ability to grow in culture.

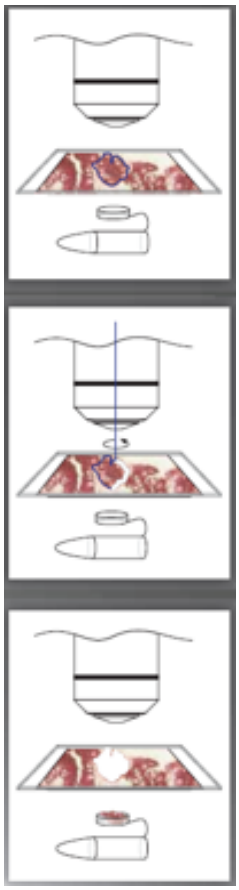

Figure 5: To make a cut, a frozen histological sample is first prepped via microtome to a thickness anywhere from $10\mu m$ to $100\mu m$. The sample is then placed onto a proprietary slide, and imaged via microscopy. The portion of interest is then separated from the sample using an ultraviolet laser and then excised via a pressure catapult or infrared light and onto a film or plastic vessel. The sample may also fall into a capture vessel due to gravity.

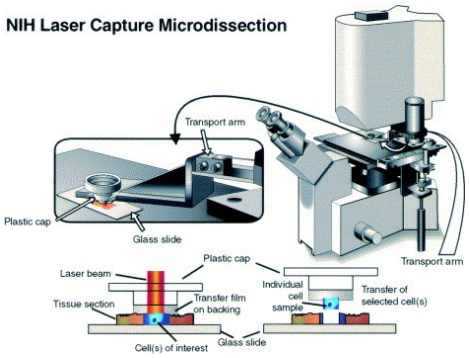

Figure 6: Manufacturers of such systems include Zeiss, Leica, and Arcturus.

Figure 7: The Leica LMD6 laser microdissection system. 150,000USD.

0.4.3 Subculture via syringe and 25 gauge needle streaking subculture onto growth media

In the methods described in (Nichols, et al., 2010), agar plugs with samples extracted from Ichip were placed into suspension within an aqueous solution. That solution was then placed in a syringe with a 25 gauge needle and deposited either back into a new Ichip for re-culture in situ or onto growth media in a petri dish. This provided domestication yields of 10-15 percent. The drawback to this method is that any extracellular structures that have formed were destroyed and the only method of intracellular communication is via diffusion. While not well understood, biofilm could be a key factor in the domestication of samples which would enable greater accessibility for analysis. It was shown in (Donofrio, et al., 2010) that siderophores from neighboring organisms impact the growth of uncultured bacteria. An important question with respect to cultivation is could the domestication rate increase significantly if the biofilm is left largely intact?

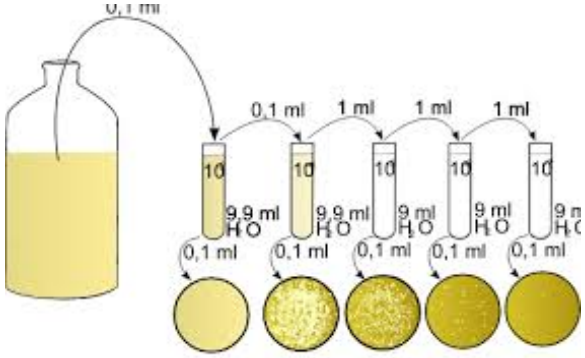

Figure 8: Serial dilution used to dilute the concentration of bacteria from a concentration of approximately 500,000 colony forming units per milliliter to 1 colony forming unit per milliliter.

0.4.4 Streaking a serial dilution onto growth media

Streaking a serial dilution onto growth media is currently the most widely adopted and performed method of separating and culturing a sample. A gram of soil is typically suspended in distilled or autoclaved water. An aliquot is then extracted and deposited in a new sample of distilled or autoclaved water free of any microbes. This process is repeated a number of times until the desired concentration is achieved and is known as a serial dilution. If a gram of soil contains on the order of a billion cells, then a 7 step serial dilution should produce 100 cells in the final dilution. This final dilution is then streaked onto growth media in a petri dish and incubated. After incubation the number of colonies formed is typically on the order of 1 percent of the final dilution concentration. The drawback to the conventional method of serial dilution of uncultured microbes is that previous forms of communication is disrupted.

0.4.5 An open source stage with sub micrometer repeatability

Recent publications have demonstrated that inexpensive open-source hardware can be configured into a system that is easy to setup and is capable of sub micrometer

repeatability. An aluminum linear translator from Thorlabs driven by a micrometer, flexible shaft, and stepper motors was demonstrated to have sub micrometer repeatability at a cost of less than USD1000 (Campbell, Eifert, & Turner, 2014). This increases confidence that inexpensive hardware can be configured for precision applications increasing the possibility of an inexpensive colony separator at a magnitude less in cost compared to the state of the art.

0.5 Materials and Methodology

0.5.1 Requirements

0.5.1.1 Functional Requirements

The intended user is a scientist in an academic or commercial research lab.

The functional requirements are prioritized from most important to least important.

1. Requirement: The process must be able to separate samples from diffusion chambers mentioned in literature. These include the oral diffusion chamber which has chambers $100\mu m$ in diameter (Sizova, et al., 2011), to micropipette tip trays which have chambers as large as $5mm$ in diameter. Justification: These are the most commonly used diffusion chambers. This machine should be compatible to process them and not require special or proprietary equipment.

2. Requirement: The process must use a cutting method that does not damage DNA or biofilm. Justification: Extracellular structures such as biofilm may be crucial to increasing domestication yields as they influence modes of intracellular communication. Thus separation must keep these structures intact. In addition, nuclear material should also be left intact which suggests avoiding ionizing radiation such as UV lasers or anything with greater energy intensity. Destructive chemicals should also be avoided.

3. Requirement: The machine must not produce any ionizing radiation or require components that are hazardous and subject to shipping restrictions. Justification: Ionizing radiation damages DNA which would contaminate specimens and compromise their survival. Hazardous equipment or processes could also invalidate the requirement that the system should be easily housed in common wet labs (usually have a safety level of 2 or below in most categories).

4. Requirement: The process must use some form of non-destructive analysis to approximate cell density. Justification: Samples will be sent for downstream processes that may involve sequencing, domestication, or screening, thus the method for identifying colonies will need to be non-destructive (example, DNA damaging radiation, chemicals that could lyse cells or denature proteins, temperatures that could denature proteins, etc).

5. Requirement: The process must be able to separate samples into at least 2 approximately equal parts. Justification: 2 was selected as the absolute minimum needed to perform numerous downstream analysis greater than those provided by the state of the art. The first being genome sequencing and the second being either subsequent subculture in situ, domestication, or screening. Ideally, at least 4 would be a better candidate as it would allow 3 additional samples for the above said downstream analysis techniques.

6. Requirement: The entire process of visualization and separation of each sample must take no more than 90 seconds for each sample.Justification: According to (Nichols, et al., 2010) a single researcher can load 20 Ichips in a single day. This leads to the following calculation:

$$20\,ichips * 400\left(\frac{chambers}{ichip}\right) = 8,000\,chambers$$

A processing time of 90 seconds per cycle would enable a machine to separate 1,000 samples a day. Thus if a researcher incubates around 20 Ichips a week, a

machine could separate the samples within 5 days assuming a culture yield of 60 percent and that chambers without samples do not require cutting time.

$$8,000\,chambers * 0.60\,yield = 4,800\,processed\,chambers$$

This would enable a lab to separate samples without the need for a dedicated person processing each individual sample and without the upfront costs of purchasing a laser dissection machine.

7. Requirement: Must separate samples into a containment vessel that is easily autoclavable as well as inexpensive to produce and maintain. (ie, capsules, small petri dishes). Justification: To reduce costs and make this as accessible as possible for researchers, this machine should be able to interface nicely with common lab materials. This contrasts with laser capture microdissection which requires proprietary films and slides.

8. Requirement: The machine must be able to operate in temperatures ranging from 55 F (13 C) to 80 F (27 C) (common bench lab temperatures). Justification: These temperatures are common bench lab temperatures.

9. Requirement: Components that cultures come into contact with must be easy to sterilize or dispose of. Justification: Contamination can compromise an entire experiment. Sterilization protocol should be easy and adhere to common sterilization techniques with similar lab equipment (sterilization via alcohol wipe or autoclaving components).

10. Requirement: Set up must take less than 10 minutes (this does not include initial fabrication/calibration). Justification: Typical centrifuge, gel electrophoresis, master mix preparations, and other common lab techniques can take around 10 minutes to set up. If the process takes longer this may make it too expensive or require too much effort and deter the user.

11. Requirement: Training to use the machine or process should take less than an hour. Justification: Processes such as streaking, preparing master mixes, pipetting, and sterilization techniques generally take an hour or less to learn the basics (not including theory). If the machine or process is too complicated to learn it will deter the user and make training too expensive.

12. Requirement: The machine must weigh less than $1500 lbm$ ($680 kg$) and fit in a standard $28 inch$ doorway. Justification: This is so that the machine is portable enough to fit in lab rooms and be transported via elevator.

13. Requirement: The machine must run on power that can be supplied via standard 110v outlets.Justification: 110v outlets and adapters to convert to 110v outlets are very common. This makes integration into a wet lab simple.

14. Requirement: Time to prep each component used in the separation process for autoclaving should take approximately 1 minute of human intervention. Justification: The time it takes to prep flasks, etc, is on the order of a minute or so.

0.5.1.2 Constraints

1. Constraint: The machine must cost less than USD2000 in material costs to produce. Justification: This is primarily due to personal financial constraints although such a price would make it as accessible as other lab equipment such as autoclaves, incubators, microscopes, etc.

2. Constraint: The first functional prototype must be produced by January 20, 2018. Functional is that it can separate a single sample autonomously. Positioning over chamber autonomously is not included. Justification: At least 1 month is needed to perform tests with a level of fidelity that is required for publications. At least 1 month is needed to write a thesis.

0.5.1.3 Engineering Requirements

The engineering requirements are prioritized from most important to least important.

1. Requirement: Cut widths must be within $0.405 - 1\mu m$ in width which is on the low end of the range for bacteria cell size. (smallest bacteria dimension is $0.2\mu m$) (National Research Council (US) Steering Group for the Workshop on Size Limits of Very Small Microorganisms, 1999). Justification: This ensures that if any bacteria are destroyed, that it should be contained to 1-3 cells in width. A geometric analysis was conducted to further justify the kerf width. Bacteria ranges in size from as small as 0.2um in width to visible to the naked eye at over $100\mu m$.

   In (Kim, et al., 2017), it defined an ultra small sample size of 10,000 cells (although "microcolonies are defined as anything with 3 cells or more in other articles, this becomes out of the scope for this current project and more in the realm of the diffusion chamber effectiveness).

   Suppose that a single cell on the conservative end, is $0.2\mu m$ in diameter and to simplify the model, is in the shape of a sphere.

   That makes the volume the following:

$$V = \frac{4}{3}\pi r^3 \tag{1}$$

$$Where\, r = \frac{0.2\mu m}{2} = 0.1\mu m$$

$$Thus\, the\, volume\, of\, the\, cell\, is\, 0.00418\mu m^3$$

   Now the geometry of a colony with the smallest sized bacteria cell known has a cell count in the ultra small range of 10,000. The assumption is made that growth occurs within a plane and that the resulting colony adopts the shape

of a single layered disk. (In reality it is probably closer to a sphere, but this analysis will assume the thickness of the diffusion chamber in use limits three dimensional growth).

Now the volume of the colony can be determined by multiplying the volume of an individual cell by the total number of cells.

$$10,000 * 0.00418\mu m^3 = 418\mu m^3$$

Since the machine will cut only in 2 dimensions, we are only concerned about surface area and the effect that the kerf width of the cut has on the sample, specifically how many cells will be destroyed.

To do this, the diameter of the colony must be determined.

The formula for the volume of a cylinder will be used to determine the diameter of the colony.

$$Volume\,of\,a\,cylinder = \pi \left(\frac{D}{2}\right)^2 h \tag{2}$$

$$D = 2\sqrt{\frac{V}{\pi h}}$$

$$h = diameter\,of\,a\,single\,cell$$

$$D = 2\sqrt{\frac{418}{0.2\pi}\left(\frac{\mu m^3}{\mu m}\right)} = 51.8\mu m$$

Thus if the colony is cut in half with a kerf width of $1\mu m$, then by using the area of a rectangle to represent the ablated area can the proportion of the colony that is destroyed be determined.

$$Area = l * w$$

$$51.8\mu m * 1\mu m = 51.8\mu m^2$$

$$\frac{51.8}{\pi * 0.1}\left(\frac{\mu m^2}{\mu m^2}\right) = 1648\,cells\,or\,16.5\,percent\,of\,the\,colony\,due\,to\,a\,single\,cut$$

While this is the absolute worst case scenario, this is not trivial. It is clear that subsequent cuts, for example, separating a colony into 4 parts would cause an intensive amount of damage for a very small sample size. In addition, sometimes when cells are damaged they release messenger signals to neighboring cells that may change gene expression or the overall physiology of the cell. Containing damage to as small an area as possible is desired to preserve the integrity and viability of the sample both for analysis and domestication.

2. Requirement: Machine must be able to cut through 0-2mm of agar material. Justification: Ichip thicknesses fall in this range

3. Requirement: A backlight or some form of illumination is needed in the following order.
   Backlight source→sample→optics
   Justification: Without a light source behind the sample, viewing the specimen will be very challenging.

4. Requirement: Feed rate for precision cutting must be about $20\mu m/s$ Justification: Minimizing damage to ultra small colonies such as those in an oral diffusion chamber will require precision cutting. Performing the cut within a reasonable amount of time is also important. If the largest colony in an oral diffusion chamber is $100\mu m$ in diameter then the length of the tool path can be described below

$$\begin{aligned} toolpath\,length &= circumference + diameter \\ &= \pi D + D \\ &= \pi(100\mu m + 100\mu m) = 630\mu m \end{aligned}$$

If 30 seconds is the maximum time allotted for cutting a sample completely then the feed rate needs to be approximately the following

$$feedrate = \left(\frac{distance}{time}\right) = \frac{630}{30}\left(\frac{\mu m}{seconds}\right) = 21\left(\frac{\mu m}{seconds}\right)$$

5. Requirement: Feed rate for sample stage must be approximately $5mm/s$. Justification: If the diffusion chamber used is a micropipette tip tray, or similar in style, then the distance center to center between chambers may be approximately

$$Center\,to\,center\,distance = 2 * diameter\,of\,chamber$$
$$= 2 * 5mm = 10mm$$

   This should be a simple operation as precision is not required for this process. Thus a feed rate of $5mm/s$ which results in a travel time of 2 seconds should be sufficient.

6. Requirement: Feed rate for capture stage must be approximately $10mm/s$. Justification: The capture containers may likely be larger than that of a micropipette tip tray and may also need to move in similar frequency to the cutting axis to reveal the backlight for microscopy.

7. Requirement: The distance that a cut sample must travel to the capture stage should be less than $4mm$. This is similar to the distance compared to those in the state of the art laser microdissection systems.

8. Requirement: The absolute positioning accuracy for each axis of the sample stage should be $+/-190\mu m$ over a range of $12mm$. Justification: The diameter of the smallest diffusion chamber was $100\mu m$. A quick estimation of the field of view for a 10x objective lens yielded a minimum length of $470\mu m$. Thus if the diameter of the smallest diffusion chamber is $100\mu m$ the error tolerance for absolute positioning can be calculated by the following:

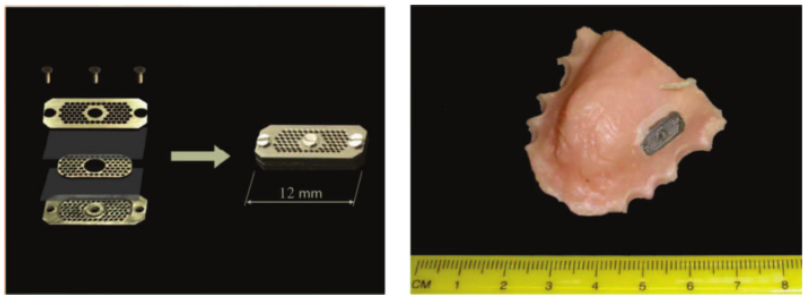

FIG 1 Minitrap used for *in vivo* cultivation of oral microorganisms. (Left) Basic design (explanations in the text). (Right) General view of the subjects' dental appliance, with the minitrap glued to a window cut in the appliance.

Figure 9: Oral Trap Diffusion Chamber. The machine must have a level of precision that can usefully operate with a workpiece of this scale.

$$Absolute\,positioning\,error\,tolerance = \frac{minimum\,FOV\,length - diameter\,of\,smallest\,chamber}{2} = \frac{470\mu m - 100\mu m}{2} = 190\mu m$$

9. Requirement: The machine components that consume electricity must be commercially readily available. Justification: The designer does not want to produce new custom components and have to thoroughly develop them. They should also be easily replaceable in the event of a failure.

10. Requirement: Process cutting methods will need a repeatability on the order of magnitude of sub micrometer per cycle (cycle being excising a sample over the entire workspace). Justification: The chamber sizes range from $100\mu m$ (see oral diffusion chamber) to $2,000\mu m$ in diameter.

    Starting from the cross sectional area of an ultra small colony with the smallest sized bacteria:

$$Area = l * w$$

$$51.8\mu m * 1\mu m = 51.8\mu m^2$$

$$\frac{51.8}{\pi * 0.1}\left(\frac{\mu m^2}{\mu m^2}\right) = 1648\, cells\, or\, 16.5\, percent\, of\, the\, colony\, due\, to\, a\, single\, cut$$

If that colony were in an oral diffusion chamber and repeat cut passes are needed, sub micrometer repeatability over the work area of the chamber is required to minimize damage.

11. Requirement: Optical and electrical components should be commercial off the shelf. Justification: This is so that they can be easily replaced by the end user.

12. Requirement: Standard 22mm objective lenses should be easily compatible with the system. Justification: Different magnifications will be needed thus common and standard 22mm objective lenses are a good candidate for the primary form of magnification.

13. Requirement: Translation in the Z axis should be greater than 2cm. Justification: The height of diffusion chambers can range from 1mm to 10mm. Thus the head of the optics platform should be able to translate to accommodate that height difference. In addition, the difference in focal length between the 4x and 10x objective lens is also approximately 1 cm.

14. Requirement: The time it takes for the stage to settle within +/- 0.5um of translation after full rapid translation in either or both axis should be less than 1 second. Justification: Process time is valuable and the machine should not be vibrating excessively.

15. Requirement: The machine should not emit noise greater than 70 decibels. Justification: The machine should not cause a disturbance louder than a normal conversation or generate excessive vibrations.

16. Requirement: Must be able to carry a sample load of at least 1N on the stage. Justification: Using the largest known Ichip which is the micropipette tip tray as a load maximum benchmark.

$$Density\,of\,water = \rho = 1\left(\frac{g}{cm^3}\right)$$

$$Total\,diffusion\,chamber\,volume\,of\,a\,micropippette\,tip\,tray = \Sigma_{n=1}96\pi r^2 h$$

$$\Sigma_{n=1}^{96} 0.5cm^2\pi * 0.2cm$$

$$Weight\,of\,tray\,filled\,with\,samples =$$

$$7.53cm^3 * 1\left(\frac{g}{cm^3}\right) + 25g\,tray\,masses * \frac{1}{1000}\left(\frac{kg}{g}\right)\left(\frac{9.81m}{s^2}\right)$$

$$= 0.319N * FOS\,of\,2.5 = 0.80N$$

0.5.2 Proposed Separation Process

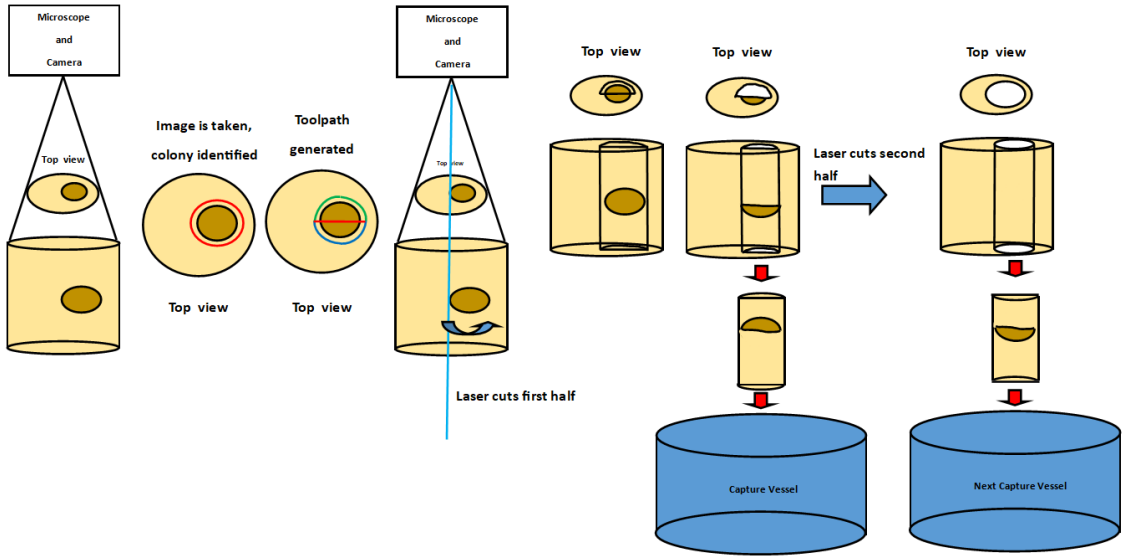

Figure 10: The proposed separation process.First the sample in the diffusion chamber and the capture vessel is positioned within the field of view of the imaging equipment. Next an image is taken and the best colony candidate is selected. A toolpath is then generated to guide the laser to separate the samples. The first sample is separated with the laser and falls into the first capture well. The capture stage then indexes to the next available well. The second sample is then excised using the laser. The second sample then falls into the capture well. The sample stage and capture stage then index to the next available sample and capture vessel.

0.5.3 System Level Architecture

The system level architecture highlights the main subsystems of the entire machine.

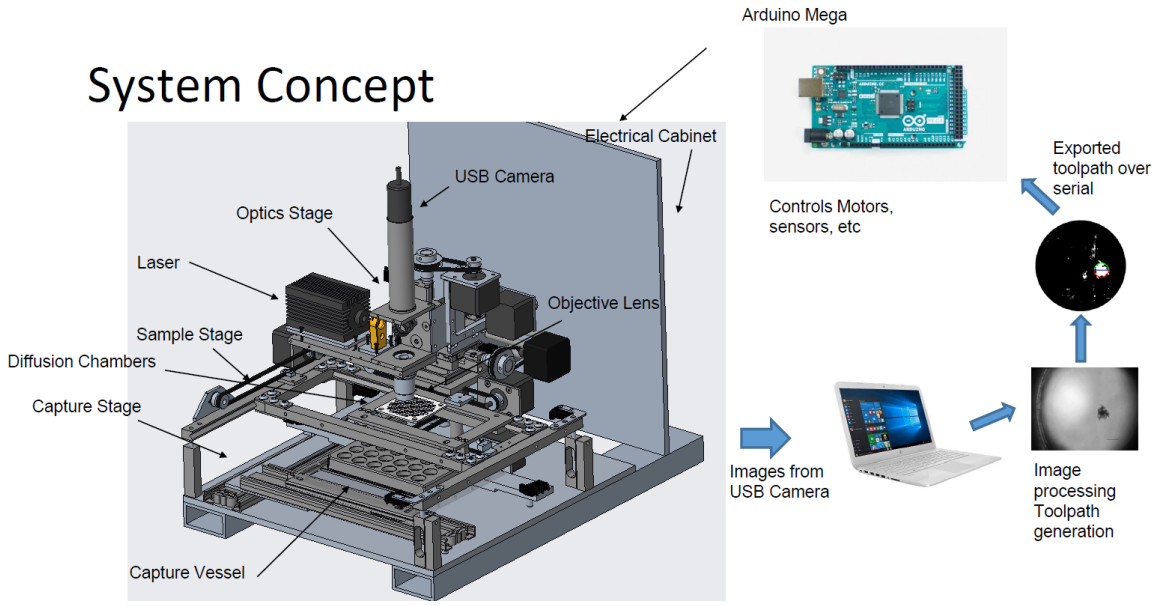

Figure 11: System Concept

These subsystems can be broken down into the following:

- Optics Stage

  The function of the optics stage is to capture images of the samples and perform the machining operations.

- Sample Stage

  The function of the sample stage is to securely house and position the diffusion chambers that house the microscopic cultures.

- Capture Stage

  The function of the capture stage is to securely house and position the capture plate, in this case a 24 well microplate.

- Electronics

  The function of the electronics is to utilize a power source to drive all actuators, sensors, and data acquisition.

- Controller/Software The function of the controller is to take both user input and sensor input and process them, taking over some of the decisions a technician might perform, and to generate instructions for the machine to perform the machining operation desired.

0.5.4 Mechanical System

0.5.4.1 Mechanical Subsystems

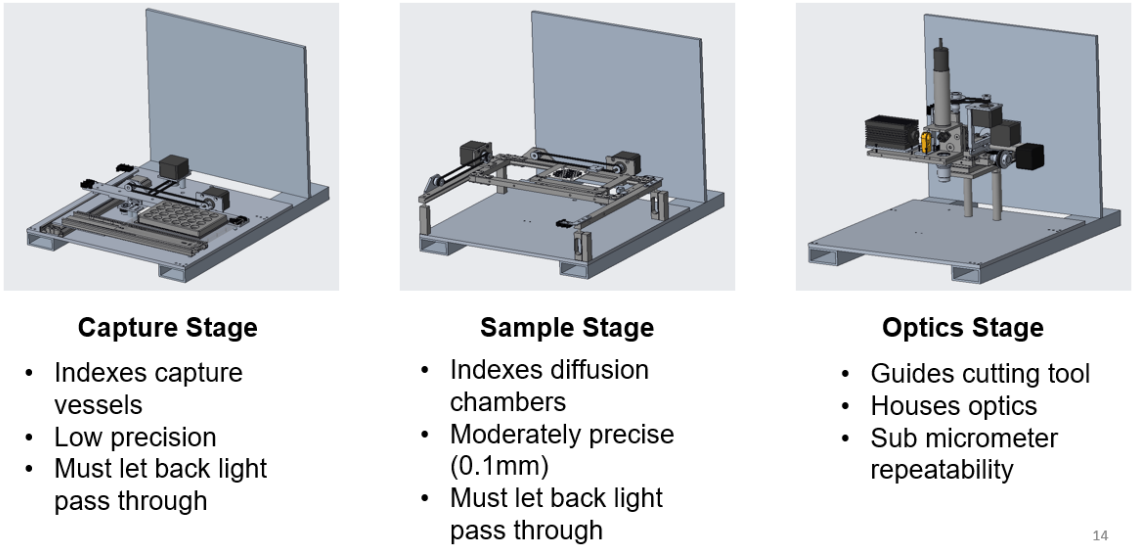

Figure 12: The three mechanical subsystems of the colony separator and their main functions and requirements.

The colony separator was modeled primarily in Creo 4.0, Fusion 360, and Solidworks 2017.

0.5.5 Optics Stage

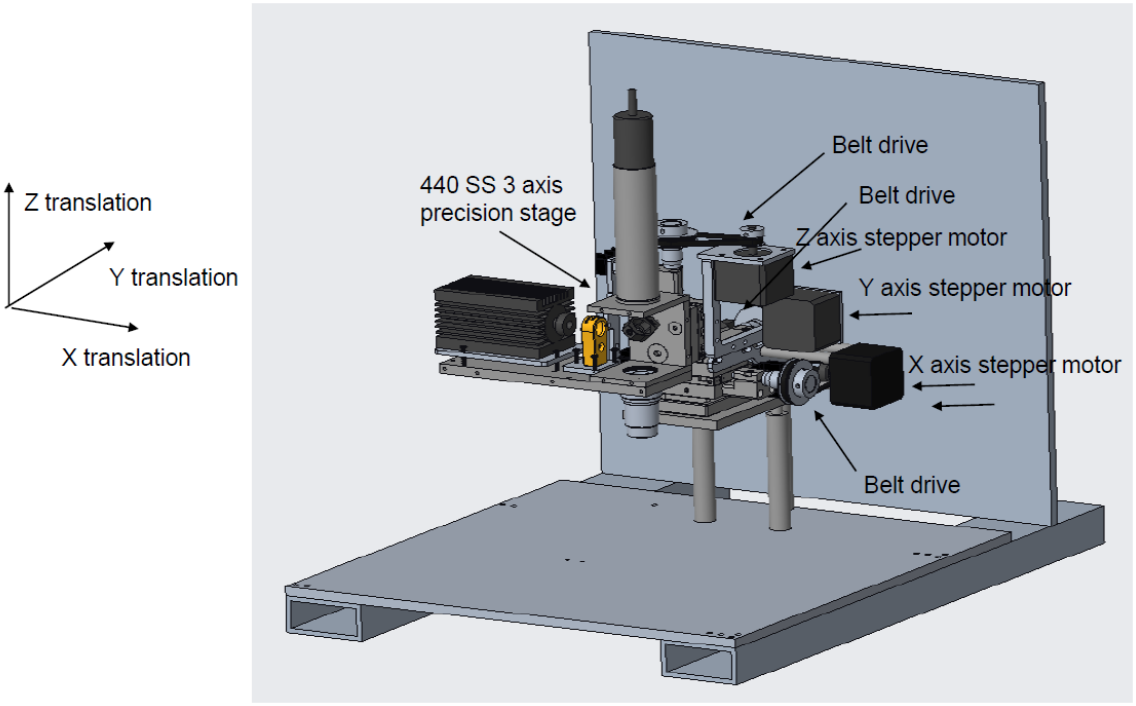

Figure 13: The overview of the optics stage

The optics stage was designed to be compact with repeatability in mind. A Newport M-461-XYZ-M ULTRAlign was selected due to cost (used on Ebay) and material. The lower coefficient of linear thermal expansion 440 stainless steel versus that of the aluminum precision stage counter part was desired. The price of the used stage was nearly equivalent to the price of the aluminum stage with the addition of included SM13 micrometers. SM13 micrometers were selected as the threaded drive due to the ease of integration, desired travel, robust construction, accuracy, and repeatability.

The X and Y axis were driven by a stepper motor and 0.125 inch MXL timing belt with a 40:15 gear ratio and 32 microsteps per step. The low microstep coupled with the smooth SM13 drive and low current selection resulted in smooth translation of the stage verified by viewing a piece of apple on a glass slide at 10x objective lens magnification. Vibrations were not visible.The Z axis was driven by a stepper motor

and 0.125 inch MXL timing belt with a 40:15 gear ratio and 8 microsteps per step. The selection of a 40:15 gear ratio was primarily due to the need for a sprocket with a large enough hub diameter to fit onto the thumb drive of the SM13 micrometers.

The Newport precision stage was then bolted to a 6.35mm thick 303 stainless steel plate that was supported by three 316 stainless steel standoffs with a 1/4-20 thread for adjustment in the Z axis. The assembly could easily be leveled using a construction bubble level and a pair of wrenches within minutes.

Upon inspection after fabrication it was realized that the stage was not ideally constrained. The 316 stainless steel standoffs act as a toroidal flexure resulting in rotation about the Z axis and some translation in the X and Y axis. Future design considerations are to constrain one of the axis with a plate standoff instead of a cylindrical standoff to increase the rigidity and prevent rotation about the Z axis (much like how modern machining centers are designed).

During visual inspection of the stage to detect the presence of unwanted vibration it appears the non ideal constrain of the optics stage did not inhibit the performance of the machine and its ability to meet the functional requirement.

0.5.5.1 Optics Stage Centers of Action

The first step in determining the center of friction and center of friction is to identify the bearing forces, external forces, and their positions. Center of action models presented in (Slocum, 1992; Trimble, 2018) are used in this analysis.

The position of the forces are represented by the following vectors.

$$P_{b1} = [X_{b1}, Y_{b1}, Z_{b1}]$$

$$P_{b2} = [X_{b2}, Y_{b2}, Z_{b2}]$$

$$P_{b3} = [X_{b3}, Y_{b3}, Z_{b3}]$$

$$P_{b4} = [X_{b4}, Y_{b4}, Z_{b4}]$$

$$P_{b5} = [X_{b5}, Y_{b5}, Z_{b5}]$$

$$P_{mg} = [X_{mg}, Y_{mg}, Z_{mg}]$$

$$P_T = [X_T, Y_T, Z_T]$$

$$P_{nest} = [X_{nest}, Y_{nest}, Z_{nest}]$$

Direction cosines are utilized to express the orientation of each force vector.

$$\Theta_{bi} = \begin{bmatrix} \alpha \\ \beta \\ \gamma \end{bmatrix} = \begin{bmatrix} cos(a) \\ cos(b) \\ cos(c) \end{bmatrix}$$

Where a, b, and c are the angles from the X, Y, and Z axis respectively.

Six equations can be used to describe the system.

$$\sum F_x = \sum_{i=1}^{5} \mu v_x + F_{mg}\alpha_{mg} + F_T\alpha_T + F_{nest}\alpha_{nest} = 0$$

$$\sum F_y = \sum F_{bi}\beta_{bi} + F_{mg}\beta_{mg} + F_T\beta_T + F_{nest}\beta_{nest} = 0$$

$$\sum F_z = \sum_{i=1}^{5} F_{bi}\gamma_{bi} + F_{mg}\gamma_{mg} + F_T\gamma_T + F_{nest}\gamma_{nest} = 0$$

$$\sum M_x = \sum_{i=1}^{5} F_{bi}(-Z_{bi}\beta_{bi} + Y_{bi}\gamma_{bi})$$
$$+F_{mg}(-Z_{mg}\beta_{mg} + Y_{mg}\gamma_{mg})$$
$$+F_T(-Z_T\beta_T + Y_T\gamma_T)$$
$$+F_{nest}(-Z_{nest}\beta_{nest} + Y_{nest}\gamma_{nest})$$

$$\sum M_y = \sum_{i=1}^{5} \mu v_x \gamma_{bi} + \sum_{i=1}^{5} F_{bi}(Z_{bi}\alpha_{bi} - X_{bi}\gamma_{bi})$$
$$F_{mg}(Z_{mg}\alpha_{mg} - X_{mg}\gamma_{mg})$$
$$F_T(Z_T\alpha_T - X_T\gamma_T)$$
$$F_{nest}(Z_{nest}\alpha_{nest} - X_{nest}\gamma_{nest})$$

$$\sum M_z = \sum_{i=1}^{5} \mu v_x \beta_{bi} + \sum_{i=1}^{5} F_{bi}(-Ybi\alpha_{bi} + X_{bi}\beta_{bi})$$
$$F_{mg}(-Y_{mg}\alpha_{mg} + X_{mg}\beta_{mg})$$
$$F_T(-Y_T\alpha_T + X_T\beta_T)$$
$$F_{nest}(-Y_{nest}\alpha_{nest} + X_{nest}\beta_{nest})$$

This leaves the following unknowns.

$$F_{b1}, F_{b2}, F_{b3}, F_{b4}, F_{b5}, v_x$$

The Matlab function *linesolve* is utilized to solve the system of equations for the unknowns.

The center of friction is calculated below.

$$X_{cof} = \frac{\sum_{i=1}^{N} F_{normali}\mu X_i}{\sum_{i=1}^{N} F_{normali}\mu}$$

$$Y_{cof} = \frac{\sum_{i=1}^{N} F_{normali}\mu Y_i}{\sum_{i=1}^{N} F_{normali}\mu}$$

$$Z_{cof} = \frac{\sum_{i=1}^{N} F_{normali}\mu Z_i}{\sum_{i=1}^{N} F_{normali}\mu}$$

This further expands into the following equations.

$$cof_X = \frac{\sum_{i=1}^{5} \mu F_{bi}\beta_{bi} X_{bi}}{\sum_{i=1}^{5} \mu F_{bi}\beta_{bi}}$$

$$cof_Y = \frac{\sum_{i=1}^{5} F_{bi}\gamma_{bi} Y_{bi}}{\sum_{i=1}^{5} F_{bi}\gamma_{bi}}$$

$$cof_Z = \frac{\sum_{i=1}^{5} F_{bi}\alpha_{bi} Z_{bi}}{\sum_{i=1}^{5} F_{bi}\alpha_{bi}}$$

The center of stiffness is also represented by a function normalized by a weighted average.

$$X_{cos} \frac{\sum_{i=1}^{5} K_{bi}\beta_{bi} X_{bi}}{\sum_{i=1}^{5} K_{bi}}$$

$$Y_{cos} \frac{\sum_{i=1}^{5} K_{bi}\gamma_{bi} Y_{bi}}{\sum_{i=1}^{5} K_{bi}}$$

$$Z_{cos} \frac{\sum_{i=1}^{5} K_{bi}\alpha_{bi} X_{bi}}{\sum_{i=1}^{5} K_{bi}}$$

A kinematic diagram helps to visualize the system.

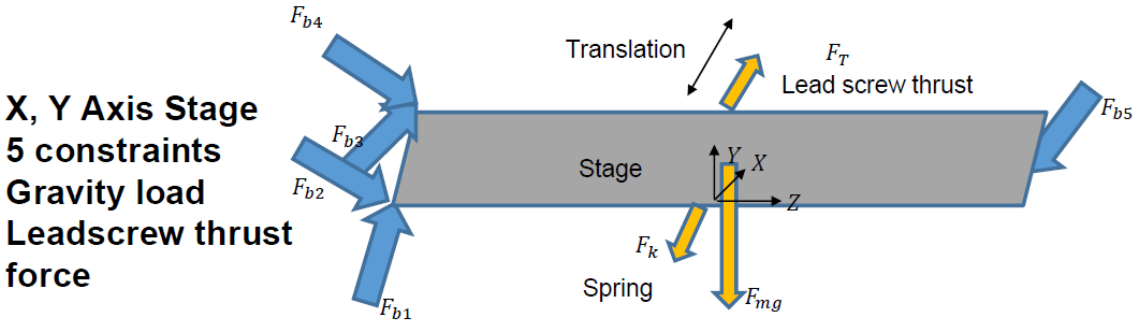

Figure 14: Kinematics of the X and Y axis of the optics stage

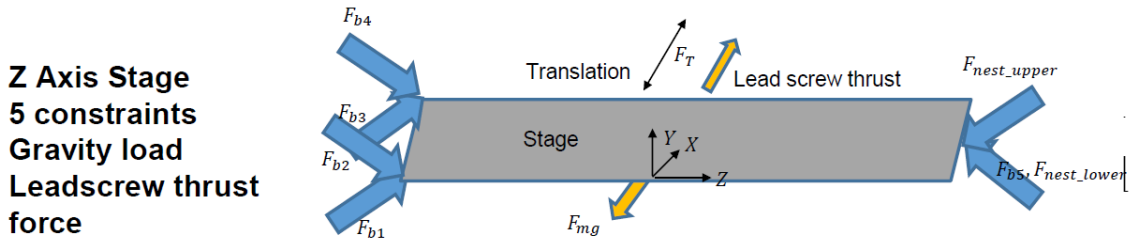

Figure 15: Kinematics of the Z axis of the optics stage

Unfortunately the preloads on the bearings are unknown but they can be estimated. Roller bearings on V grooves will be used to model the bearings. 10 440c SS roller bearings will be estimated on each side of the stage. The objective is to estimate the preload to solve for the bearing forces.

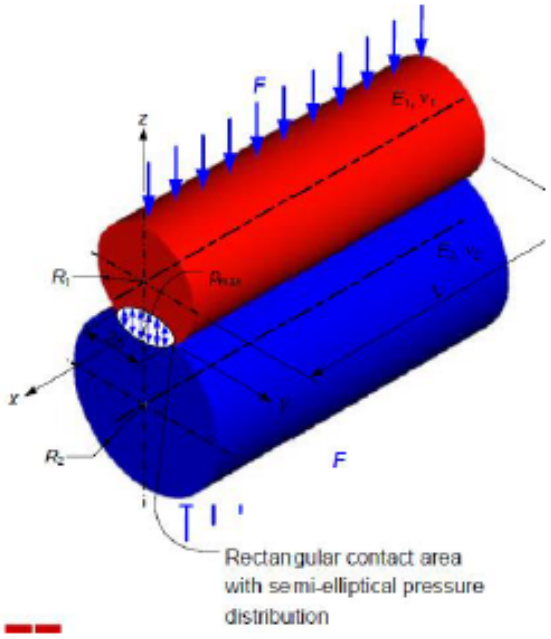

Figure 16: Diagram of the contact area between two cylinders due to Hertzian contact stresses.

The calculation begins by determining the contact area between two cylinders. R_2 in this case is equivalent to infinity since the surface is flat. R_1 is equivalent to

$0.00075m$. E is $200GPa$ and Poisson's ratio $v = 0.28$. Lastly L or the length of the roller bearing is $0.0015m$.

$$contact\,area = \sqrt{\frac{8F\left(\frac{1-v^2}{E}\right)}{\pi L\left(\frac{1}{R_1}+\frac{1}{R_2}\right)}}$$

Next the pressure on the cylinders is calculated. The idea preload stress is where the change in deflection will be minimal.

$$\sigma_{max} = \frac{2F}{\pi bL} = \frac{2F}{\pi L\sqrt{\frac{8F\left(\frac{1-v^2}{E}\right)}{\pi L\left(\frac{1}{R_1}+\frac{1}{R_2}\right)}}}$$

A plot with stress as a function of force is then generated to visualize the value of F where the change in stress is minimized.

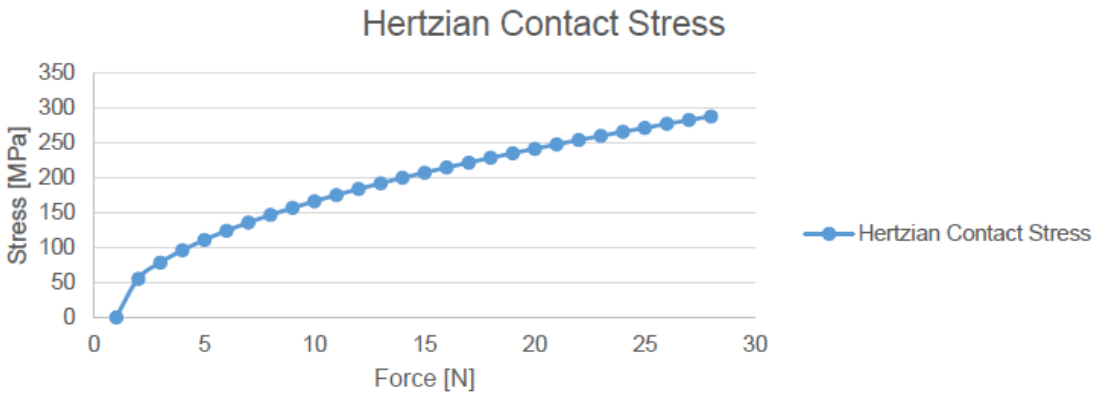

Figure 17: Plot of the stress curve as a function of force for two roller bearings.

15N is selected as the predicted preload resulting in a total nesting force of 150N.

For the X and Y Axis stage. With no translation forces:

$$F_T = 0,\ F_{b1} = -37.5,\ F_{b2} = -30.5,\ F_{b3} = 7.5,\ F_{b4} = 14.4,\ F_{b5} = -1.1,\ v_x = 0\frac{m}{s}$$

$$COF_{XYZ} = \begin{bmatrix} 0.02 \\ 0 \\ -0.02 \end{bmatrix}$$

With translation forces:

$$F_T = 0.6,\ F_{b1} = -37.4,\ F_{b2} = -30.4,\ F_{b3} = 7.4,\ F_{b4} = 14.3,\ F_{b5} = -1.1,\ v_x = 23\frac{m}{s}$$

$$COF_{XYZ} = \begin{bmatrix} 0.02 \\ 0 \\ -0.02 \end{bmatrix}$$

For the Z axis stage.

$$F_T = 0,\ F_{b1} = -37.5,\ F_{b2} = -30.5,\ F_{b3} = 7.5,\ F_{b4} = 14.4,\ F_{b5} = -1.1,\ v_x = 0\frac{m}{s}$$

$$COF_{XYZ} = \begin{bmatrix} 0.02 \\ 0 \\ -0.02 \end{bmatrix}$$

With translation forces:

$$F_T = 0.6,\ F_{b1} = -37.4,\ F_{b2} = -30.4,\ F_{b3} = 7.4,\ F_{b4} = 14.3,\ F_{b5} = -1.1,\ v_x = 23\frac{m}{s}$$

$$COF_{XYZ} = \begin{bmatrix} 0.02 \\ 0 \\ -0.02 \end{bmatrix}$$

In conclusion, the 0.6N should be more than enough thrust force to drive the stage.

It is also non trivial to mention that the expected COF in Z should be at 0 so the model created to determine COF may need to be reevaluated.

To calculate the center of stiffness the deflection at each bearing will first need to be determined.

Deflection will be calculated based on Hertzian contact stresses between two cylinders represented by the following equations.

$$contact\,area = \sqrt{\frac{8F\left(\frac{1-v^2}{E}\right)}{\pi L\left(\frac{1}{R_1} + \frac{1}{R_2}\right)}}$$

$$\delta = \frac{2F(1-v^2)}{\pi LE}\left(\frac{2}{3} + ln\left(\frac{4R_1}{b}\right) + ln\left(\frac{4R_2}{b}\right)\right)$$

The forces on each bearing was just found previously.

The deflections at each point compute to the following:

$$\delta_{b1} = 3.7e^{-6}m$$

$$\delta_{b2} = 3.0e^{-6}m$$

$$\delta_{b3} = 7.6e^{-7}m$$

$$\delta_{b4} = 4.5e^{-6}m$$

$$\delta_{b5} = 1.1e^{-7}m$$

The equation for stiffness will be utilized for each bearing.

$$k = \frac{F}{\delta}$$

$$k_{b1} = 1.0e^{7}\left(\frac{N}{m}\right)$$

$$k_{b2} = 1.0e^{7}\left(\frac{N}{m}\right)$$

$$k_{b3} = 9.8e^{6}\left(\frac{N}{m}\right)$$

$$k_{b4} = 9.9e^{6}\left(\frac{N}{m}\right)$$

$$k_{b5} = 9.4e^{6}\left(\frac{N}{m}\right)$$

The center of stiffness can then be calculated using the following equations:

$$X_{cos}\frac{\sum_{i=1}^{5} K_{bi}\beta_{bi}X_{bi}}{\sum_{i=1}^{5} K_{bi}}$$

$$Y_{cos}\frac{\sum_{i=1}^{5} K_{bi}\gamma_{bi}Y_{bi}}{\sum_{i=1}^{5} K_{bi}}$$

$$Z_{cos}\frac{\sum_{i=1}^{5} K_{bi}\alpha_{bi}X_{bi}}{\sum_{i=1}^{5} K_{bi}}$$

$$COS_{XYZ} = \begin{bmatrix} 0.02 \\ 0 \\ 0.02 \end{bmatrix}$$

The Z position looks suspicious and the model should be reviewed. Other than that, the center of stiffness is near the other centers of action and near the point at which the translation force is applied which is ideal.

0.5.5.2 Optics Stage Actuator Performance

Newport SM13 micrometers came with the 3 axis stage that was purchased and meets the functional requirements. Initial observations concluded that the amount of static friction and starting torque needed to turn the micrometers was greater than expected.

To determine the stiction a very approximate test was conducted by hanging a known mass at the radius of the drive and increasing the mass until the micrometer turned. The starting torque was found to be approximately 0.03Nm.

Starting the analysis from a speed requirement standpoint, the engineering requirement for the rapid rate of the optics stage was $1\left(\frac{mm}{s}\right)$. The pitch of the SM13 micrometer is 0.5 mm. The selected microstep setting was 32 microsteps per step after some experimenting to reduce vibrations from the inertia of the rotor and still achieve adequate repeatability.

The number of microsteps needed to drive the lead screw 1mm was calculated by the following.

$$32\left(\frac{microsteps}{step}\right) * 200\left(\frac{full\,steps}{revolution}\right) * \frac{1}{0.5}\left(\frac{revolution}{mm}\right) * 1\,mm = 12800\,microsteps$$

The period for each microstep can then be calculated by the following

$$T = \left(\frac{1 * 10^6}{12800}\right)\left(\frac{\mu seconds}{microsteps}\right) = 78\mu seconds$$

That duration is well within the capability of the electrical hardware selected.

To determine if the motor could output the torque needed the motor pull out torque curve was referenced.

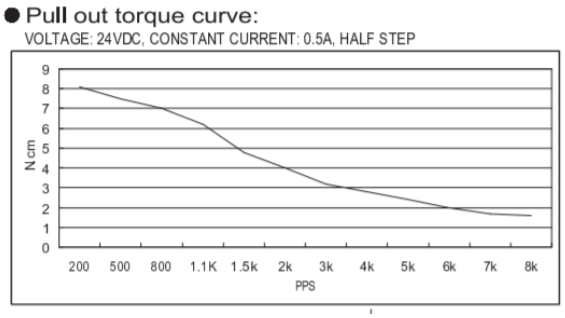

Figure 18: The motor pull out curve for the NEMA14 SY35ST28-0504A stepper motor

To determine the pulses per second or PPS the period for the microstep is multiplied by the ratio of the number of microsteps to full steps.

$$T_{fullstep} = 70 * 10^{-6}s\left(\frac{32}{1}\right)\left(\frac{microsteps}{fullstep}\right) = 0.00224s = period\, full\, step$$

$$PPS = \frac{1}{T_{fullstep}} = \frac{1}{0.00224}\left(\frac{pulse}{second}\right) = 446PPS$$

At $446PPS$ the holding torque is equivalent to $7.5Ncm$.

Next was to calculate the torque loss due to the use of microstepping by the following calculation.

$$T_{INC} = T_{HFS}(sin(\frac{90}{\frac{microsteps}{step}}) \tag{3}$$

$$T_{INC} = 7.5Ncm(sin(\frac{90}{\frac{32\,microsteps}{step}})$$

$$T_{INC} = 4.0Ncm$$

Next was to calculate the force after the transmission.

$$T_{INC} * transmission\,ratio = 4.0Ncm * \frac{40}{15} = 11.6Ncm = 0.116Nm$$

The actuator design has enough torque to drive the stage.

0.5.5.3 Vibration Analysis

To determine if the system will vibrate too much due to the inertia of the stepper motor rotors microstepping, a quick analysis was performed with a simple model.

The following assumptions are made:

Stage mass = $2kg$

Rotor mass = $30g$

Microstep period = $500us$

Rotor radius = $0.008m$

Worst case scenario - no damping - modeling a harmonic oscillator

Cantilever beam

Frequency at 32 microsteps (most repeatable with low vibration) considered

Inertia of the stage omitted due to high damping

The magnitude of the force and the deflection of the cantilever beam is determined.

First the number of microsteps per revolution is calculated.

$$200\left(\frac{fullsteps}{1\,rev}\right)\frac{32}{1}\left(\frac{microsteps}{full\,step}\right) = 6400\left(\frac{microsteps}{rev}\right)$$

The angular displacement per microstep is then calculated.

$$\alpha = \frac{2\pi}{1}\left(\frac{rad}{rev}\right)\frac{1}{6400}\left(\frac{rev}{microsteps}\right) = 9.8e^{-4}rad$$

The centroid of the rotor is found using centroid of a sector, in this case to the extend of a semi circle representing the half of the rotor that causes a force to deflect the end of the cantilever beam.

$$R = \frac{4r}{3\pi}$$

A triangular velocity profile is assumed (although as pointed out during my defense, stepper motors do not display a singular triangular velocity profile. The coils are magnetized and the rotor turns at full force. The rotor overshoots and then reverse direction and returns until it reaches equilibrium with the coils thus even within the rotor itself is there oscillation within each step).

The initial angular velocity is calculated.

$$\omega_0 = \frac{4.9e^{-4}}{500-250}\left(\frac{rad}{us}\right) = 2e^{-6}\left(\frac{rad}{s}\right)$$

The angular acceleration is then calculated.

$$\alpha = \frac{\omega_f - \omega_0}{t_2 - t_1} = \frac{0 - 2e^{-6}}{500-250}\left(\frac{rad}{us}\right) = 8e^{-9}\left(\frac{rad}{s^2}\right)$$

The lateral force is then calculated.

$$F = m_{rotor}r\alpha = 0.03kg * 0.003m * 8e^{-9}\left(\frac{rad}{s^2}\right) = 7e^{-13}N$$

The following assumptions about the cantilever beam used to model the optics supports are listed below:

$\rho = 7700\left(\frac{kg}{m^3}\right)$

A=$0.01m^2$

L=$0.1m$

E=$200GPa$

The moment of inertia of the vertical support (assuming a square cross sectional area) for only one of the columns as a conservative estimate is then calculated.

$$I = \frac{1}{12}bh^3 = \frac{1}{12}(0.01)^4 = 8.3e^{-10}m^4$$

The deflection due to the previously calculated lateral load is then calculated.

$$\delta = \frac{FL^3}{3EI} = \frac{7e^{-13}N0.1m^3}{3 * 200GPa * 8.3e^{-10}m^4} = 1.4e^{-18}m$$

The natural frequencies are then calculated for a cantilever beam.

The k values are listed below:

$$k_{n=1} = 1.875$$

$$k_{n=1} = 4.694$$

$$k_{n=1} = 7.855$$

$$k_{n=1} = 10.996$$

The natural frequencies for a cantilever beam can be calculated using the equation below:

$$\omega_n = k^2\sqrt{\frac{EI}{A\rho L^4}}$$

And finally the natural frequencies are found to be the following:

$$\omega_{n=1} = 51Hz$$

$$\omega_{n=2} = 320Hz$$

$$\omega_{n=3} = 900Hz$$

$$\omega_{n=4} = 1800Hz$$

The frequency of the motor is calculated below:

$$f_{motor} = \frac{1}{microstep\,period} = \frac{1}{500\mu s} = 2kHz$$

The conclusion is that the motor frequency is somewhat close to the 4th natural frequency. Deflection is very low and damping was not considered. Excessive vibration is not likely however including a better model of the velocity profile of the rotor would be a non trivial task.

0.5.6 Sample Stage

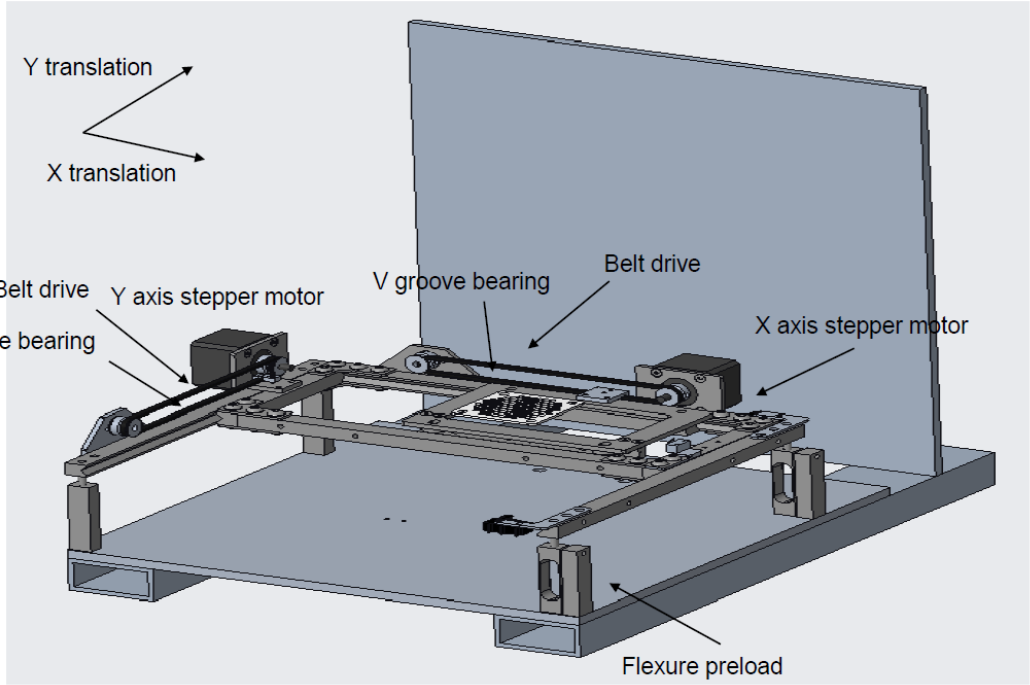

Figure 19: Overview of the sample stage.

The sample stage was designed to minimize the Z length profile. This was due to minimize any forces that could change the trajectory of a separated sample such as a draft. To accomplish this, rectangular extruded 303 stainless steel bars were machined with a V groove to accommodate bearing balls. The nesting force to preload the bearings was accomplished with 303 stainless steel flexures. 303 stainless steel was

selected due to the availability, good machinability, and higher yield strength when compared to aluminum. About 1 mm of compliance was estimated to accommodate the geometric tolerances of the stage.

Each stage was driven by a stepper motor and 0.125 inch MXL timing belt with a 1:1 gearing ratio and 8 microsteps per step.

The sample stage platform was machined out of 17-4 PH, a stainless steel that is moderately difficult to machine. The material was selected for its magnetic and corrosion resistant properties. The magnetic properties were desired for the application of a flexible means to clamp down diffusion chambers of different sizes to the sample stage platform.

Due to the requirement that the back light must be positioned on the same axis as the USB camera, placing the belt drive along the center of stiffness of each axis came with challenges.

0.5.6.1 Sample Stage Centers of Action

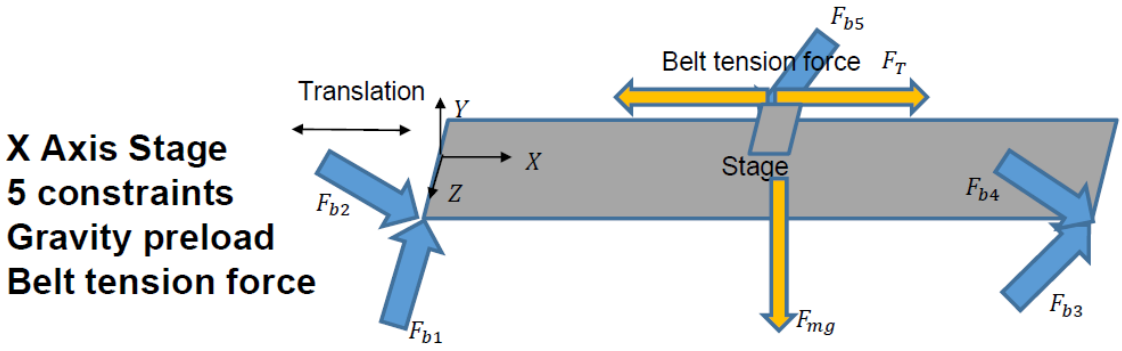

Figure 20: Kinematics of the X Axis Sample Stage

The position vectors are then assigned.

$$P_{b1} = \begin{bmatrix} 0 & 0.003 & 0.045 \end{bmatrix}$$
$$P_{b2} = \begin{bmatrix} 0 & -0.003 & 0.045 \end{bmatrix}$$
$$P_{b3} = \begin{bmatrix} 0.12 & 0.003 & 0.045 \end{bmatrix}$$
$$P_{b4} = \begin{bmatrix} 0.12 & -0.003 & 0.045 \end{bmatrix}$$
$$P_{b5} = \begin{bmatrix} 0.06 & -0.003 & 0.06 \end{bmatrix}$$
$$P_{mg} = \begin{bmatrix} 0.06 & 0 & 0 \end{bmatrix}$$
$$P_{FT} = \begin{bmatrix} 0.06 & 0.005 & -0.05 \end{bmatrix}$$

Followed by the direction cosine vectors.

$$\Theta_{b1} = \Theta b3 = \begin{bmatrix} 0 \\ \frac{1}{\sqrt{2}} \\ -\frac{1}{\sqrt{2}} \end{bmatrix} \Theta_{b2} = \Theta_{b4} \begin{bmatrix} 0 \\ -\frac{1}{\sqrt{2}} \\ -\frac{1}{\sqrt{2}} \end{bmatrix} \Theta_{b5} = \begin{bmatrix} 0 \\ -\frac{1}{\sqrt{2}} \\ \frac{1}{\sqrt{2}} \end{bmatrix} \Theta_{mg} = \begin{bmatrix} 0 \\ -1 \\ 0 \end{bmatrix} \Theta_{FT} = \begin{bmatrix} 1 \\ 0 \\ 0 \end{bmatrix}$$

Mass is assumed to be $0.5kg$.

The results are the following: With no translation forces: All forces are in Newtons.

$$F_T = 0,\ F_{b1} = -20.2,\ F_{b2} = 1.7,\ F_{b3} = -20.2,\ F_{b4} = 1.7,\ F_{b5} = -37,\ v_x = 0\left(\frac{m}{s}\right)$$

The steady state velocity comes out to zero which is expected with no translation forces.

The center of friction is calculated to be the following:

$$COF_{XYZ} = \begin{bmatrix} 0.06 \\ 0 \\ -0.035 \end{bmatrix}$$

When a translation force is applied the following bearing forces are resolved to the values below:

$$F_T = 0.7,\ F_{b1} = -20.3,\ F_{b2} = -1.7,\ F_{b3} = -20.2,\ F_{b4} = 1.7,\ F_{b5} = -37,\ v_x = 28\frac{m}{s}$$

The steady state velocity comes out positive and greater than the 5mm/s needed although this does not factor in static friction and acceleration of the stage.

$$COF_{XYZ} = \begin{bmatrix} 0.06 \\ 0 \\ -0.035 \end{bmatrix}$$

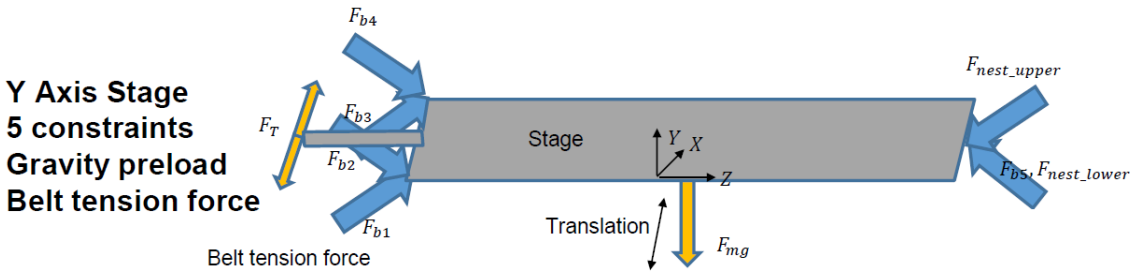

Figure 21: Kinematics of the Y Axis Sample Stage

$$P_{b1} = \begin{bmatrix} 0 & 0.003 & -0.14 \end{bmatrix}$$
$$P_{b2} = \begin{bmatrix} 0 & -0.003 & -0.14 \end{bmatrix}$$
$$P_{b3} = \begin{bmatrix} 0.12 & 0.003 & -0.14 \end{bmatrix}$$
$$P_{b4} = \begin{bmatrix} 0.12 & -0.003 & -0.14 \end{bmatrix}$$
$$P_{b5} = \begin{bmatrix} 0.06 & 0.003 & 0.14 \end{bmatrix}$$
$$P_{mg} = \begin{bmatrix} 0.06 & 0 & 0 \end{bmatrix}$$
$$P_{FT} = \begin{bmatrix} 0.06 & 0.005 & -0.15 \end{bmatrix}$$
$$P_{nestupper} = \begin{bmatrix} 0.06 & -0.003 & -0.14 \end{bmatrix}$$
$$P_{nestlower} = \begin{bmatrix} 0.06 & -0.003 & -0.14 \end{bmatrix}$$

Followed by the direction cosine vectors.

$$\Theta_{b1} = \Theta b3 = \begin{bmatrix} 0 \\ \frac{1}{\sqrt{2}} \\ \frac{1}{\sqrt{2}} \end{bmatrix} \Theta_{b2} = \Theta_{b4} \begin{bmatrix} 0 \\ -\frac{1}{\sqrt{2}} \\ \frac{1}{\sqrt{2}} \end{bmatrix} \Theta_{b5} = \Theta_{nestlower} \begin{bmatrix} 0 \\ \frac{1}{\sqrt{2}} \\ -\frac{1}{\sqrt{2}} \end{bmatrix}$$

$$\Theta_{mg} = \begin{bmatrix} 0 \\ -1 \\ 0 \end{bmatrix} \Theta_{FT} = \begin{bmatrix} 1 \\ 0 \\ 0 \end{bmatrix} \Theta_{nestupper} = \begin{bmatrix} 0 \\ -\frac{1}{\sqrt{2}} \\ -\frac{1}{\sqrt{2}} \end{bmatrix}$$

Mass is assumed to be $1.0kg$.

The results are the following: With no translation forces: All forces are in Newtons.

$$F_T = 0,\ F_{b1} = 21.5,\ F_{b2} = 25.5,\ F_{b3} = 21.5,\ F_{b4} = 25.5,\ F_{b5} = -5.9,\ v_x = 0\left(\frac{m}{s}\right)$$

The steady state velocity comes out to zero which is expected with no translation forces.

The center of friction is calculated to be the following:

$$COF_{XYZ} = \begin{bmatrix} 0.06 \\ 0 \\ -0.02 \end{bmatrix}$$

When a translation force is applied the following bearing forces are resolved to the values below:

$$F_T = 0.7,\ F_{b1} = 22.5,\ F_{b2} = 26.5,\ F_{b3} = 20.6,\ F_{b4} = 24.5,\ F_{b5} = -5.9,\ v_x = 28\frac{m}{s}$$

The steady state velocity comes out positive and greater than the 5mm/s needed although this does not factor in static friction and acceleration of the stage.

$$COF_{XYZ} = \begin{bmatrix} 0.06 \\ 0 \\ -0.02 \end{bmatrix}$$

0.5.6.2 Sample Stage Actuator Performance

The engineering requirement for the rapid rate of the capture stage was 5mm/s.

The following assumptions were made:

The mass of the stage is 1.3 kg

The coefficient of friction for the rolling bearing balls on the v groove ways is conservatively estimated at 0.005.

The lever arm of the sprocket is equal the half the pitch diameter and can be expressed with the following equation.

$$Pitch\,diameter = 0.382\,inches = 9.70mm$$

$$Lever\,arm = \frac{pitch\,diameter}{2} = 4.85mm = 4.85 * 10^{-3}m$$

The tension force that can be produced by the stepper motor drive system was then calculated.

Starting from the desired speed given the pitch diameter. The engineering requirement calls for 5mm/s.

$$The\,circumference\,of\,the\,sprocket = pitch\,diameter * \pi$$

$$= 4.85mm * \pi$$

$$= 15.2mm$$

$$5\left(\frac{mm}{s}\right) * \frac{1}{15.2}\left(\frac{rev}{mm}\right) = 0.33rps$$

To reduce the amount of vibration from the stepper motors the drivers were configured for the maximum number of microsteps per step at a ratio of 8 microsteps per full step.

Thus to achieve 0.33rps, the maximum period for a microstep is calculated by the following.

The number of microsteps to full step is first calculated.

$$8\left(\frac{microsteps}{full\,step}\right) * 200\left(\frac{full\,step}{revolution}\right) = 1600\left(\frac{microsteps}{revolution}\right)$$

Then the number of microsteps required per second is calculated by the following.

$$1600\left(\frac{microsteps}{revolution}\right) * 0.33\left(\frac{revolutions}{second}\right) = 528\left(\frac{microsteps}{second}\right)$$

The period which determines the delay between sending a high and low step is derived from the period needed to obtain the desired speed and calculated by the following.

$$\frac{1 * 10^6}{528}\left(\frac{\mu seconds}{microsteps}\right) = 1890\left(\frac{\mu seconds}{microstep}\right)$$

The next step executed was to determine if the stepper motor can output the torque needed to drive the stage. The equivalent full step number of pulses was first calculated.

$$528\left(\frac{microsteps}{second}\right) * \frac{1}{8}\left(\frac{full\,steps}{microsteps}\right) = 66\left(\frac{full\,steps}{second}\right)\left(\frac{pulse}{full\,steps}\right) = 66\,pulses\,per\,second$$

At 66 pulses per second the pull out torque can be expected to be around 8 Ncm. To be conservative, 50 percent, or 4 Ncm of the pull out torque will be used from here on.

Due to microstepping, the output torque from the motor is significantly smaller (Budimir, 2013).

$$T_{INC} = T_{HFS}(sin(\frac{90}{\frac{microsteps}{step}})$$

$$T_{INC} = 4Ncm(sin(\frac{90}{\frac{8\,microsteps}{step}})$$

$$T_{INC} = 0.78Ncm$$

Next the tension force on the MXL timing belt is calculated.

$$F_T = \frac{\tau}{r}$$

$$Where\, F_T = tension\, force$$

$$\tau = motor\, torque = 4Ncm$$

$$and\, r = lever\, arm\, of\, sprocket = 0.49cm$$

$$F_T = \frac{0.78}{0.49}\left(\frac{Ncm}{cm}\right) = 0.38N$$

Next a free body diagram was construction to estimate if the tension force is great enough to overcome the friction due to the rolling resistance of the bearing balls within the V groove.

To estimate the friction forces a quick static stress analysis was performed on the flexure providing the preload for the sample stage X axis. The resulting force vector was then incorporated into a free body diagram of the bearing to estimate the normal force and ultimately the friction force.

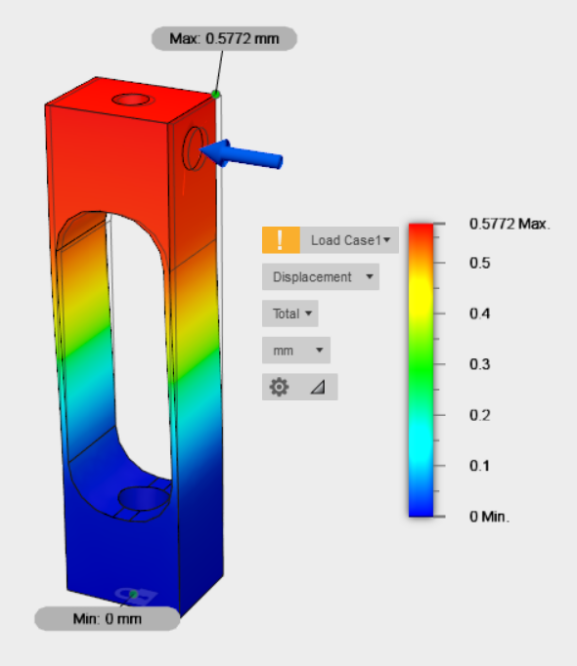

Figure 22: A quick static stress analysis in Fusion 360 was performed on a flexure to determine the maximum displacement before yielding. The resulting force which would be generated by an adjusting screw was 50N. Two flexures are used to preload the sample stage X axis

There are 4 bearing balls on each side of the stage. The designed is over constrained and utilizes elastic averaging. In addition, it is highly unlikely that the drive will be placed near the center of action of the stage thus two analysis will be performed. The first will be to determine the centers of action, the second is to determine the magnitude of the reactions at the bearings with a drive off the center of friction. The objective of that study is to determine if the preload generated by the flexure is sufficient to prevent excessive angular errors.

The forces on each bearing in the V groove can be described by the following diagram.

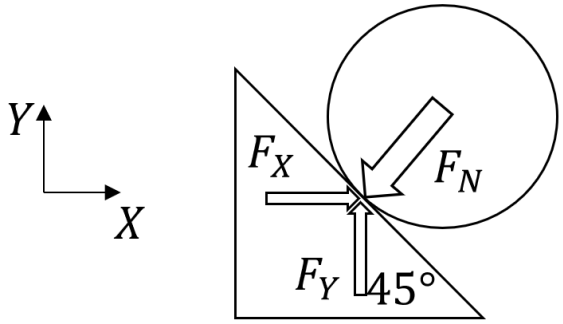

Figure 23: 2 dimensional free body diagram of the stage and reaction forces at the interface between the bearing ball and the V-groove.

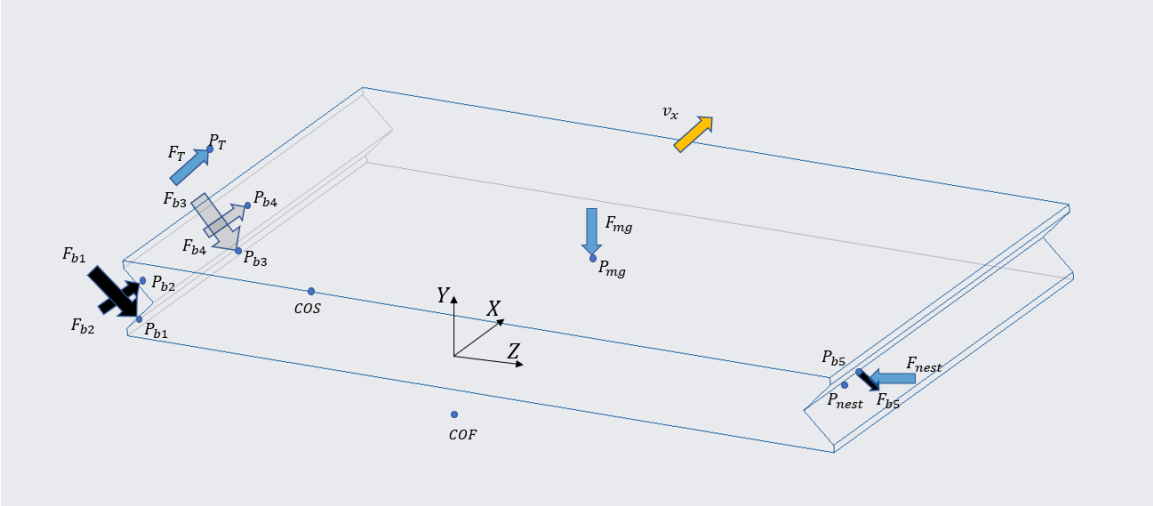

Figure 24: 3D dimensional free body diagram of the stage and reaction forces.

The linear bearings span half of the depth of the stage in Y thus there are two extremes to the moments generated. To get an estimate of the magnitude of the moments generated and the belt tension needed to overcome the static friction, 3 different models were created using the following system of equations. The work coordinate system is represented in the diagram.

The direction cosines of each force are represented by the following:

$$\Theta_{b1} = \Theta_{b3} = \begin{bmatrix} 0 \\ -\frac{1}{\sqrt{2}} \\ \frac{1}{\sqrt{2}} \end{bmatrix} \Theta_{b2} = \Theta_{b4} = \begin{bmatrix} 0 \\ \frac{1}{\sqrt{2}} \\ \frac{1}{\sqrt{2}} \end{bmatrix} \Theta_{b5} = \begin{bmatrix} 0 \\ \frac{1}{\sqrt{2}} \\ -\frac{1}{\sqrt{2}} \end{bmatrix} \Theta_{mg} = \begin{bmatrix} 0 \\ -1 \\ 0 \end{bmatrix} \Theta_{T} = \begin{bmatrix} 1 \\ 0 \\ 0 \end{bmatrix} \Theta_{nest} = \begin{bmatrix} 0 \\ 0 \\ -1 \end{bmatrix}$$

Many variables can be assigned values and are described below.

μ is substituted with the rolling resistance of a bearing ball in a v groove which is 0.005 (Amroll, 2018).

$$F_{mg} = m * g = 1.3kg * 9.81 \left(\frac{m}{s^2}\right) = 12.8N$$

$$F_{nest} = 100N$$

The tension force will be omitted for now since we want to find the center of stiffness and friction first.

$$F_T = 0N$$

The values for the position vectors are assigned. Units are in meters.

$$P_{b1} = [0, -0.003, -0.135]$$

$$P_{b2} = [0, 0.003, -0.135]$$

$$P_{b3} = [0.05, -0.003, -0.135]$$

$$P_{b4} = [0.05, 0.003, -0.135]$$

$$P_{b5} = [0.025, 0.003, 0.135]$$

$$P_{mg} = [0.05, 0, 0]$$

$$P_T = [-0.14, 0.05, 0.006]$$

$$P_{nest} = [0.025, 0, 0.135]$$

The solution is the following values.

$$F_{b1} = 35.4N$$
$$F_{b2} = 30.8N$$
$$F_{b3} = 35.4N$$
$$F_{b4} = 30.8N$$
$$F_{b5} = -9.0N$$
$$v_x = 0 \left(\frac{m}{s}\right)$$

The velocity looks correct since there are no forces in X.

Applying the following tension force in X will provide a steady state velocity in the X direction.

$$F_T = 0.05N$$

The solution is the following values.

$$F_{b1} = 35.4N$$
$$F_{b2} = 30.9N$$
$$F_{b3} = 35.3N$$
$$F_{b4} = 30.8N$$
$$F_{b5} = -9.0N$$
$$v_x = 0.08 \left(\frac{m}{s}\right)$$

The velocity is positive, greater than 0, and sounds about right in terms of magnitude.

Now the preload and the belt tension is set to 0. The expected answer is only reaction forces in the forces pointing against gravity.

The solution is the following values.

$$F_{b1} = 0N$$

$$F_{b2} = -4.5N$$

$$F_{b3} = 0N$$

$$F_{b4} = -4.5N$$

$$F_{b5} = -9.0N$$

$$v_x = 0.0\left(\frac{m}{s}\right)$$

There are no forces on $B1$ and $B3$ as expected. In addition, there is no velocity and $B2$, $B4$, and $B5$ are equivalent in direction. A quick check for the forces in Y is conducted to see if they equate to the weight of the stage.

$$\beta_{b2} * F_{b2} = 3.19N$$

$$\beta_{b4} * F_{b4} = 3.19N$$

$$\beta_{b5} * F_{b5} = 6.38N$$

$$3.18N + 3.18N + 6.37N = 12.8N$$

$$weight = 12.8N$$

They do equate.

However, the tension force in the belt that was recently calculated was 0.38N.

Assigning 0.38N to F_T and running the model again yields the following reaction forces.

The solution is the following values.

$$F_{b1} = 36.0N$$

$$F_{b2} = 31.0N$$

$$F_{b3} = 34.7N$$

$$F_{b4} = 30.7N$$

$$F_{b5} = -9.0N$$

$$v_x = 0.08\left(\frac{m}{s}\right)$$

There is a difference in magnitude between F_{b1} and F_{b3} of about 1.3N as well as a difference in magnitude between F_{b2} and F_{b4} of 0.3N. The stage will have a slight tendency to rotate. The center of friction and center of stiffness are calculated to further the analysis.

The center of friction with no nesting force or belt tension force results in the following values:

$$Center\,of\,friction = \begin{bmatrix} 0m \\ -0.025m \\ 0m \end{bmatrix}$$

The results are as expected.

When a 100N nesting force is added in the negative Z axis the resulting center of friction resolves to the following values.

$$Center\,of\,friction = \begin{bmatrix} 0m \\ -0.025m \\ 0m \end{bmatrix}$$

The center of stiffness is then approximated. The spring constant for the bearing points will be calculated from the cantilever geometry of the stage supports. Displacement due to Hertzian contact forces will be ignored since they are likely to be much smaller in magnitude than the stage support deflections.

To simply the model the same simply supported beam will be used for both sides. In addition the stage will be situated in the center where the bending moment will be the greatest and thus the deflections will be maximized. This may provide both the stiffness at each bearing and the linear deflection at that point.

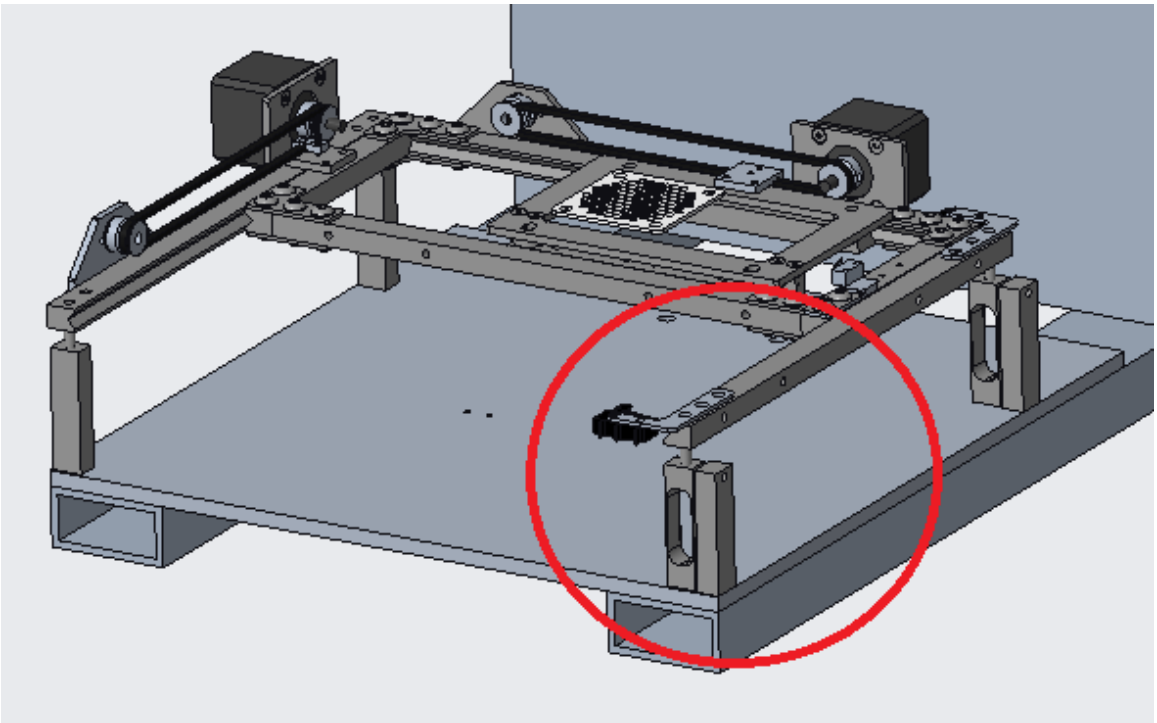

Figure 25: The area of interest for the stiffness study.

The resulting model can be represented by the following diagram.

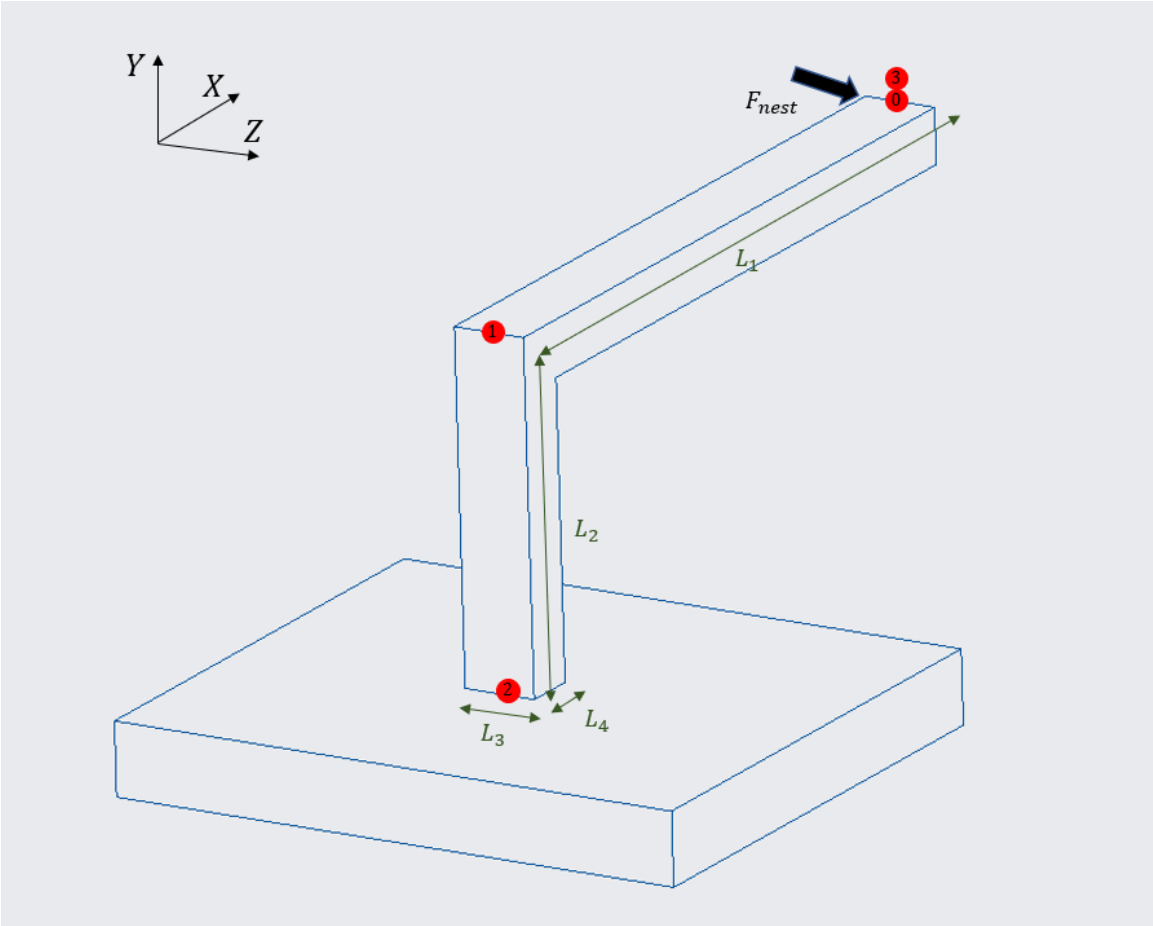

Figure 26: The simply supported beam (visually cut in half) that makes up the support for the stage and the stage preload. Three locations are marked to set up the homogeneous transformation matrices.

The force is equivalent to the preload force which is 50N in magnitude at each support in the Z axis. The cross sectional area of the beam is also constant.

The moment of inertia will first be calculated.

$$I = \frac{1}{12}bh^3 \tag{4}$$

$$b = L_3 = 0.0127m$$

$$h = L_4 = 0.0095m$$

$$I = 9.07 * 10^{-10} m^4$$

The homogeneous transformation matrices are then set up as shown below.

All material properties were used from (Azom, 2018; ASM, 2018).

From 0 to 1 deflection in X is caused by the nesting force.

$$dL_{01z} = \frac{F_{nest}(2 * L_1)^3}{48 E_{303} I}$$

$${}^0T_1 = \begin{bmatrix} 1 & 0 & 0 & -L_1 \\ 0 & 1 & 0 & 0 \\ 0 & 0 & 1 & dL_{01z} \\ 0 & 0 & 0 & 1 \end{bmatrix}$$

From 1 to 2 the errors are deflection in X due to the nesting force and torsion about Z due to the moment generated from 0 to 1.

$$J_T = \beta L_3 L_4^3 = 0.174 * 0.0127m * 0.009m^3 = 1.61 * 10^{-9} m^4$$

$$dL_{12z} = \frac{F_{nest} L_2^3}{3 E_{303} I}$$

$$\varphi_z = -\frac{F_{nest} L_1 L_2}{G_{303} J_T}$$

$${}^1T_2 = \begin{bmatrix} cos\varphi & -sin\varphi & 0 & 0 \\ sin\varphi & cos\varphi & 0 & -L_2 \\ 0 & 0 & 1 & dL_{12z} \\ 0 & 0 & 0 & 1 \end{bmatrix}$$

From 2 to 3 is pure translation.

$$^{2}T_{3} = \begin{bmatrix} 1 & 0 & 0 & 0 \\ 1 & 0 & 0 & L_1 \\ 0 & 0 & 1 & L_2 \\ 0 & 0 & 0 & 1 \end{bmatrix}$$

$$^{0}T_{3} = {}^{0}T_{1}{}^{1}T_{2}{}^{2}T_{3}$$

This results in the simple matrix.

$$^{0}T_{3} = \begin{bmatrix} 1 & 0 & 0 & 0 \\ 0 & cos\varphi & -sin\varphi & -L_2 + L_2 cos\varphi \\ 0 & sin\varphi & cos\varphi & dL_{01z} + dL_{12z} - L_1 sin\varphi \\ 0 & 0 & & 1 \end{bmatrix}$$

The following values are substituted.

$$L_1 = 0.127m$$

$$L_2 = 0.0508m$$

$$L_3 = 0.0127m$$

$$L_4 = 0.0095m$$

$$E_{303} = 193GPa$$

$$G_{303} = 77.2GPa$$

The matrix from 0 to 3 computes to the following.

$$^{0}T_{3} = \begin{bmatrix} 1 & 0 & 0 & 0 \\ 0 & 0.999 & -0.004 & -4.94 * 10^{-7} \\ 0 & 0.004 & 0.999 & 4.43 * 10^{-4} \\ 0 & 0 & & 1 \end{bmatrix}$$

The greatest amount of compliance is in the Z axis by a magnitude of 3 thus only the stiffness in Z will be considered.

The resulting deflection in Z is 0.00044m.

The stiffness at that specific bearing can then be determined.

$$K_z = F/\delta = \frac{100}{0.00044}\left(\frac{N}{m}\right) = 227000N/m$$

The center of stiffness can then be resolved in Z which comes out to the following.

$$Z_{COS} = -0.081m$$

The resulting diagram of the centers of action of the sample stage are shown below.

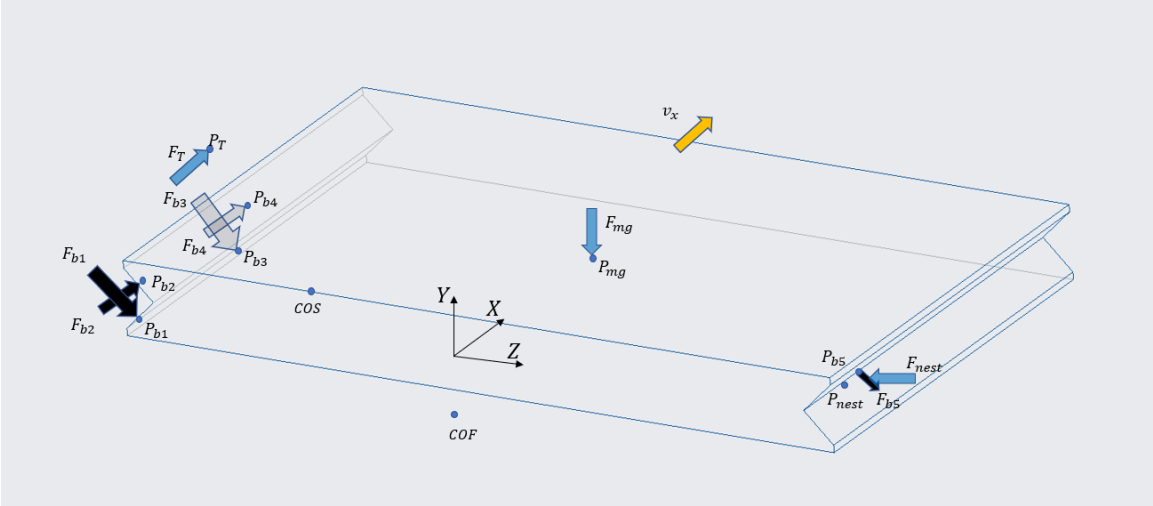

Figure 27: The sample stage with the different reaction forces, center of stiffness, and center of friction.

0.5.7 Capture Stage

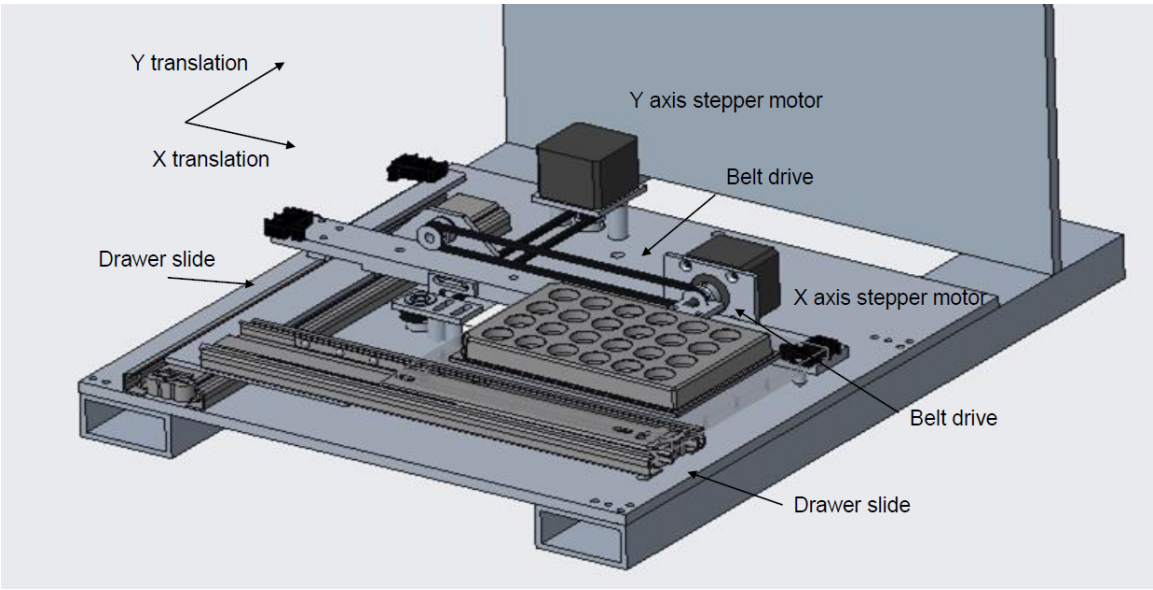

Figure 28: Overview of the Capture Stage

The capture stage was constrained in both X and Y by a stainless steel drawer slide purchased from Mcmaster-Carr. Originally the design incorporated two drawer slides for the Y axis but this led to over constraint that generated too much friction on the bearings and exceeded the torque output of the stepper motor.

A polycarbonate plate 6.4mm in thickness was used as the stage platform to support any capture vessels such as a 24 well microplate. Polycarbonate was selected due to availability and the need for a back light to transmit light through the sample and into the USB camera in the optical assembly.

To fully constrain the Z axis of the stage two PVC pegs were placed on the far end.

Each stage was driven by a stepper motor and 0.125 inch MXL timing belt with a 1:1 gearing ratio and 8 microsteps per step.

Due to the requirement that the back light must be positioned on the same axis as the USB camera placing the belt drive along the center of stiffness of each axis

came with challenges.

0.5.7.1 Capture Stage Centers of Action

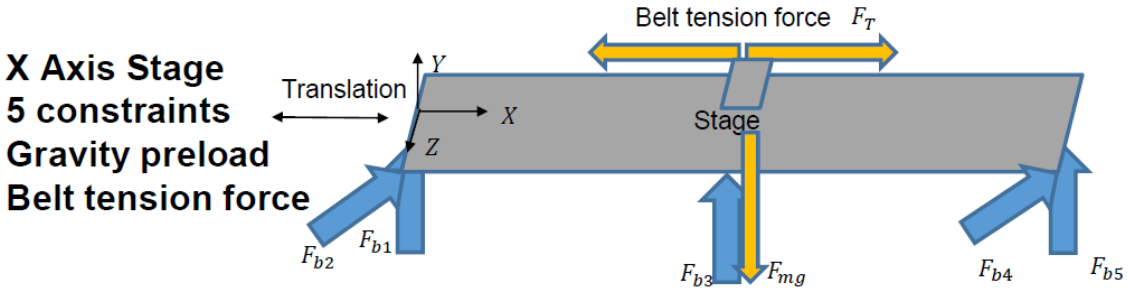

Figure 29: Kinematics of X axis capture stage.

The position vectors are then assigned.

$$P_{b1} = \begin{bmatrix} 0 & -0.003 & 0.04 \end{bmatrix}$$
$$P_{b2} = \begin{bmatrix} 0 & -0.003 & 0.06 \end{bmatrix}$$
$$P_{b3} = \begin{bmatrix} 0.075 & -0.003 & 0.06 \end{bmatrix}$$
$$P_{b4} = \begin{bmatrix} 0.15 & -0.003 & 0.06 \end{bmatrix}$$
$$P_{b5} = \begin{bmatrix} 0.15 & -0.003 & 0.04 \end{bmatrix}$$
$$P_{mg} = \begin{bmatrix} 0.075 & 0 & 0 \end{bmatrix}$$
$$P_{FT} = \begin{bmatrix} 0.075 & 0.005 & -0.07 \end{bmatrix}$$

Followed by the direction cosine vectors.

$$\Theta_{b1} = \Theta b3 = \begin{bmatrix} 0 \\ 1 \\ 0 \end{bmatrix} \Theta_{b2} = \Theta_{b4} \begin{bmatrix} 0 \\ 0 \\ -1 \end{bmatrix} \Theta_{b5} = \begin{bmatrix} 0 \\ 1 \\ 0 \end{bmatrix} \Theta_{mg} = \begin{bmatrix} 0 \\ -1 \\ 0 \end{bmatrix} \Theta_{FT} = \begin{bmatrix} 1 \\ 0 \\ 0 \end{bmatrix}$$

Mass is assumed to be $0.5kg$.

The results are the following: With no translation forces: All forces are in Newtons.

$$F_T = 0,\ F_{b1} = -7.4,\ F_{b2} = 0,\ F_{b3} = 9.8,\ F_{b4} = 0,\ F_{b5} = -7.4,\ v_x = 0\left(\frac{m}{s}\right)$$

The steady state velocity comes out to zero which is expected with no translation forces.

The center of friction is calculated to be the following:

$$COF_{XYZ} = \begin{bmatrix} 0.075 \\ 0 \\ 0 \end{bmatrix}$$

When a translation force is applied the following bearing forces are resolved to the values below:

$$F_T = 0.7,\ F_{b1} = -7.4,\ F_{b2} = -0.1,\ F_{b3} = 9.8,\ F_{b4} = 0.1,\ F_{b5} = -7.4,\ v_x = 28\frac{m}{s}$$

The steady state velocity comes out positive and greater than the 5mm/s needed although this does not factor in static friction and acceleration of the stage.

The center of friction does shift a bit in the X axis.

$$COF_{XYZ} = \begin{bmatrix} 0.074 \\ 0 \\ 0 \end{bmatrix}$$

In conclusion, the 0.7N for tension in the belt should be enough to drive the stage.

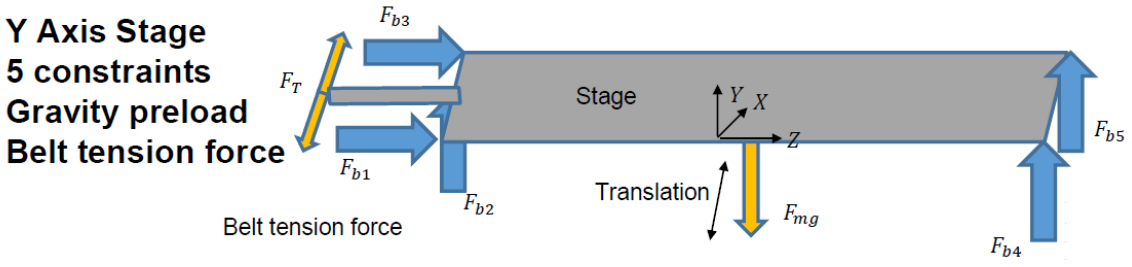

Figure 30: Kinematics of Y axis capture stage.

The position vectors are then assigned.

$$P_{b1} = \begin{bmatrix} 0 & -0.003 & -0.14 \end{bmatrix}$$
$$P_{b2} = \begin{bmatrix} 0.12 & -0.003 & -0.14 \end{bmatrix}$$
$$P_{b3} = \begin{bmatrix} 0.24 & -0.003 & -0.14 \end{bmatrix}$$
$$P_{b4} = \begin{bmatrix} 0 & -0.02 & 0.14 \end{bmatrix}$$
$$P_{b5} = \begin{bmatrix} 0.24 & -0.02 & 0.14 \end{bmatrix}$$
$$P_{mg} = \begin{bmatrix} 0.12 & 0 & 0 \end{bmatrix}$$
$$P_{FT} = \begin{bmatrix} 0.12 & 0.005 & -0.15 \end{bmatrix}$$

Followed by the direction cosine vectors.

$$\Theta_{b1} = \Theta b5 = \begin{bmatrix} 0 \\ 1 \\ 0 \end{bmatrix} \Theta_{b2} = \Theta_{b3} \begin{bmatrix} 0 \\ 0 \\ 1 \end{bmatrix} \Theta_{b4} = \begin{bmatrix} 0 \\ 1 \\ 0 \end{bmatrix} \Theta_{mg} = \begin{bmatrix} 0 \\ -1 \\ 0 \end{bmatrix} \Theta_{FT} = \begin{bmatrix} 1 \\ 0 \\ 0 \end{bmatrix}$$

Mass is assumed to be $1.0kg$.

The results are the following: With no translation forces: All forces are in Newtons.

$$F_T = 0,\ F_{b1} = -4.9,\ F_{b2} = 0,\ F_{b3} = 0,\ F_{b4} = 0,\ F_{b5} = -4.9,\ v_x = 0\left(\frac{m}{s}\right)$$

The steady state velocity comes out to zero which is expected with no translation forces.

The center of friction is calculated to be the following:

$$COF_{XYZ} = \begin{bmatrix} 0.12 \\ 0 \\ 0 \end{bmatrix}$$

When a translation force is applied the following bearing forces are resolved to the values below:

$$F_T = 0.7,\ F_{b1} = -4.9,\ F_{b2} = 1.0,\ F_{b3} = -1.0,\ F_{b4} = 0,\ F_{b5} = -4.9,\ v_x = 28\frac{m}{s}$$

The steady state velocity comes out positive and greater than the 5mm/s needed although this does not factor in static friction and acceleration of the stage.

$$COF_{XYZ} = \begin{bmatrix} 0.11 \\ 0 \\ 0 \end{bmatrix}$$

In conclusion, the 0.7N for tension in the belt should be enough to drive the stage.

0.5.8 Error Budget

To estimate the errors of the system an error budget matrix was created using the example presented in (Trimble, Yammamoto, & Li, 2016; Slocum, 1992). The machine loop included in the matrix starts at the apex of the objective lens to the position of the sample within the diffusion chamber. A total of 21 homogeneous transformation matrices were created to model the system. The following equation demonstrates how the calculation was undertaken.

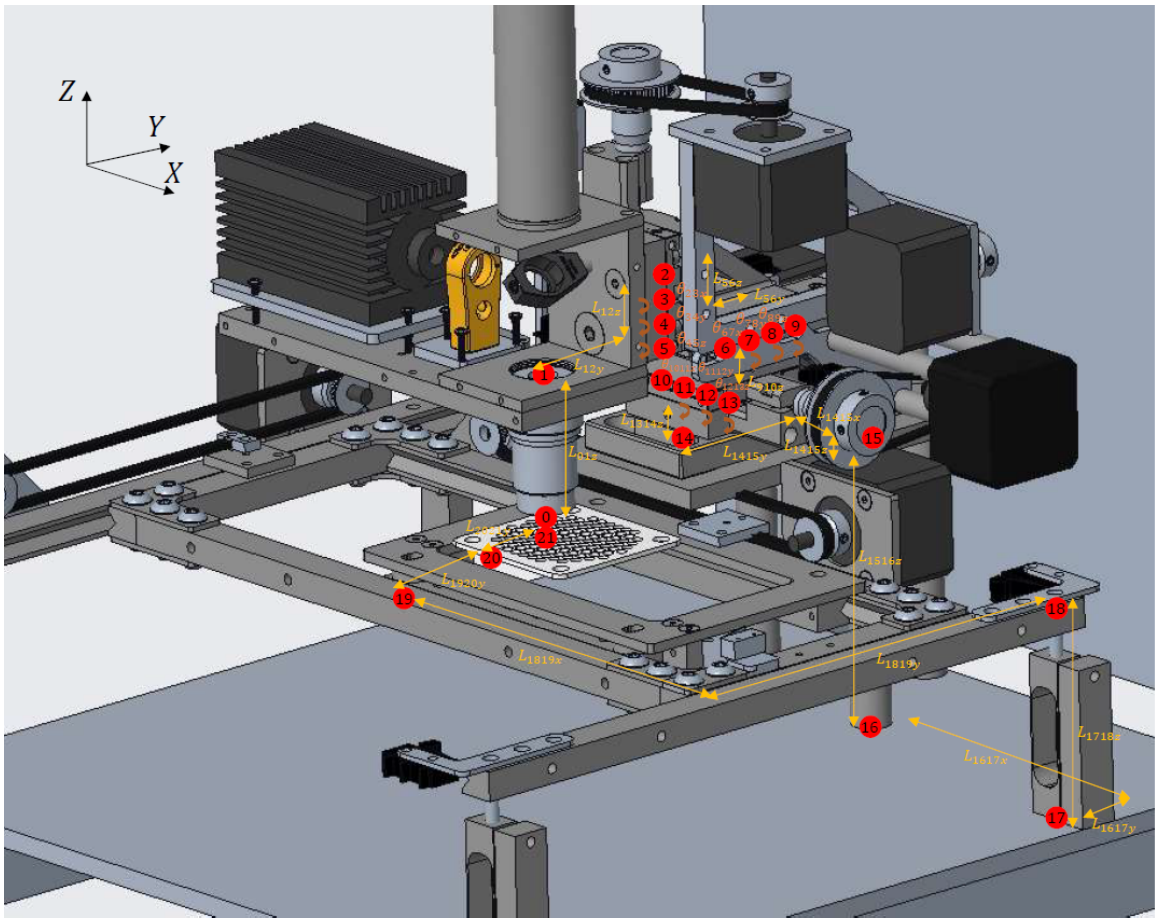

Figure 31: The location of each HTM. All maintain the same XYZ orientation.

$$\prod_{n=0}^{21} {}^{n-1}T_n$$

Expanding the product yields the following format of the expression.

$${}^{0}T_{21} = {}^{0}T_1 {}^{1}T_2 {}^{2}T_3 ... {}^{n-1}T_n$$

To model the repeatability of the machine, inertial loads were omitted due to the low accelerations of the system. Angular errors were also omitted assuming non-slip conditions (i.e. roller bearings would return to the same location on the ways). Only errors due to thermal expansion were included. To model the accuracy of the machine, angular errors were included in addition to the errors due to thermal expansion. From

T_0 to T_1 the primary error is due to thermal expansion of the aluminum objective lens tube. The expansion error, dL_{01z} is determined by the following equation.

$$dL_{01z} = \alpha_{6061} * L_{01z} * \Delta T$$

$$^0T_1 = \begin{bmatrix} 1 & 0 & 0 & 0 \\ 0 & 1 & 0 & 0 \\ 0 & 0 & 1 & L_{01z} - dL_{01z} \\ 0 & 0 & 0 & 1 \end{bmatrix}$$

From T_1 to T_2 the primary error is due to thermal expansion of the 303 stainless steel components. The expansion error, dL_{12y} and dL_{12z} are determined by the following equations.

$$dL_{12y} = \alpha_{303} * L_{12y} * \Delta T$$

$$dL_{12z} = \alpha_{303} * L_{12z} * \Delta T$$

$$^1T_2 = \begin{bmatrix} 1 & 0 & 0 & 0 \\ 0 & 1 & 0 & L_{12y} + dL_{12y} \\ 0 & 0 & 1 & L_{12z} - dL_{12z} \\ 0 & 0 & 0 & 1 \end{bmatrix}$$

From T_2 to T_3 the primary error is angular due to variations in roller diameter, surface roughness, and parallelism of the stage components. The angular error is provided by the manufacturer, Newport, and is specified at a maximum of $100\mu rad$ in roll, pitch, and yaw, of each axis. To easily account for the angular error in each axis and to keep the order each is calculated consistent, the error is designated its own matrix. Therefore ${}^2T_3$, ${}^3T_4$, and ${}^4T_5$ are all superimposed and share the same origin. When determining repeatability under non slip conditions, the angular errors are omitted from the error budget matrix.

$$ {}^2T_3 = \begin{bmatrix} 1 & 0 & 0 & 0 \\ 0 & cos(\theta_{23}) & sin(\theta_{23}) & 0 \\ 0 & -sin(\theta_{23}) & cos(\theta_{23}) & 0 \\ 0 & 0 & 0 & 1 \end{bmatrix} $$

$$ {}^3T_4 = \begin{bmatrix} cos(\theta_{34}) & 0 & -sin(\theta_{34}) & 0 \\ 0 & 1 & 0 & 0 \\ sin(\theta_{34}) & 0 & cos(\theta_{34}) & 0 \\ 0 & 0 & 0 & 1 \end{bmatrix} $$

$$ {}^4T_5 = \begin{bmatrix} cos(\theta_{45}) & sin(\theta_{45}) & 0 & 0 \\ -sin(\theta_{45}) & cos(\theta_{45}) & 0 & 0 \\ 0 & 0 & 1 & 0 \\ 0 & 0 & 0 & 1 \end{bmatrix} $$

From T_5 to T_6 the primary error is due to thermal expansion of the 440 stainless steel components of the stage. The expansion error, dL_{56y} and dL_{56z} are determined

by the following equations.

$$dL_{56y} = \alpha_{440} * L_{56y} * \Delta T$$

$$dL_{56z} = \alpha_{440} * L_{56z} * \Delta T$$

$$^{5}T_{6} = \begin{bmatrix} 1 & 0 & 0 & 0 \\ 0 & 1 & 0 & L_{56y} + dL_{56y} \\ 0 & 0 & 1 & L_{56z} + dL_{56z} \\ 0 & 0 & 0 & 1 \end{bmatrix}$$

From T_6 to T_7 the primary error again is angular due to variations in roller diameter, surface roughness, and parallelism of the stage components. $^{6}T_{7}$, $^{7}T_{8}$, and $^{8}T_{9}$ are all superimposed and share the same origin.

$$^{6}T_{7} = \begin{bmatrix} 1 & 0 & 0 & 0 \\ 0 & cos(\theta_{67}) & sin(\theta_{67}) & 0 \\ 0 & -sin(\theta_{67}) & cos(\theta_{67}) & 0 \\ 0 & 0 & 0 & 1 \end{bmatrix}$$

$$^{7}T_{8} = \begin{bmatrix} cos(\theta_{78}) & 0 & -sin(\theta_{78}) & 0 \\ 0 & 1 & 0 & 0 \\ sin(\theta_{78}) & 0 & cos(\theta_{78}) & 0 \\ 0 & 0 & 0 & 1 \end{bmatrix}$$

$$ {}^{8}T_{9} = \begin{bmatrix} cos(\theta_{89}) & sin(\theta_{89}) & 0 & 0 \\ -sin(\theta_{89}) & cos(\theta_{89}) & 0 & 0 \\ 0 & 0 & 1 & 0 \\ 0 & 0 & 0 & 1 \end{bmatrix} $$

From T_9 to T_{10} the primary error is due to thermal expansion of the 440 stainless steel components of the stage. The expansion error, dL_{910z} are determined by the following equation.

$$ dL_{56z} = \alpha_{440} * L_{910z} * \Delta T $$

$$ {}^{9}T_{10} = \begin{bmatrix} 1 & 0 & 0 & 0 \\ 0 & 1 & 0 & 0 \\ 0 & 0 & 1 & L_{910z} + dL_{910z} \\ 0 & 0 & 0 & 1 \end{bmatrix} $$

From T_{10} to T_{11} the primary error again is angular due to variations in roller diameter, surface roughness, and parallelism of the stage components. ${}^{10}T_{11}$, ${}^{11}T_{12}$, and ${}^{12}T_{13}$ are all superimposed and share the same origin.

$$
{}^{10}T_{11} = \begin{bmatrix} 1 & 0 & 0 & 0 \\ 0 & cos(\theta_{1011}) & sin(\theta_{1011}) & 0 \\ 0 & -sin(\theta_{1011}) & cos(\theta_{1011}) & 0 \\ 0 & 0 & 0 & 1 \end{bmatrix}
$$

$$
{}^{11}T_{12} = \begin{bmatrix} cos(\theta_{1112}) & 0 & -sin(\theta_{1112}) & 0 \\ 0 & 1 & 0 & 0 \\ sin(\theta_{1112}) & 0 & cos(\theta_{1112}) & 0 \\ 0 & 0 & 0 & 1 \end{bmatrix}
$$

$$
{}^{12}T_{13} = \begin{bmatrix} cos(\theta_{1213}) & sin(\theta_{1213}) & 0 & 0 \\ -sin(\theta_{1213}) & cos(\theta_{1213}) & 0 & 0 \\ 0 & 0 & 1 & 0 \\ 0 & 0 & 0 & 1 \end{bmatrix}
$$

From T_{13} to T_{14} the primary error is due to thermal expansion of the 440 stainless steel components of the stage. The expansion error dL_{1314z} are determined by the following equation.

$$
dL_{1314z} = \alpha_{440} * L_{1314z} * \Delta T
$$

$$
{}^{13}T_{14} = \begin{bmatrix} 1 & 0 & 0 & 0 \\ 0 & 1 & 0 & 0 \\ 0 & 0 & 1 & L_{1314z} + dL_{1314z} \\ 0 & 0 & 0 & 1 \end{bmatrix}
$$

From T_{14} to T_{15} the primary error is due to thermal expansion of the 303 stainless steel platform. The expansion errors dL_{1415x}, dL_{1415y}, and dL_{1415z} are determined by the following equations.

$$dL_{1415x} = \alpha_{303} * L_{1415z} * \Delta T$$

$$dL_{1415y} = \alpha_{303} * L_{1415y} * \Delta T$$

$$dL_{1415z} = \alpha_{303} * L_{1415z} * \Delta T$$

$$^{14}T_{15} = \begin{bmatrix} 1 & 0 & 0 & L_{1415x} + dL_{1415x} \\ 0 & 1 & 0 & L_{1415y} + dL_{1415y} \\ 0 & 0 & 1 & L_{1415z} + dL_{1415z} \\ 0 & 0 & 0 & 1 \end{bmatrix}$$

From T_{15} to T_{16} the primary error is due to thermal expansion of the 316 stainless steel support standoff. The expansion error dL_{1516z} are determined by the following equation.

$$dL_{1516x} = \alpha_{316} * L_{1516z} * \Delta T$$

$$
{}^{15}T_{16} = \begin{bmatrix} 1 & 0 & 0 & 0 \\ 0 & 1 & 0 & 0 \\ 0 & 0 & 1 & L_{1516z} + dL_{1516z} \\ 0 & 0 & 0 & 1 \end{bmatrix}
$$

From T_{16} to T_{14} the primary error is due to thermal expansion of the 6061 aluminum plate. Due to the length of the component and the higher coefficient of linear thermal expansion increased access to airflow on the bottom of the plate was incorporated to improve heat transfer from the machine to the aluminum to the air. The expansion errors dL_{1617x} and dL_{1617y} are determined by the following equations.

$$
dL_{1617x} = \alpha_{6061} * L_{1617x} * \Delta T
$$

$$
dL_{1617y} = \alpha_{6061} * L_{1617y} * \Delta T
$$

$$
{}^{16}T_{17} = \begin{bmatrix} 1 & 0 & 0 & L_{1617x} + dL_{1617x} \\ 0 & 1 & 0 & L_{1617y} + dL_{1617y} \\ 0 & 0 & 1 & 0 \\ 0 & 0 & 0 & 1 \end{bmatrix}
$$

From T_{17} to T_{18} the primary error is due to thermal expansion of the 303 stainless steel components of the stage. The expansion error dL_{1718z} is determined by the following equation.

$$dL_{1718z} = \alpha_{303} * L_{1718z} * \Delta T$$

$$^{17}T_{18} = \begin{bmatrix} 1 & 0 & 0 & 0 \\ 0 & 1 & 0 & 0 \\ 0 & 0 & 1 & L_{1718z} + dL_{1718z} \\ 0 & 0 & 0 & 1 \end{bmatrix}$$

From T_{18} to T_{19} the primary error is due to thermal expansion of the 303 stainless steel components of the stage. The expansion errors dL_{1819x} and dL_{1819y} are determined by the following equations.

$$dL_{1819x} = \alpha_{303} * L_{1819x} * \Delta T$$

$$dL_{1819y} = \alpha_{303} * L_{1819y} * \Delta T$$

$$^{18}T_{19} = \begin{bmatrix} 1 & 0 & 0 & L_{1819x} + dL_{1819x} \\ 0 & 1 & 0 & L_{1819y} + dL_{1819y} \\ 0 & 0 & 1 & 0 \\ 0 & 0 & 0 & 1 \end{bmatrix}$$

From T_{19} to T_{20} the primary error is due to thermal expansion of the 303 stainless steel components of the stage. The expansion error dL_{1920y} is determined by the

following equation.

$$dL_{1920y} = \alpha_{303} * L_{1920y} * \Delta T$$

$$^{19}T_{20} = \begin{bmatrix} 1 & 0 & 0 & 0 \\ 0 & 1 & 0 & L_{1920y} + dL_{1920y} \\ 0 & 0 & 1 & 0 \\ 0 & 0 & 0 & 1 \end{bmatrix}$$

And lastly, the homogenous transformation matrix to account for the translation in Y of the diffusion chamber. If the diffusion chamber is not constrained on the platform it is assumed that thermal expansion occurs equidistant from the center.

$$^{20}T_{21} = \begin{bmatrix} 1 & 0 & 0 & 0 \\ 0 & 1 & 0 & L_{2021y} \\ 0 & 0 & 1 & 0 \\ 0 & 0 & 0 & 1 \end{bmatrix}$$

The resulting linear translations calculated using Matlab with small angle approximations omitted came out to the following.

The following small angle approximations were applied:

$$sin\theta = 0$$

$$cos\theta = 1$$

$$\theta^2 = 0$$

$$\theta^3 = 0$$

The resulting linear translations with the errors is represented by the vector R.

$$^0R_{21} = \begin{bmatrix} \delta_x \\ \delta_y \\ \delta_z \end{bmatrix}$$

The errors in X, Y, and Z can be substituted using the expanded cells below.

$$\delta_x = L_{1415x} + L_{1617x} + L_{1819x} + \alpha_{303}L_{1415x}\Delta T - \alpha_{303}L_{1819x}\Delta T + \alpha_{6061}L_{1617x}\Delta T$$

$$\delta_y = L_{12y} + L_{56y} + L_{1415y} + L_{1617y} + L_{1819y} + L_{1920y} + L_{2021y} + \alpha_{303}L_{12y}\Delta T$$
$$+\alpha_{440}L_{56y}\Delta T + \alpha_{303}L_{1415y} + \alpha_{6061}L_{1617y}\Delta T - \alpha_{303}L_{1819y}\Delta T + \alpha_{303}L_{1920y}\Delta T$$
$$+\alpha_{bk602POM}L_{2021}\Delta T$$

$$\delta_z = L_{01z} + L_{12z} + L_{56z} + L_{910z} + L_{1314z} + L_{1415z} + L_{1516z} + L_{1718z} + z - L_{12z}\alpha_{303}\Delta T$$
$$+L_{56z}\alpha_{440}\Delta T + L_{910z}\alpha_{440}\Delta T + L_{1415z}\alpha_{303}\Delta T + L_{1314z}\alpha_{440}\Delta T + L_{1516z}\alpha_{316}\Delta T$$
$$-L_{1718z}\alpha_{303}\Delta T - L_{01z}\alpha_{6061}\Delta T$$

To estimate the error during a non slip repeatability test (translating distance x, then translating distance -x) all sources of error except those due to thermal expansion were considered when setting up the homogeneous transformation matrices.

$$^{0}T_{21ideal} = \begin{bmatrix} 1 & 0 & 0 & 0 \\ 0 & 1 & 0 & 0 \\ 0 & 0 & 1 & 0 \\ 0 & 0 & 0 & 1 \end{bmatrix}$$

$$^{0}T_{21error} = \begin{bmatrix} 1 & 0 & 0 & 5.02 * 10^{-7} \\ 0 & 1 & 0 & 5.02 * 10^{-7} \\ 0 & 0 & 1 & 1.05 * 10^{-5} \\ 0 & 0 & 0 & 1 \end{bmatrix}$$

$$R_{error} = (^{0}T_{21error} - {}^{0}T_{21ideal})R_{xyz}$$

$$R_{error} = \left(\begin{bmatrix} 1 & 0 & 0 & 5.02 * 10^{-7} \\ 0 & 1 & 0 & 5.02 * 10^{-7} \\ 0 & 0 & 1 & 1.05 * 10^{-5} \\ 0 & 0 & 0 & 1 \end{bmatrix} - \begin{bmatrix} 1 & 0 & 0 & 0 \\ 0 & 1 & 0 & 0 \\ 0 & 0 & 1 & 0 \\ 0 & 0 & 0 & 1 \end{bmatrix} \right) \begin{bmatrix} x \\ y \\ z \\ 1 \end{bmatrix}$$

$$R_{error} = \begin{bmatrix} 5.02 * 10^{-7} \\ 5.02 * 10^{-7} \\ 1.05 * 10^{-5} \\ 1 \end{bmatrix}$$

To estimate the accuracy error, the angular errors of each axis of the stage was included.

$$
{}^{0}T_{21error} = \begin{bmatrix} 1.00 & 3.00 * 10^{-4} & -3.00 * 10^{-4} & -2.55 * 10^{-5} \\ -3.00 * 10^{-4} & 1 & 3.00 * 10^{-4} & 1.03 * 10^{-5} \\ 3.00 * 10^{-4} & -3.00 * 10^{-4} & 1.00 & 2.67 * 10^{-5} \\ 0 & 0 & 0 & 1 \end{bmatrix}
$$

0.5.9 Laser Power Analysis

To determine if the 2 watt 445nm laser diode has the right wavelength and power density to vaporize the agar work piece an analysis was conducted using the Beer-Lambert law. The estimated power after efficiency loss after all optical elements is 75 percent or 1.5W leaving 0.5W to enter the sample. 50 percent is lost as it transmits through the dichroic mirror (50 percent transmission and reflectance ratio). The remaining 25 percent is due to reflectance and absorbance of the objective lens as well as the assumption of lower than stated power output of the laser. The estimated laser diameter is $1\mu m$. And the assumed sample thickness is $2mm$.

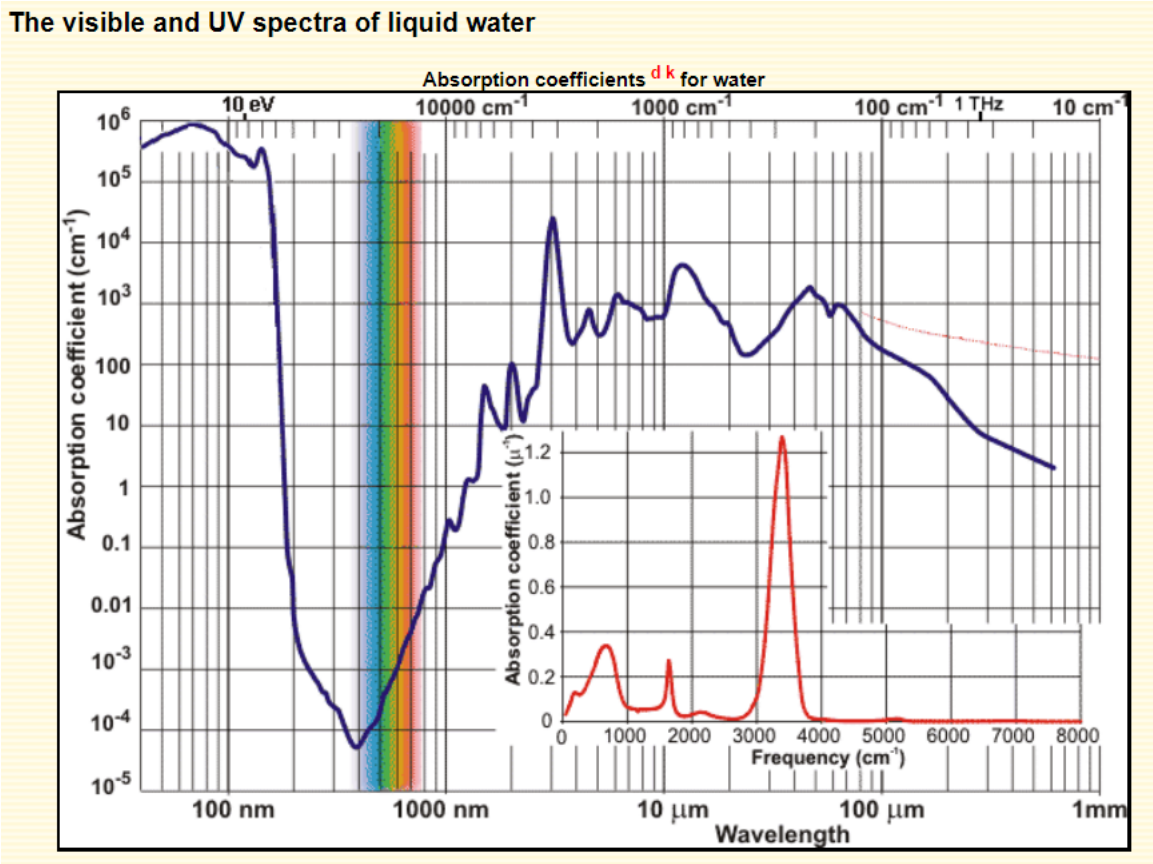

Figure 32: Absorption of light for water.

The wavelength of the laser is specified as 445 nm. The absorbtion coefficient from the figure above for water intersects at about $10^{-4.2}$ or $6.309cm^{-1}$ (Chaplin, 2018).

This is then input into the Beer-Lambert absorption equation.

$$A = -log_{10}\frac{I}{I_0} \tag{5}$$

Where I is the transmitted intensity of light (leaving the medium) and I_0 is the incident intensity of light (entering the medium). The absorption coefficient found from the figure above can be used to determine the amount of light absorbed in the medium by the following equation.

$$Where\,\frac{I}{I_0} = e^{-\alpha_\lambda * L}$$

Where α_λ is the absorption coefficient found from figure X and L is the thickness of the material.

Substituting these values results in the following calculation

$$e^{-10^{-3.2}m*0.002m} = 0.999$$

$$A = -log_{10}(0.999) = 4.3 * 10^{-4}\, Watts$$

Now looking at a cube of agar 1 μm by 1 μm by $2mm$ thick results in the following volume.

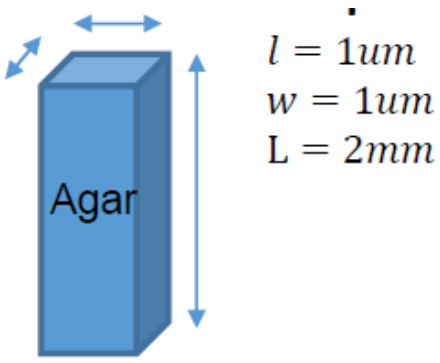

Figure 33: An agar rectangular prism with a cross sectional area approximately equivalent in area to the beam.

$$V = l * w * h = (1 * 10^{-6}m)(1 * 10^{-6}m) * (0.002m) = 2.0 * 10^{-15}m^3$$

Finding the mass of the water for that volume

$$mass = \rho * v = 998\left(\frac{kg}{m^3}\right)(2 * 10^{-15}m^3)\frac{1000}{1}\left(\frac{g}{kg}\right) = 2 * 10^{-9}g$$

Assuming the machine is operating at 20°C the change in temperature to reach vaporization is 80°C.

The heat of vaporization for water is $\frac{2260Kg}{kg}$.

Next finding the amount of energy needed to ablate the sample cube using heat capacity.

First calculating the amount of energy need to heat the near liquid sample.

$$q = cm\Delta T \tag{6}$$

$$= 4.18\left(\frac{J}{gC}\right) * 2 * 10^{-9}g * 80C = 6.7 * 10^{-7}J$$

Then calculating the heat of vaporization.

$$2260\left(\frac{J}{g}\right) * 2 * 10^{-9} = 4.5 * 10^{-6}J$$

Total energy needed to ablate the sample agar cube is calculated by the following

$$q_total = q_{20C-100C} + q_{vaporization}$$

$$= 6.7 * 10^{-7}J + 4.5 * 10^{-6}J = 5.1 * 10^{-6}J$$

To find how long it will take to ablate this cube the following calculation is made

$$T_{ablation} = 5.1 * 10^{-6}J\left(\frac{1s}{4.3 * 10^{-4}J}\right) = 10ms$$

If the thickness is constant and the area always assumed to be a square of sizes $1\mu m$ then the rate is $1\mu m$ per $0.01seconds$.

Now taking into account the distance the laser would need to cover for a small sample size.

Assuming a circular sample of diameter $0.1mm$.

$$perimeter = \pi D + D$$

$$= \pi(0.0001m) + 0.0001m$$

$$= 4.1 * 10^{-4}m$$

Now to find the amount of time it would take to cut that length.

$$4.1 * 10^{-4}m\frac{0.01\,seconds}{1 * 10^{-6}m} = 4\,seconds$$

Now assuming a large sample of diameter 2mm.

$$perimeter = \pi D + D$$
$$= \pi(0.002m) + 0.002m$$
$$= 0.008m$$

Now to find the amount of time it would take to cut that length.

$$0.008m \frac{0.01, seconds}{1 * 10^{-6}m} = 80\, seconds$$

The laser appears to be able to cut fast enough in theory. In addition, the calculations assumed the absorbance of water. The agar samples will have increasing opacity as agar concentration is increased resulting in greater absorbance and likely reduced cutting time.

A quick test was conducted with the 2 watt laser on hand to get a better approximation of the cutting performance on agar.

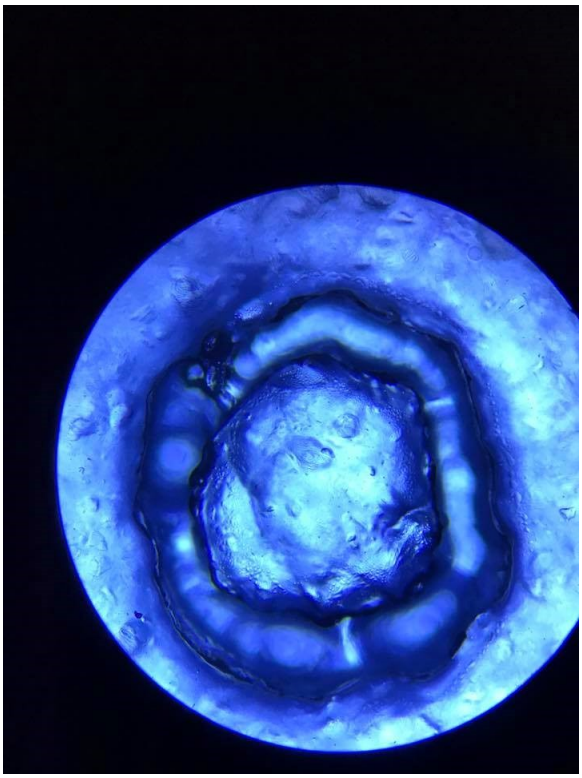

Figure 34: A test cut in high concentration agar. Focus was adjusted until sample started producing smoke. The kerf width was very roughly estimated at 250μ m.

The test was on a sample about $2mm$ in thickness and took an amount of time less than a minute.

Further testing revealed that obtaining a $1\mu m$ spot diameter for the laser beam may not be as trivial as first anticipated.

A quick estimation of beam diameter can be calculated using the waist beam equation (Newport, 2018) which assumes a Gaussian distribution of the beam.

$$2\omega_0 = \frac{4\lambda}{\pi}\frac{F}{D} \tag{7}$$

Where λ is the wavelength of the laser beam.
F is the focal length of the lens.
D is the diameter of the collimated laser beam before entering the lens.
And ω_0 is the radius of the exiting beam.

Assuming that the focal length of the 10x objective lens is around $F = 0.002m$, that λ is equal to $445 * 10^{-9}m$, and that $D = 0.001m$ based on tests with the lens on the laser to collimate the beam.

The resulting expected waist beam can be calculating by substituting those values into the waist beam equation.

$$2\omega_0 = \frac{4 * (445 * 10^{-9}m)}{\pi} \frac{0.002m}{0.001m}$$
$$= 1.1\mu m.$$

This is very close to the desired value of a spot diameter no greater than $1\mu m$.

Next the spot diameter for a beam exiting a 4x objective lens was estimated.

Assuming that the focal length of the 4x objective lens is around $F = 0.016m$, that λ is equal to $445 * 10^{-9}m$, and that $D = 0.001m$ based on tests with the lens on the laser to collimate the beam.

The resulting expected waist beam can be calculating by substituting those values into the waist beam equation.

$$2\omega_0 = \frac{4 * (445 * 10^{-9}m)}{\pi} \frac{0.016m}{0.001m}$$
$$= 9.1\mu m.$$

That value is quite far from the desired value and may require a lens with greater power (larger radius of curvature) for a shorter focal length or perhaps a collimator between the laser and the lens to generate a larger diameter collimated beam.

`https://www.newport.com/n/gaussian-beam-optics`

Due to budget constraints the 2 watt laser was selected without any additional optical components.

0.5.10 Optical Sub System

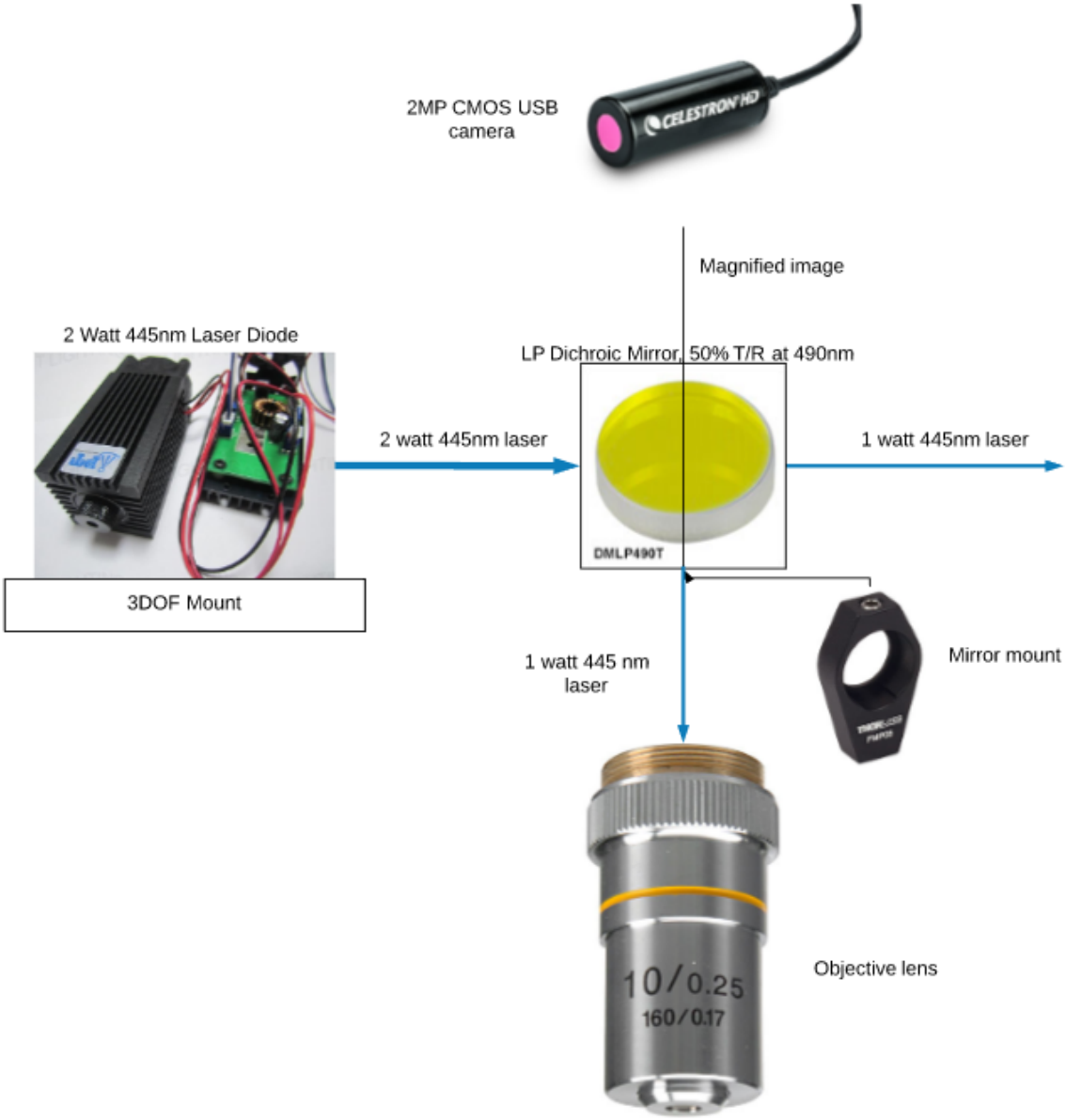

Figure 35: Block diagram of the optics subsystem

The optical subsystem consists of a digital eyepiece, white LED backlight with plano convex lens, a 2 watt 445 nm laser diode, a dichroic mirror with 50 percent transmittance and reflectance at 490nm, and either a 4x or 10x objective lens.

0.5.11 Material Selection

Large variations in stresses and ultimately deflections are not expected. However, temperature gradients due to the several heat sources are of concern. Errors in the system due to thermal expansion could compromise the performance of the system.

Thus, in areas that are sensitive to thermal expansion such as those with long characteristic lengths, materials with low coefficients of linear thermal expansion were selected.303 and 316 stainless steel were selected.

17-4 PH was used for the sample stage due its magnetic properties. A diffusion chamber could rest on a thin piece of aluminum and the top of the chamber sandwiched with another thin piece of aluminum. Magnets could then be used to both hold the position of the chamber and provide clamping force.

For components that would be too costly to manufacture such as the base frame and non precision systems, 6061 was utilized.

0.5.12 Electrical System

0.5.12.1 Control Sub System Level Architecture

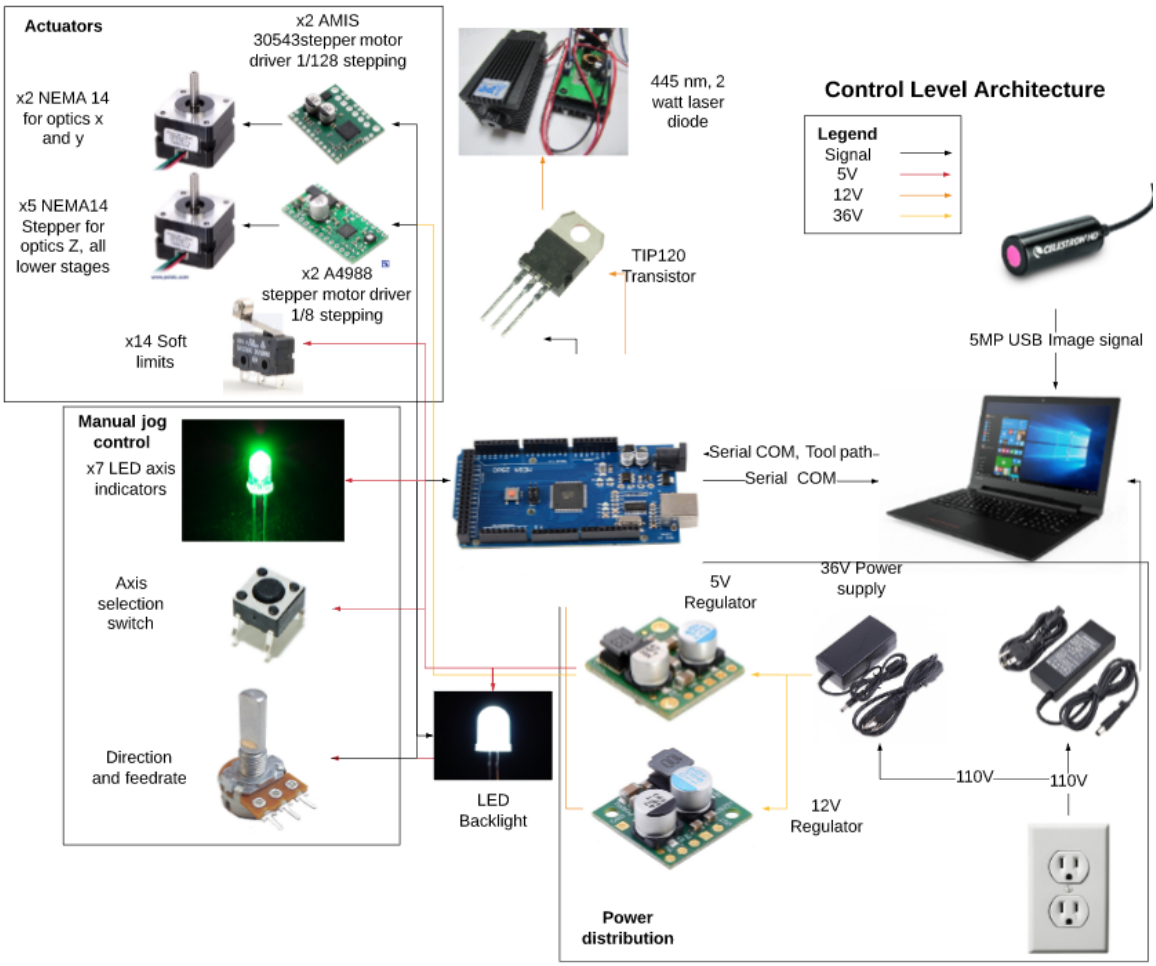

Figure 36: Control system architecture block diagram

0.5.12.2 Power Budget

Power Budget				
Sources				
Part	Qty	Current [A]	Voltage [V]	Power [w]
36V 4A (Main Power Source)	1	4	36	**144**
12V Regulator D24V22F5	1	2.5	12	**30**
5V Regulator	1	2.5	5	**12.5**
Loads				
36V				
5x NEMA 14 Stepper	5	0.3	36	10.8
2x NEMA 14 Stepper	2	0.5	36	18
AMIS 30543 Driver	2	0.012	37	0.444
A4988 Driver	5	0.008	36	0.288
			Subtotal	**29.5**
12V				
2 watt 445 nm laser diode	1	0.17	12	2
			Subtotal	**2**
5V				
Arduino Mega	1	0.2	5	1
Potentiometer	1	0.05	5	0.25
LEDs	20	0.02	5	0.1
			Subtotal	**1.4**
			Total	**32.9**

Figure 37: Table detailing how power was distributed throughout the system.

The current limits for the optics stepper motors were set to reduce the amount of missed microsteps within the 32 microstep setting. The value of 0.5A was determined empirically. The current limit for all of the remaining stepper motors at 0.3A was also determined empirically. The sinks in the power budget assumed continuous power draw. This would not happen (unless in the future synchronous movement was implemented) thus it represents the worst case scenario. In conclusion the power draw

from the sinks is significantly less than the power that the sources can deliver.

Below is a diagram illustrating how power is distributed to the system components.

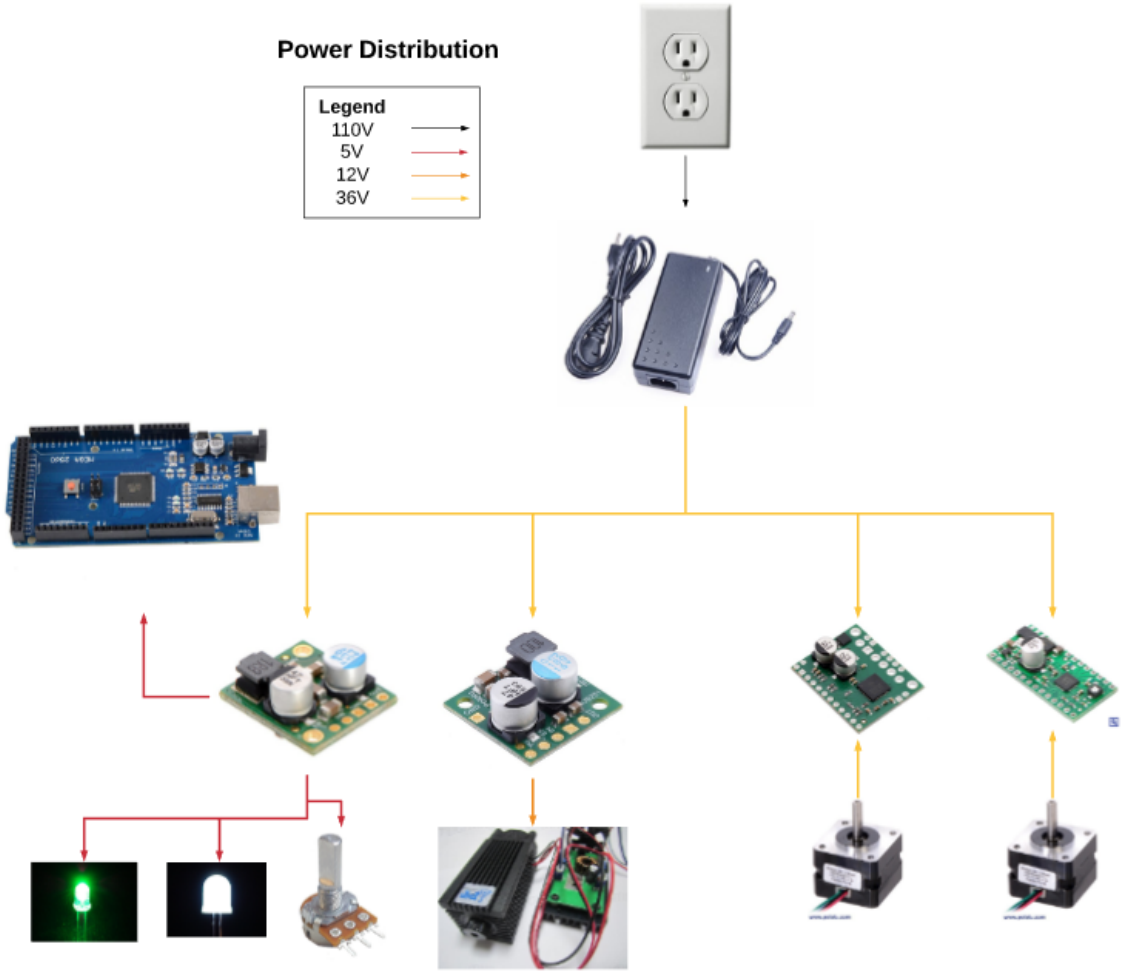

Figure 38: Diagram detailing how power was distributed throughout the system.

0.5.12.3 PCBs

Custom printed circuit boards were designed and fabricated to modularize the electronics and increase the reliability of the electrical system.

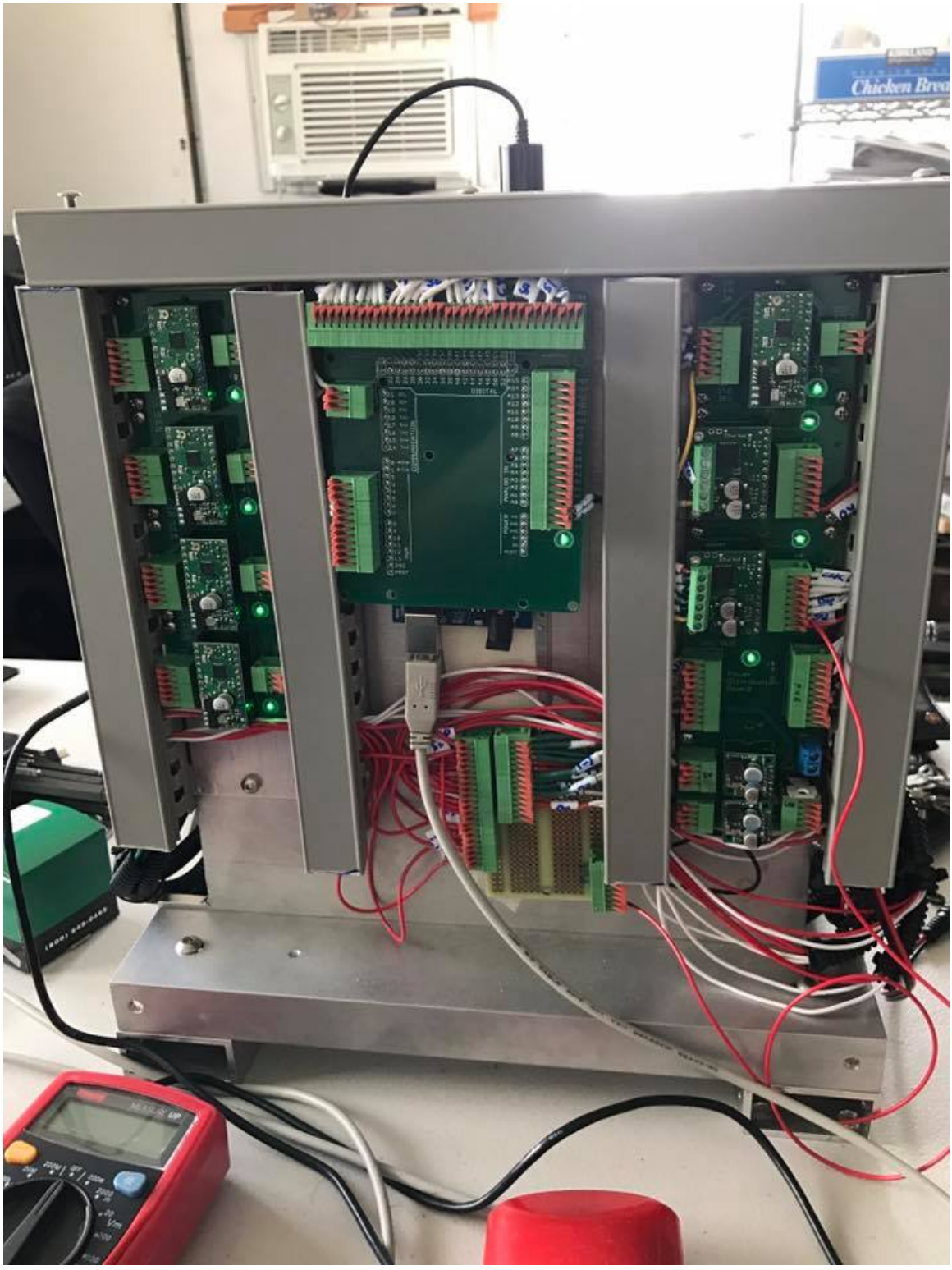

Figure 39: The electrical cabinet housing the driver, controller, and power distribution board in a modular system. Wire raceways aid in the organization of cables.

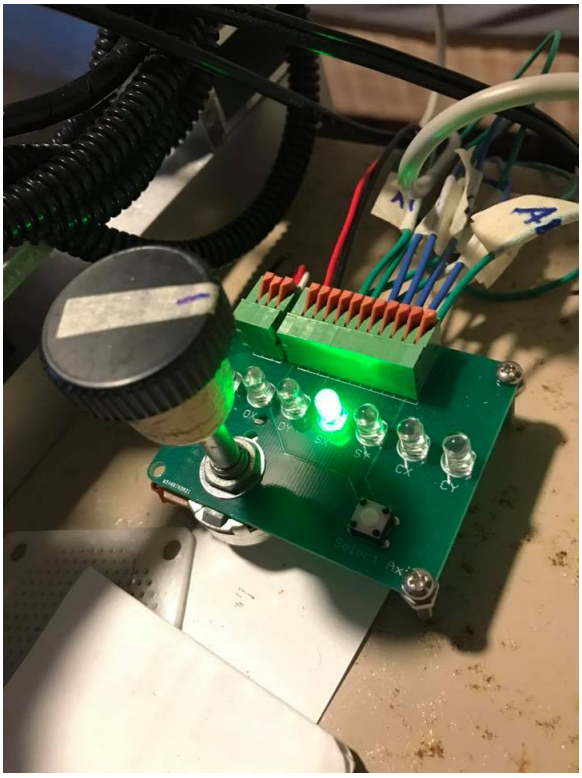

Figure 40: The manual jog controller PCB featuring LED lights indicating the axis under control, an axis selector switch, and a hand wheel using a 100K potentiometer.

0.5.13 Software System

0.5.13.1 Detailed Logic Flow Chart

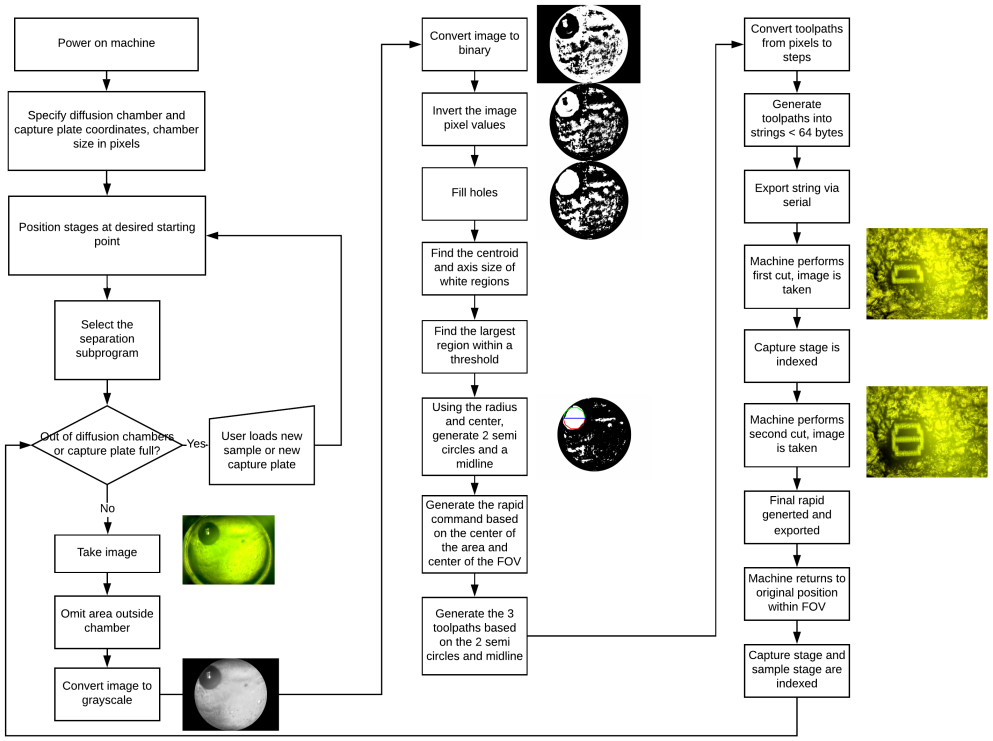

Figure 41: Logic diagram of the software controller.

0.5.13.2 Controller

An Arduino Mega was selected as the controller for the colony separator due to the low cost, memory capacity, quantity of I/O pins, availability, and familiarity with the board and the programming environment. In addition the ease of parsing strings sent via serial communication between Matlab and Arduino increased the viability of using the microcontroller as a control solution.

0.5.13.3 Image Analysis

The objective of the image analysis software is to acquire an image from the USB digital camera, isolate the best colony candidate, and then produce a toolpath that can separate the colony into two parts of approximately equal cell count.

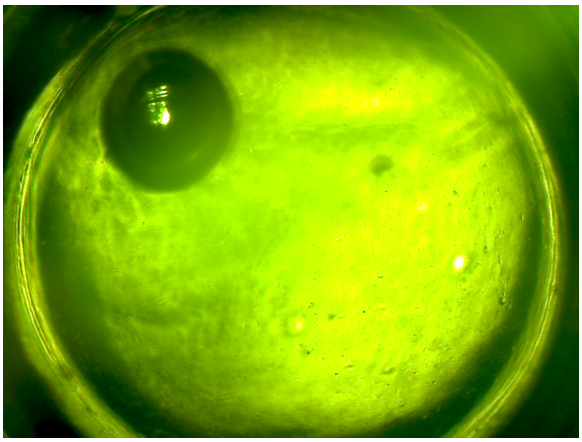

Figure 42: An example sample diffusion chamber with an object, in this case a bubble, of greater opacity than its surroundings. The contrast is similar to that of a bacteria colony.

Initially edge detection was proposed as the method to isolate the colony, but too many artifacts made the method unreliable.

Contour plotting was explored with the derivative of the values assessed as a method to identify the colony. However, the peak in the center, a result of glare through the apex of the bubble complicated the method. A diffuser to more evenly scatter the illumination from the backlight could substantially improve the glare situation but due to time constraints a software based solution was explored.

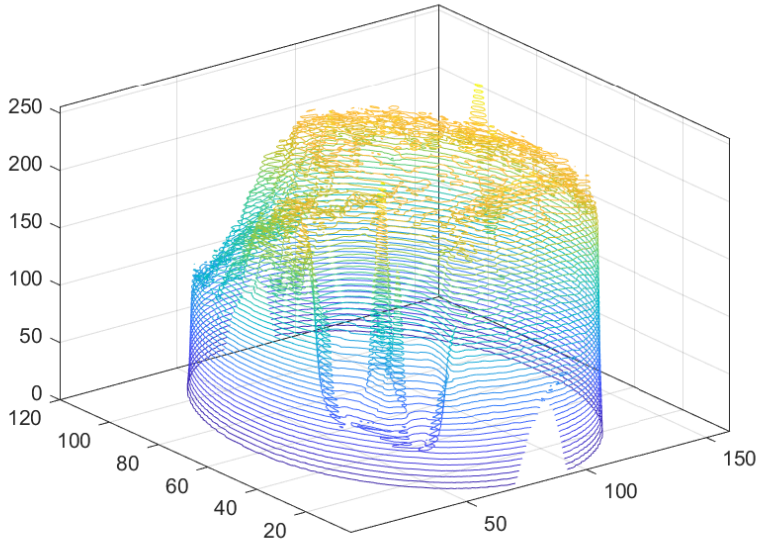

Figure 43: 3D contour plot of the example sample diffusion chamber from the previous figure. The bubble can be seen in the lower left hand corner with the glare represented as a peak.

After some trial and error using the different image processing tools in Matlab, a solution to identify a potential colony (assumed to be a more opaque region in the chamber) was realized. The process first assumes that the colony separator is equipped with a 4x objective lens. The pixel size of the image is 1600x1200. The radius of the selected diffusion chamber is about $1mm$. The most effective setting for the radius of the dish was found to be 1200/2. The next step employs the function mesh grid to set up 2D coordinates of the X and Y values of the image. The center of the dish in cartesian coordinates is then found. All areas except for the dish itself are then assigned a value of 0 or completely black to filter the diffusion chamber housing material from the image. The image is then converted to grayscale to simplify the pixel values. Next the image is converted into a binary image with a sensitivity of 0.5. The inverse of the image is then executed preparing it for the Matlab function imfill. The result is continuous areas with no holes in the center of them. The centroid and

diameters of each continuous area is found. The results can number immensely and only the largest object is of interest (assumed to be a colony). A top candidate is found by filtering all the areas with a diameter greater than 200 pixels and less than 1000 pixels. This filters out any small glares, debris, and the chamber itself. With the radius and center coordinates of the top candidate known, the top semi circle path of the circular contour is calculated converting the data from polar coordinates to cartesian.

$$x = x_{origin} + rcos(\theta) \tag{8}$$

$$y = y_{origin} + rsin(\theta) \tag{9}$$

The first semicircle is plotted from $\theta = 0 to \pi$ over 5 increments. The second semicircle is plotted from $\theta = \pi to 2\pi$ over 5 increments.

The midline, or the cut that separates the sample into two parts is generated by a line through the center of circle and parallel to the X axis. It is calculated using the maximum and minimum x coordinates.

The algorithm was tested on sample images with high contrast.

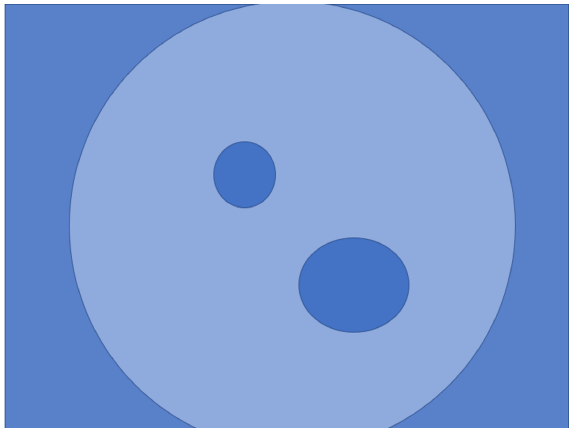

Figure 44: Test image 1.

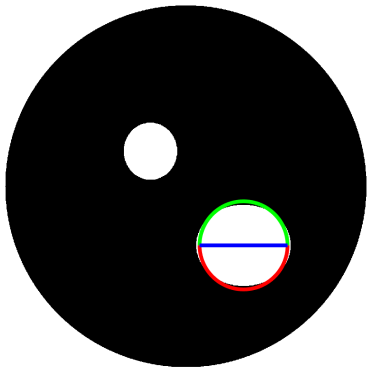

Figure 45: Test image 1 with toolpath.

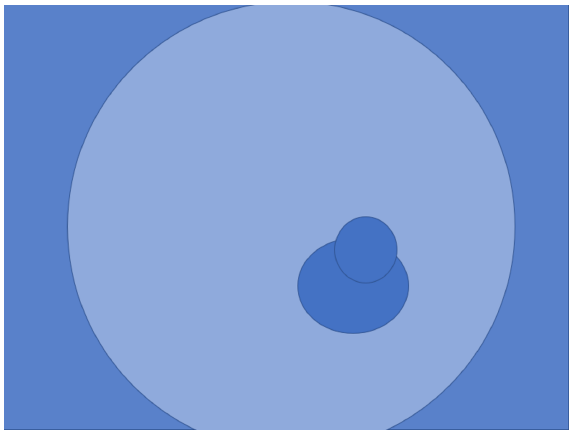

Figure 46: Test image 2.

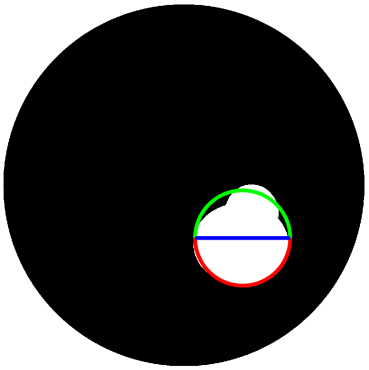

Figure 47: Test image 2 with toolpath.

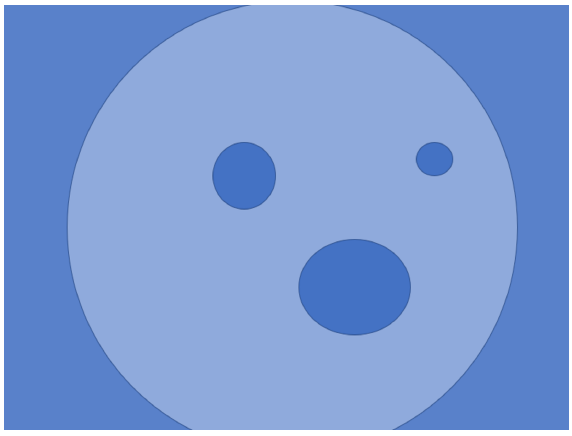

Figure 48: Test image 3.

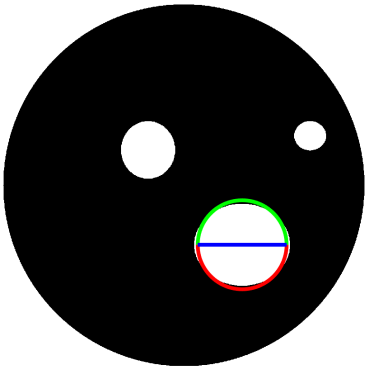

Figure 49: Test image 3 with toolpath.

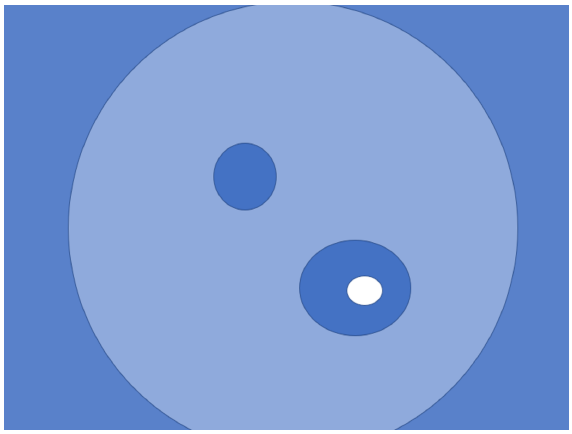

Figure 50: Test image 4.

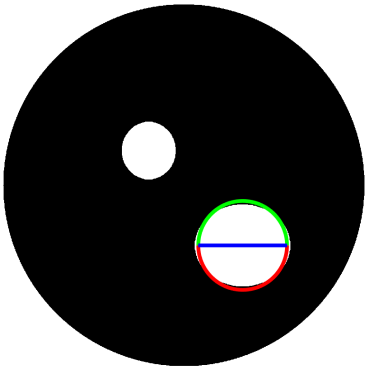

Figure 51: Test image 4 with toolpath.

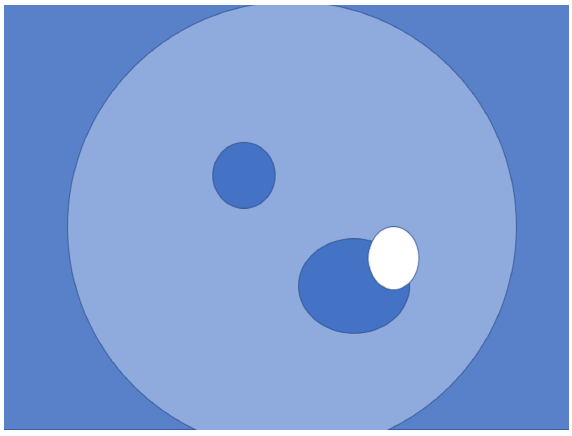

Figure 52: Test image 5.

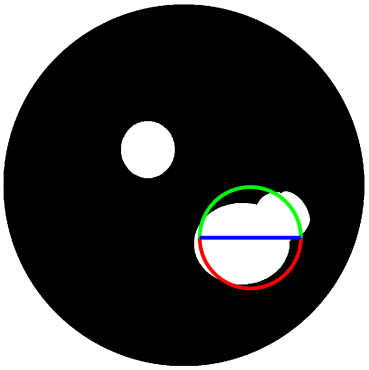

Figure 53: Test image 5 with toolpath.

And finally the image analysis on an actual diffusion chamber image. In this case the bubble in the image is representative of a colony.

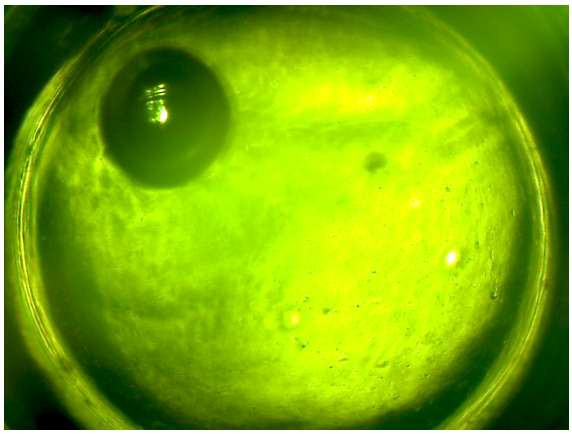

Figure 54: Test image 6, an actual agar diffusion chamber with an off center bubble representative of a colony.

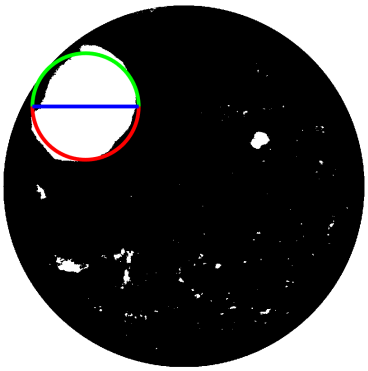

Figure 55: Test image 6 with toolpath.

Testing the image processing algorithm on diffusion chambers with bubbles and small debris is appropriate since they look very similar to chambers that contain a bacteria colony incubated in Ichips.

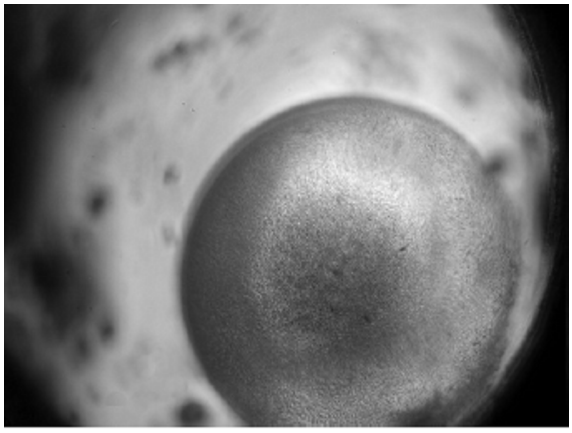

Figure 56: The original image of the diffusion chamber from (Nichols, et al., 2010) with a large bacteria colony.

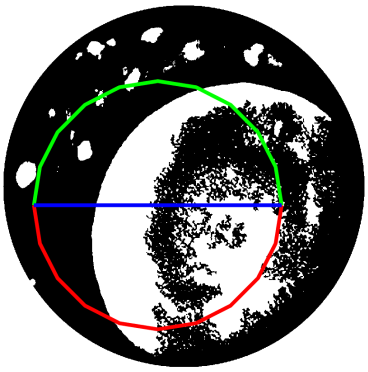

Figure 57: The diffusion chamber from (Nichols, et al., 2010). processed with the image processing algorithm.

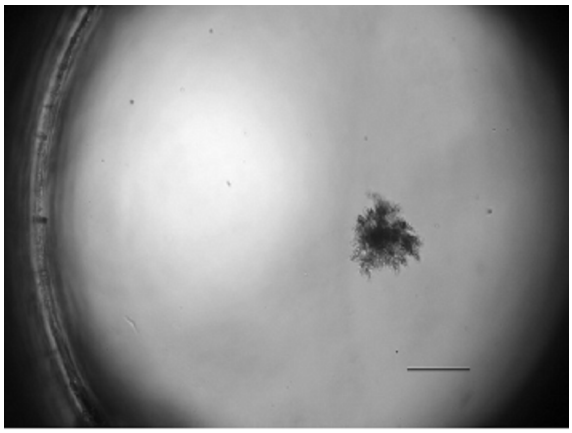

Figure 58: The original image of the diffusion chamber from (Nichols, et al., 2010) with a large bacteria colony.

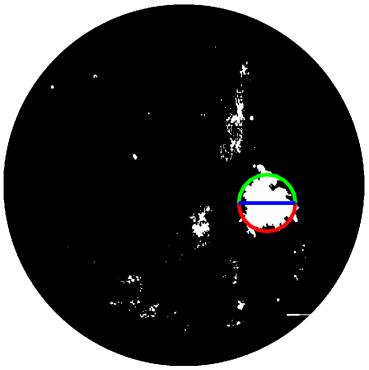

Figure 59: The diffusion chamber from (Nichols, et al., 2010) processed with the image processing algorithm.

0.5.13.4 Toolpath Generation

The toolpaths are created using the coordinates generated during image analysis. The first toolpath is a rapid translation from the center of the field of view to the X maximum value of the midline of the circle. The first toolpath is made by concatenating the top semi circle and the midline. The second toolpath is made by the bottom semi circle. The final toolpath is a rapid translation back to the center of the field of view. Since the Arduino Mega has a serial buffer of 64 bytes the toolpaths are broken into 6 different strings. Those strings are the initial rapid, the first half of toolpath 1, the second half of toolpath 1, the first half of toolpath 2, the second half of toolpath 2, and the final rapid.

Toolpaths are exported in the following format via serial communication to the Arduino microcontroller.

<N,Xcoord, Ycoord, Xcoord, Ycoord.....>>

Where N represents the subprogram that will be initiated (rapid, cutting, etc), Xcoord is the number of steps in X, and Ycoord is the number of steps in Y. The resulting cut is accomplished by translating one axis at a time.

0.6 Manufacturing

Much of the machining was completed on a Tormach PCNC440 CNC Mill and a Tormach 15L Slant-Pro CNC lathe equipped with gangtooling.

Finding the right speeds, feeds, depth of cut, radial cut, etc was a non trival task especially for more difficult to machine components such as the stainless steels.

All machining parameters are listed using the Imperial system.

0.6.1 CNC Machining Aluminum Components

To machine the various aluminum components high speed steel, cobalt steel, and carbide tool bits were utilized as well as TRIM 210 synthetic coolant.

Due to the more forgiving speeds and feeds of aluminum, speeds and feeds typically hovered around 500 surface feet per minute and 0.001 inches per tooth.

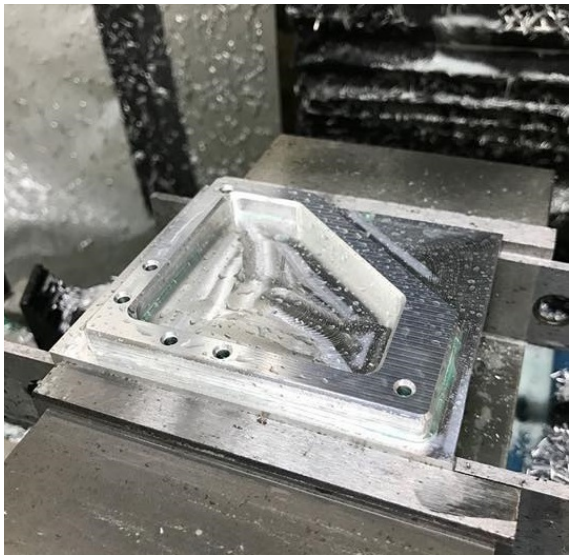

Figure 60: CNC machining motor mount with adaptive clearing toolpaths.

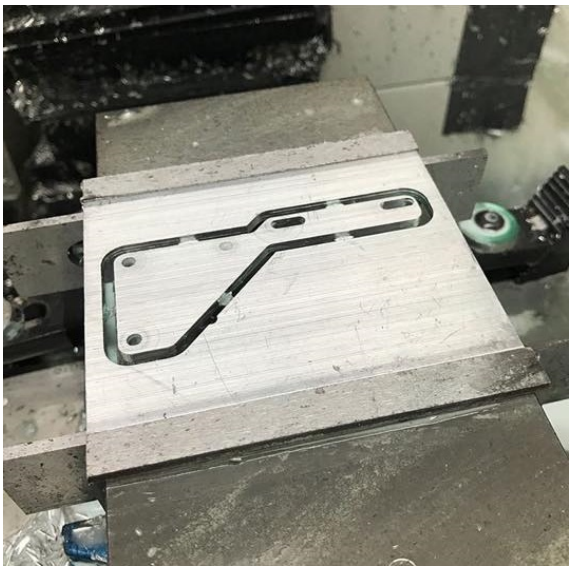

Figure 61: CNC machining motor mount with tabs

0.6.2 CNC Machining Stainless Steel Components

Machining the various stainless steels required more research and trial and error. Cobalt steel drill bits were exclusively used for machining stainless steels.

303 is known as an easy to machine stainless steel. Typical speeds used were about 90 surface feet per minute with a feed 0.0005 inches per tooth for 5 flute Lakeshore carbide 0.125" diameter endmills. For larger bits (3/8" 5 flute endmill, a feed of about 0.001 inches per tooth were used. Typical depth of cut for pocketing was about 0.01 inches. If a milling machine with a lot more torque at low speeds were used then utilizing the entire length of cut would yield higher material removal rate (MRR).

17-4 PH is a more difficult stainless steel to machine and very conservative speeds were implemented. The main bit used to machine the 17-4 PH inner stage was a 0.125 inch diameter, 5 fluke Lakeshore carbide carbide endmill. The speeds used were about 90 surface feet per minute and 0.0004 inches per tooth. Depth of cut did not exceed 0.01 inches.

Due to the low torque and low horsepower of the PCNC 440 countersinking proved a challenge. In the future the alternative method of countersinking with a ball endmill is highly recommended.

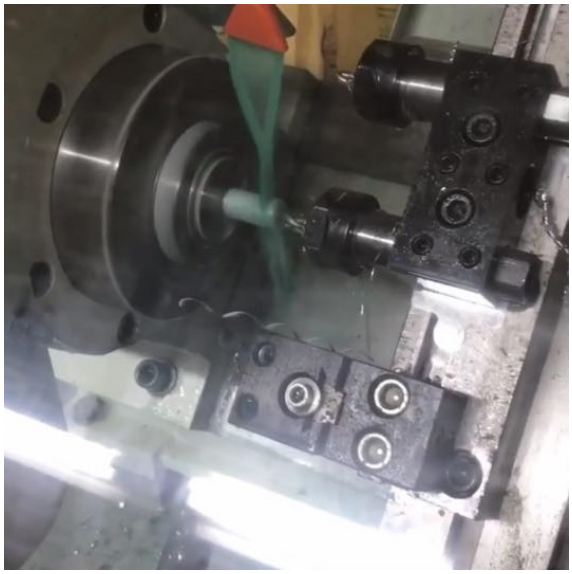

Figure 62: Rigid tapping 316 rods for the optics supports

Figure 63: CNC machining the linear bearing V groove with a drill mill carbide endmill.

Figure 64: The finished machined 17-5 PH. Machine time was about 2 hours using a 1/8" 5 flute carbide endmill.

Figure 65: The V groove with the bearing balls and delrin bearing cage. This particular linear bearings are used for the sample stage.

The computer aided manufacturing component of Fusion360 was used extensively in developing the toolpaths for manufacturing the components.

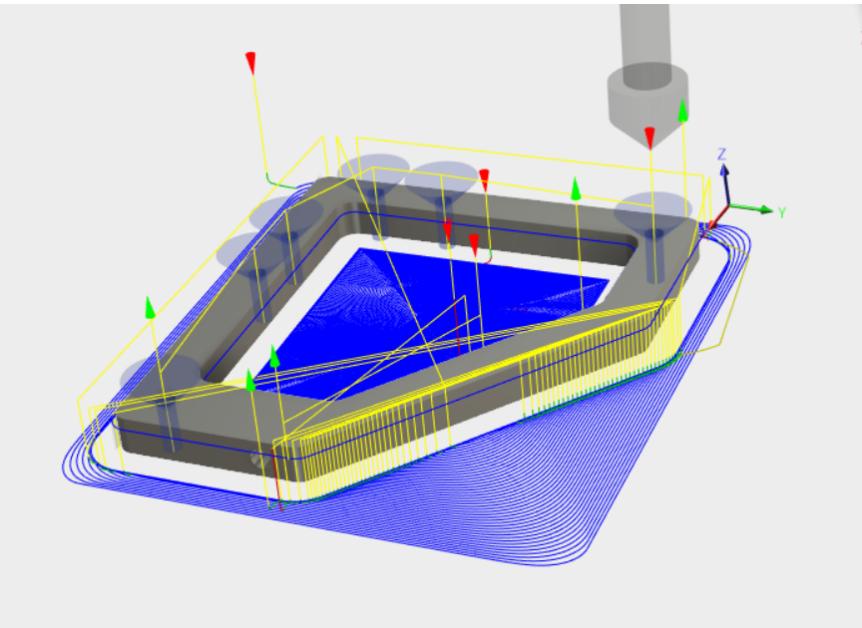

Figure 66: The toolpath generated in Fusion360 for machining one of the motor mounts. Adaptive clearing was utilized to keep cutter engagement.

0.7 Budget

The material cost to replicate the colony separator is presented in the budget below.

Component	Price	Qty	Total	Vendor
Frame				
12"x12"x0.25" 6061 Plate	$ 45.00	2	$ 90.00	Mcmaster-Carr
2"x1"x1/8" W	$ 26.81	1	$ 26.81	Mcmaster-Carr
4'x8' 0.04" Thick 6061 Sheet	$ 40.00	1	$ 40.00	Royal Metals
Vibration Dampening Sandwich Mount with Stud	$ 1.88	4	$ 7.52	Mcmaster-Carr
Misc Fasteners, Aluminum Sheet	$ 150.00	1	$ 150.00	Mcmaster-Carr
		Total	**$ 314.33**	
Capture Stage				
304 SS Drawer Slide	$ 25.88	2	$ 51.76	Mcmaster-Carr
Polycarbonate Plate (6"x6"x0.25")	$ 4.78	1	$ 4.78	Mcmaster-Carr
15T MXL Timing Belt Pulley	$ 10.02	4	$ 40.08	Mcmaster-Carr
R3-2Z SS Ball Bearing	$ 6.38	2	$ 12.76	Mcmaster-Carr
NEMA 14 Bipolar Stepper Motor	$ 12.95	2	$ 25.90	Pololu
SPDT Limit Switch 3 Pin	$ 0.85	4	$ 3.40	Pololu
MXL Timing Belt 13.2"	$ 3.11	2	$ 6.22	Mcmaster-Carr
6061 3/8"x1"x12"	$ 3.33	1	$ 3.33	Mcmaster-Carr
		Total	**$ 148.23**	
Sample Stage				
17-4 PH SS sheet 6"x6"x1/8"	$ 37.03	1	$ 37.03	Mcmaster-Carr
303 SS 1/2"x3/8"x12" Bar	$ 17.08	6	$ 102.48	Mcmaster-Carr
304 Brush SS Strip 2"x12"x0.063"	$ 9.95	1	$ 9.95	Mcmaster-Carr
15T MXL Timing Belt Pulley	$ 10.02	4	$ 40.08	Mcmaster-Carr
R3-2Z SS Ball Bearing	$ 6.38	2	$ 12.76	Mcmaster-Carr
NEMA 14 Bipolar Stepper Motor	$ 12.95	2	$ 25.90	Pololu
SPDT Limit Switch 3 Pin	$ 0.85	4	$ 3.40	Pololu
MXL Timing Belt 13.2"	$ 3.11	2	$ 6.22	Mcmaster-Carr
7/32 440C Hardened Bearing Ball	$ 9.74	1	$ 9.74	Mcmaster-Carr
		Total	**$ 247.56**	
Optics Stage				
Newport 461 XYZ M Stage	$ 1,543.00	1	$ 1,543.00	Newport
Newport SM13 Micrometer	$ 77.00	3	$ 231.00	Newport
NEMA 14 Bipolar Stepper Motor	$ 12.95	3	$ 38.85	Pololu
SPDT Limit Switch 3 Pin	$ 0.85	6	$ 5.10	Pololu
40T MXL Timing Belt Pulley	$ 14.20	3	$ 42.60	Mcmaster-Carr
15T MXL Timing Belt Pulley	$ 10.02	3	$ 30.06	Mcmaster-Carr
303 SS 3/16"x2"x12" Bar	$ 12.36	1	$ 12.36	Mcmaster-Carr
303 SS 1/4"x1-1/2"x6" Bar	$ 15.92	1	$ 15.92	Mcmaster-Carr
303 SS 1/4"x5"x6" Bar	$ 38.92	1	$ 38.92	Mcmaster-Carr
316 SS 1/2" Rod 12" Long	$ 6.66	2	$ 13.33	Mcmaster-Carr
6061 1" OD 3/4" ID 6" Long Tube	$ 5.14	1	$ 5.14	Mcmaster-Carr
		Total	**$ 1,976.28**	

Figure 67: Budget Page 1

Optics				
2 Watt 425nm Laser Diode with Focuser	$ 75.00	1	$ 75.00	Ebay
4x, 10x, 40x Objective Lens	$ 179.95	1	$ 179.95	Celestron
Dichroic Mirror	$ 113.00	1	$ 113.00	Thorlabs
Dichoric Mirror Mount	$ 34.00	1	$ 34.00	Thorlabs
2MP CMOS USB Digital Eyepiece	$ 69.95	1	$ 69.95	Celestron
		Total	**$ 471.90**	
Control				
Arduino Mega	$ 13.00	1	$ 13.00	Ebay
AMIS 30543 Stepper Motor Driver	$ 19.95	2	$ 39.90	Pololu
A4988 Stepper Motor Driver	$ 9.95	5	$ 49.75	Pololu
36V 4A Power supply	$ 20.00	1	$ 20.00	Amazon
TIP120	$ 0.25	1	$ 0.25	Ebay
Computer	$ 300.00	1	$ 300.00	Best Buy
Display Monitor	$ 100.00	1	$ 100.00	Best Buy
Keyboard and Mouse	$ 20.00	1	$ 20.00	Best Buy
Custom Printed Circuit Boards	$ 80.00	1	$ 80.00	PCBway
USB hub	$ 7.00	1	$ 7.00	Misc
24 AWG Wire	$ 5.00	7	$ 35.00	Pololu
5V Voltage Regulator	$ 8.95	1	$ 8.95	Pololu
12V Voltage Regulator	$ 9.95	1	$ 9.95	Pololu
Spring Terminal Blocks	$ 4.95	46	$ 227.70	Adafruit
Potentiometer 100kOhm	$ 1.50	1	$ 1.50	Ebay
Cable Raceway	$ 8.65	1	$ 8.65	Digikey
Cable Sleeving	$ 43.95	1	$ 43.95	Digikey
Misc (LEDs, resistors, etc)	$ 3.00	1	$ 3.00	Digikey
		Total	**$ 968.60**	
Consumables				
Carbide Endmills	$ 150.00	1	$ 150.00	Lakeshore Carbide
TRIM C210/1 Synthetic Coolant	45.69	2	$ 91.38	Amazon
Agar Powder 2 Ounce	5.2	1	$ 5.20	Amazon
		Total	**$ 246.58**	
		Total	**$ 4,373.48**	

Figure 68: Budget Page 2

It is non trivial to mention that the realized version of the colony separator required approximately 200 hours of CNC programming and machining. Using a quote from a local CNC machine shop at 175USD per hour (Precision Machinery and Tooling LLC, 2018), the cost to machine the components comes out to 35,000USD. Thus the total cost the replicate the machine comes out to 39,400 USD. While this is significantly less expensive then an entry level laser capture microdissection unit,

the costs are still quite high.

In future iterations, the sample stage, which was the component that required the most machining time, could be replaced with a design that is less machining intensive

In addition, some of the more expensive items such as the stages and micrometers could be purchased used significantly reducing the costs.

Presented are the actual expenditures to realize the colony separator and the price discrepancy.

Component	Price	Qty	Total	Vendor
Frame				
12"x12"x0.25" 6061 Plate	$ 45.00	2	$ 90.00	Mcmaster-Carr
2"x1"x1/8" W	$ 26.81	1	$ 26.81	Mcmaster-Carr
4'x8' 0.04" Thick 6061 Sheet	$ 40.00	1	$ 40.00	Royal Metals
Vibration Dampening Sandwich Mount with Stud	$ 1.88	4	$ 7.52	Mcmaster-Carr
Misc Fasteners, Aluminum Sheet	$ 150.00	1	$ 150.00	Mcmaster-Carr
		Total	**$ 314.33**	
Capture Stage				
304 SS Drawer Slide	$ 25.88	2	$ 51.76	Mcmaster-Carr
Polycarbonate Plate (6"x6"x0.25")	$ 4.78	1	$ 4.78	Mcmaster-Carr
15T MXL Timing Belt Pulley	$ 10.02	4	$ 40.08	Mcmaster-Carr
R3-2Z SS Ball Bearing	$ 6.38	2	$ 12.76	Mcmaster-Carr
NEMA 14 Bipolar Stepper Motor	$ 12.95	2	$ 25.90	Pololu
SPDT Limit Switch 3 Pin	$ 0.85	4	$ 3.40	Pololu
MXL Timing Belt 13.2"	$ 3.11	2	$ 6.22	Mcmaster-Carr
6061 3/8"x1"x12"	$ 3.33	1	$ 3.33	Mcmaster-Carr
		Total	**$ 148.23**	
Sample Stage				
17-4 PH SS sheet 6"x6"x1/8"	$ 37.03	1	$ 37.03	Mcmaster-Carr
303 SS 1/2"x3/8"x12" Bar	$ 17.08	6	$ 102.48	Mcmaster-Carr
304 Brush SS Strip 2"x12"x0.063"	$ 9.95	1	$ 9.95	Mcmaster-Carr
15T MXL Timing Belt Pulley	$ 10.02	4	$ 40.08	Mcmaster-Carr
R3-2Z SS Ball Bearing	$ 6.38	2	$ 12.76	Mcmaster-Carr
NEMA 14 Bipolar Stepper Motor	$ 12.95	2	$ 25.90	Pololu
SPDT Limit Switch 3 Pin	$ 0.85	4	$ 3.40	Pololu
MXL Timing Belt 13.2"	$ 3.11	2	$ 6.22	Mcmaster-Carr
7/32 440C Hardened Bearing Ball	$ 9.74	1	$ 9.74	Mcmaster-Carr
		Total	**$ 247.56**	
Optics Stage				
Newport 461 XYZ M Stage w/ 3 SM13 Mics	$ 489.00	1	$ 489.00	Ebay
NEMA 14 Bipolar Stepper Motor	$ 12.95	3	$ 38.85	Pololu
SPDT Limit Switch 3 Pin	$ 0.85	6	$ 5.10	Pololu
40T MXL Timing Belt Pulley	$ 14.20	3	$ 42.60	Mcmaster-Carr
15T MXL Timing Belt Pulley	$ 10.02	3	$ 30.06	Mcmaster-Carr
303 SS 3/16"x2"x12" Bar	$ 12.36	1	$ 12.36	Mcmaster-Carr
303 SS 1/4"x1-1/2"x6" Bar	$ 15.92	1	$ 15.92	Mcmaster-Carr
303 SS 1/4"x5"x6" Bar	$ 38.92	1	$ 38.92	Mcmaster-Carr
316 SS 1/2" Rod 12" Long	$ 6.66	2	$ 13.33	Mcmaster-Carr
6061 1" OD 3/4" ID 6" Long Tube	$ 5.14	1	$ 5.14	Mcmaster-Carr
		Total	**$ 691.28**	

Figure 69: Expenditures Page 1. Costs were reduced significantly since some components were sourced secondhand.

Optics				
2 Watt 445nm Laser Diode with Focuser	$ 75.00	1	$ 75.00	Ebay
4x, 10x, 40x Objective Lens	$ 179.95	1	$ 179.95	Celestron
Dichroic Mirror	$ 113.00	1	$ 113.00	Thorlabs
Dichoric Mirror Mount	$ 34.00	1	$ 34.00	Thorlabs
2MP CMOS USB Digital Eyepiece	$ 69.95	1	$ 69.95	Celestron
		Total	**$ 471.90**	
Control				
Arduino Mega	$ 13.00	1	$ 13.00	Ebay
AMIS 30543 Stepper Motor Driver	$ 19.95	2	$ 39.90	Pololu
A4988 Stepper Motor Driver	$ 9.95	5	$ 49.75	Pololu
36V 4A Power supply	$ 20.00	1	$ 20.00	Amazon
TIP120	$ 0.25	1	$ 0.25	Ebay
Computer	$ 300.00	1	$ 300.00	Best Buy
Display Monitor	$ 100.00	1	$ 100.00	Best Buy
Keyboard and Mouse	$ 20.00	1	$ 20.00	Best Buy
Custom Printed Circuit Boards	$ 80.00	1	$ 80.00	PCBway
USB hub	$ 7.00	1	$ 7.00	Misc
24 AWG Wire	$ 5.00	7	$ 35.00	Pololu
5V Voltage Regulator	$ 8.95	1	$ 8.95	Pololu
12V Voltage Regulator	$ 9.95	1	$ 9.95	Pololu
Spring Terminal Blocks	$ 4.95	46	$ 227.70	Adafruit
Potentiometer 100kOhm	$ 1.50	1	$ 1.50	Ebay
Cable Raceway	$ 8.65	1	$ 8.65	Digikey
Cable Sleeving	$ 43.95	1	$ 43.95	Digikey
Misc (LEDs, resistors, etc)	$ 3.00	1	$ 3.00	Digikey
		Total	**$ 968.60**	
Consumables				
Carbide Endmills	$ 150.00	1	$ 150.00	Lakeshore Carbide
TRIM C210/1 Synthetic Coolant	45.69	2	$ 91.38	Amazon
Agar Powder 2 Ounce	5.2	1	$ 5.20	Amazon
		Total	**$ 246.58**	
		Total	**$ 3,088.48**	

Figure 70: Expenditures Page 2

0.8 Experimental Setup

0.8.1 Basic Machine Characteristics

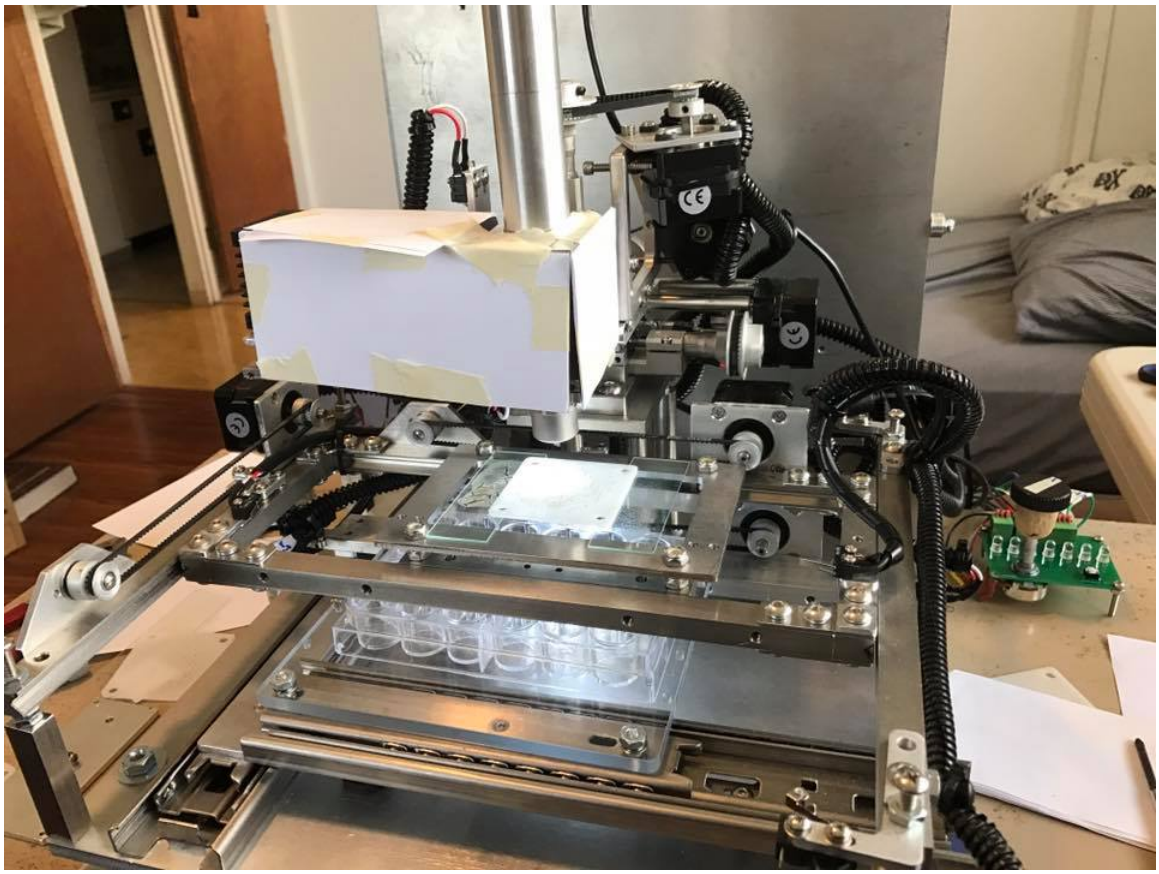

Figure 71: The colony Separator

0.8.1.1 Size of Machine

The objective of this test is to determine the machine dimensions, the machine foot print, and the machine mass.

Materials and Methods

A yardstick was used to measure the height, width, and length of the machine. The coordinate system is defined as such: The height is parallel to the Z axis of the optics stage, the width is parallel to the X axis of the optics stage, and the length is parallel

to the Y axis of the optics stage.

The machine foot print includes the manual jog controller. The width is defined as parallel to the X axis of the optics stage and the depth is defined as parallel to the Y axis of the optics stage.

The machine mass was measured using a digital kitchen scale. 3 measurements were taken and the average calculated.

0.8.1.2 4x Objective Lens FOV

Objective

The objective of this test is to estimate the field of view of the 4x objective lens empirically. Based on previous observations, it is likely that the 4x objective lens will be used the most during any cutting operation since the field of view can fit a diffusion chamber that is about 1 mm in diameter.

Methods and Materials

To determine the field of view a sample image with very sharp features was selected. The apple core prepared sample was determined to be a suitable candidate.

Estimation of the height of the field of view was first conducted.

A feature on the apple core was selected and the stage manually moved such so that the feature was placed on the far right of the field of view. The z axis of the optics stage was adjusted manually until the image came into sharp focus. The reading on the SM13 micrometer was recorded and remained unchanged throughout the process.

The optics stage was then manually jogged until the feature translated to the opposite side of the field of view. The reading on the SM13 micrometer was then recorded. The procedure was repeated 10 times.

The procedure was then repeated for measuring the width of the field of view.

0.8.1.3 10x Objective Lens FOV

The objective of this test is to estimate the field of view of the 10x objective lens empirically. Based on previous observation, it is likely that the 10x objective lens will be used only for very small chambers such as the oral diffusion chamber which has a diffusion chamber diameter of $100\mu m$. Due to the higher resolution the 10x objective lens is also an initial candidate for testing the repeatability of the device.

0.8.1.4 40x Objective Lens FOV

The objective of this test is to estimate the field of view of the 40x objective lens empirically. Based on previous observation, it is likely that the 40x objective lens will be used only for very small chambers such as the oral diffusion chamber which has a diffusion chamber diameter of $100\mu m$. Due to the higher resolution the 40x objective lens is also an initial candidate for testing the repeatability of the device although challenges such as getting the image into focus may present itself.

0.8.1.5 Linear Repeatability in Optics Stage X Axis

Objective To determine if the machine has sub micrometer repeatability over the length of the diameter of a small diffusion chamber quantified as $< 1\mu$m repeatability over a distance of 100μm in the X axis.

Methods and Materials

Using a 40x objective lens translate a distance of $100\mu m$ in one direction and then return $100\mu m$. Use a reference such as the apple core slide to determine repeatability (similar to that paper on the open source stage). 10 cycles per translation. Utilize machine vision tools to aid in the quantifying the repeatability.

0.8.1.6 Linear Repeatability in Optics Stage Y Axis

Objective To determine if the machine has sub micrometer repeatability over the length of the diameter of a small diffusion chamber quantified as $< 1\mu$m repeatability

over a distance of 100μm in the Y axis.

Methods and Materials

Using a 40x objective lens translate a distance of $100\mu m$ in one direction and then return $100\mu m$. Use a reference such as the apple core slide to determine repeatability (similar to that paper on the open source stage). 10 cycles per translation.

0.8.1.7 Emulated Ballbar Test

Objective: To quantify the repeatability of motion in both X and Y axis of the optics stage over a work area needed to process a large sample in a small diffusion chamber.

Methods and Materials

Using a 10x objective lens (due to the larger field of view) navigate to 12 different points spaced $\frac{\pi}{6}$ radians apart with a radius of $50\mu m$.Use a reference such as the apple core slide to determine repeatability (similar to that paper on the open source stage). 10 cycles per translation. Using machine vision tools, attempt to quantify the repeatability and plot the elliptical path similar to a ballbar test used for the tables of machining centers. The plot should also provide more insight to the overall accuracy of each axis (if it is not circular then errors are beginning to propagate).

0.8.2 Separation Process Characteristics

0.8.2.1 Cutting Beam Properties

Objective: To determine how beam diameter varies as a function of Z position and laser duration. This is important since it will give insight on how thick a workpiece can be machined. The specifications of the optical components are unknown and the exiting beam is not collimated.

Variables:

Cut hole diameter [μm]

Z position [mm]

Laser duration [s]

Methods and Materials

A piece of blank printer paper was placed onto the sample stage of the colony separator and secured with two glass slides until visibly flat. A 4x objective lens was used for the cutting process. An initial cut was made without translating the slide. The Z axis was adjusted until the edges of the recently cut hole came into focus. This Z position was recorded and used as the reference height for all future image acquisitions.

Several trials were conducted varying the Z position of the optics stage, and the duration that the laser was fired. The diameter of each cut was measured by converting the major diameter of the hole in pixels and converting it to micrometers based on the known field of view for the 4x objective lens. Trials were conducted until the shortest laser duration to cut a hole was achieved and a plot displaying the relationship between cut diameter, Z position, and laser duration was plotted.

0.8.2.2 Cutting Parameters

Objective: To determine the set of parameters that results in the small kerf width and quickest feed rate.

Based on initial testing, running the feed rate too slowly resulted in the agar sample curling up due to the evaporation of water. This curling and scrapping of the work piece was suspected due to the dehydration of the local site resulting in an initial expansion followed by a rapid contraction and ablation of material which changed the geometry of the work piece.

It became non trivial to explore the effects of changing certain parameters to find a manufacturing process that could avoid this unwanted warping of the material.

The variables considered included the cut length, the axis, the number of passes, the agar concentration, and the feed rate.

Methods and Materials

Cut a length of 500um in X with 1 pass, 2 passes, and 3 passes

Variables Cut length (constant at 500um) Axis (X and Y) Passes (1, 2, 3) Agar concentration (start at 7.5 percent, may reduce) Feed rate (start at a microstep period of 3010 us).

0.9 Results

0.9.1 Basic Machine Characteristics

Mass and overall dimensions

Size of Machine The height was 410mm, the width 360mm, and the length 410 mm. This meets the functional requirement that the system does not take up too much lab bench space.

Footprint of Machine The footprint of the machine had a width of 500mm and a depth of 410mm. This meets the functional requirement that the system does not take up too much lab bench space.

Mass of Machine

Machine Mass	
Trial	Mass [kg]
1	12.6
2	12.6
3	12.6

The average mass of the machine was found to be 12.6 Kg (error unknown but likely on the order of 0.5kg). This meets the functional requirement for machine mass.

0.9.1.1 Determination of Field of View for 4x Objective Lens

Standard deviation was computing using the sample method expressed in the equation below.

$$\sigma = \sqrt{\frac{\sum(X - \bar{X})^2}{n-1}} \tag{10}$$

Field of view for 4x objective lens

Trial	X_i [mm]	X_f [mm]	ΔX [mm]
1	4.023	2.818	1.205
2	4.018	2.816	1.202
3	4.020	2.813	1.207
4	4.018	2.814	1.204
5	4.019	2.810	1.209
6	4.017	2.813	1.204
7	4.016	2.811	1.205
8	4.017	2.811	1.206
9	4.015	2.811	1.204
10	4.015	2.813	1.202
		Mean	1.205
		σ_{sample}	0.002

The horizontal field of view length is found empirically to be $1.205mm$. The vertical field of view length is calculated using the sensor camera size (1200x1600 pixels).

$$FOV_{vertical} = FOV_{horizontal} * camera\,size = 1.205mm * \frac{1200}{1600}\left(\frac{pixels}{pixels}\right)$$

$$= 0.900mm$$

$$1\,pixel = 0.3\mu m\,wide$$

$$Error = (+/- 0.15\mu m)$$

Thus the field of view at 4x magnification is $900\mu m$ by $1210\mu m$, or $1.09 * 10^6 \mu m^2$.

0.9.1.2 Determination of Field of View for 10x Objective Lens

Field of view for 10x objective lens

Trial	X_i [mm]	X_f [mm]	ΔX [mm]
1	3.753	3.283	0.470
2	3.754	3.283	0.471
3	3.753	3.283	0.470
4	3.754	3.283	0.471
5	3.754	3.282	0.472
6	3.754	3.282	0.472
7	3.754	3.283	0.471
8	3.754	3.282	0.472
9	3.755	3.283	0.472
10	3.752	3.283	0.469
		Mean	0.471
		σ_{sample}	0.001

The horizontal field of view length is found empirically to be $0.471mm$. The vertical field of view length is calculated using the sensor camera size (1200x1600 pixels).

$$FOV_{vertical} = FOV_{horizontal} * camera\,size = 0.471mm * \frac{1200}{1600}\left(\frac{pixels}{pixels}\right)$$

$$= 0.350mm$$

$$1\,pixel = 0.12\mu m\,wide$$

$$Error = (+/- 0.06\mu m)$$

Thus the field of view at 10x magnification is $350\mu m$ by $470\mu m$, or $1.7 * 10^5 \mu m^2$.

0.9.1.3 Determination of Field of View for 40x Objective Lens

Field of view for 40x objective lens

Trial	X_i [mm]	X_f [mm]	ΔX [mm]
1	6.353	6.240	0.113
2	6.353	6.237	0.116
3	6.351	6.237	0.114
4	6.351	6.236	0.115
5	6.35	6.238	0.112
6	6.351	6.237	0.114
7	6.349	6.238	0.111
8	6.351	6.237	0.114
9	6.35	6.237	0.113
10	6.35	6.236	0.114
		Mean	0.114
		σ_{sample}	0.001

$$FOV_{vertical} = FOV_{horizontal} * camera\,size = 0.114mm * \frac{1200}{1600}\left(\frac{pixels}{pixels}\right)$$

$$= 0.09mm$$

$$1\,pixel = 0.03\mu m\,wide$$

$$Error = (+/- 0.015\mu m)$$

Thus the field of view at 40x magnification is $90\mu m$ by $110\mu m$, or $10.0 * 10^3 \mu m^2$.

The length of each magnification is quickly compared to their respective field of view lengths to further validate the measurements.

$$\frac{FOV_{V4x}}{FOV_{V10x}} = \frac{10x}{4x}$$

$$\frac{900}{350} = 2.6$$

$$\frac{10}{4} = 2.5$$

That is approximately equal.

$$\frac{FOV_{V10x}}{FOV_{V40x}} = \frac{40x}{10x}$$
$$\frac{350}{90} = 3.9$$
$$\frac{40}{10} = 4.0$$

That is approximately equal.

$$\frac{FOV_{V4x}}{FOV_{V40x}} = \frac{40x}{4x}$$
$$\frac{900}{90} = 10$$
$$\frac{40}{4} = 10$$

In conclusion, the field of view for each magnification has been determined empirically.

Objective: To determine if the machine has sub micrometer repeatability over the length of the diameter of a small diffusion chamber over a distance of 100μm in the X axis.

The specific sub program to translate the X axis a total of $75\mu m$ is presented below. The feed factor of 11 is to add $11\mu s$ to each microstep period resulting in a feed rate of approximately $0.1mm$ per second. Printing the step count is executed to validate that the appropriate number of steps have been counted.

```
else if (operation[0] == 6 && operation[1] == NULL) {
  Serial.print(optics_x_stepcount);
  feed_factor = 11;
  optics_x(5120, 1);
  Serial.print(optics_x_stepcount);
  optics_x(5120, -1);
```

```
  operation[0] = 2;
  Serial.print(optics_x_stepcount);
}
```

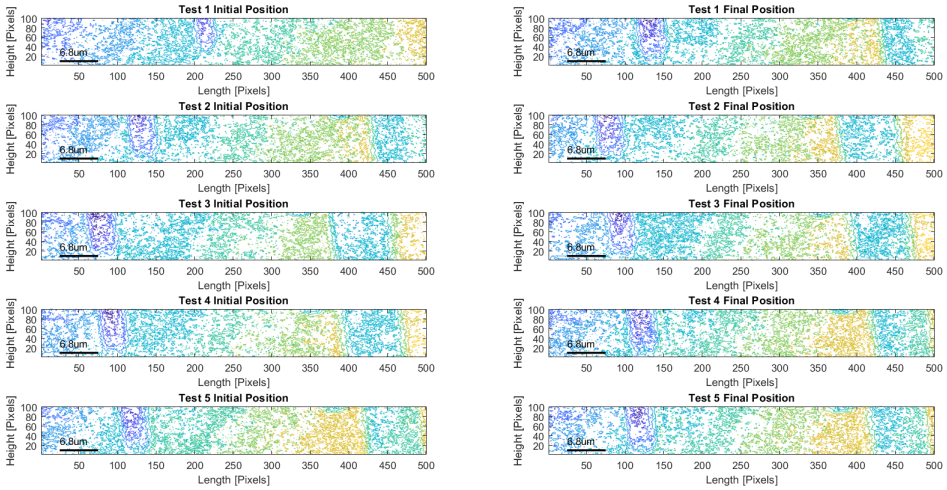

Figure 72: The positioning repeatability of tests 6 through 10. The purple region indicates the filament of apple core and is the reference object.

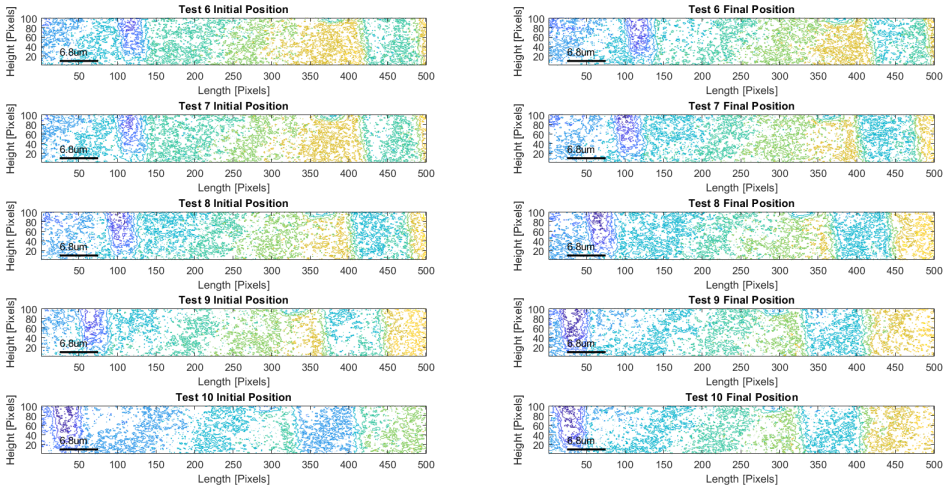

Figure 73: The positioning repeatability of tests 1 through 5. The purple region indicates the filament of apple core and is the reference object.

The only tests that appear to be anywhere near sub micrometer repeatable are test 5, 6, and 10.

What may be occurring is that the stepper motor may not be producing enough torque due to the very fine microstep settings. During the test presented above the motors were programmed to have a supply of $350mA$. This could be increased up to $500mA$ per phase. Thus to observe the effects of greater current and thus greater torque output (and ultimately more heat generation), a test was performed with $500mA$ being supplied to the motors.

The feature changed due to a repositioning of the slide.

The same sub program from the previous test is implemented.

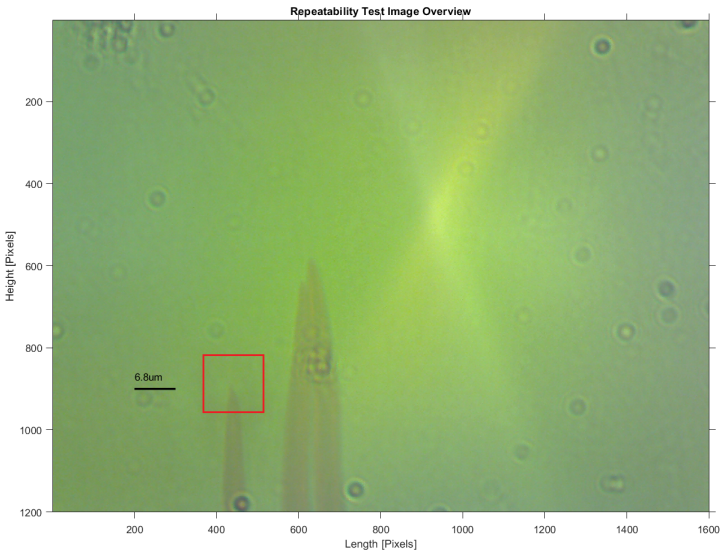

Figure 74: The setup for the second repeatability test in the X axis over a total travel distance of 75μm. The box in the red indicates the area of interest for subsequent figures.

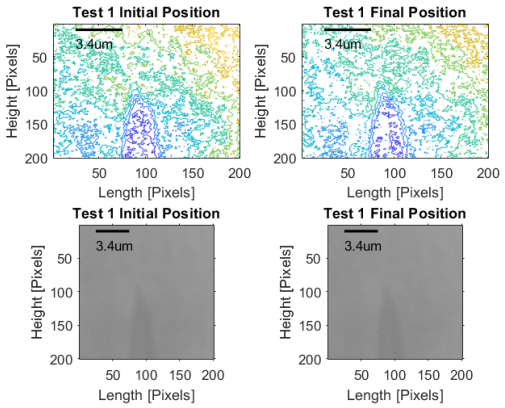

Figure 75: Repeatability Test 2 Trial 1

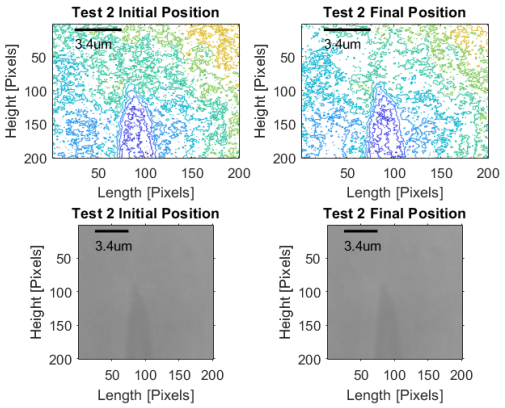

Figure 76: Repeatability Test 2 Trial 2

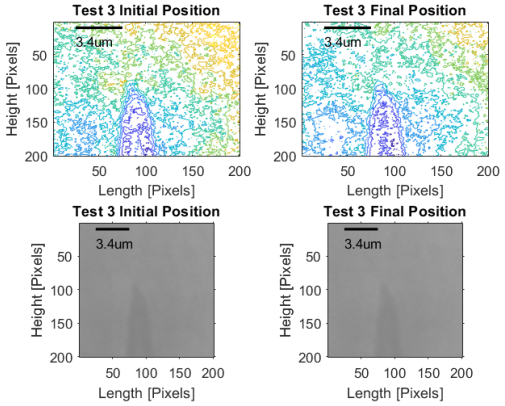

Figure 77: Repeatability Test 2 Trial 3

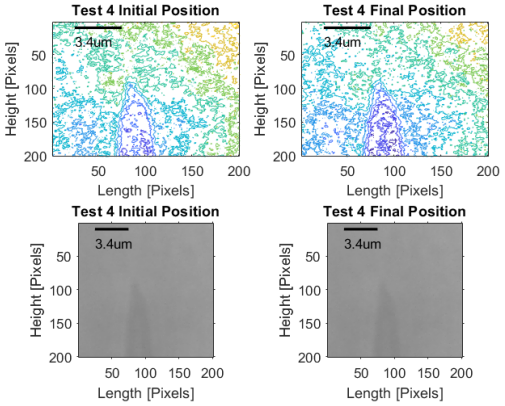

Figure 78: Repeatability Test 2 Trial 4

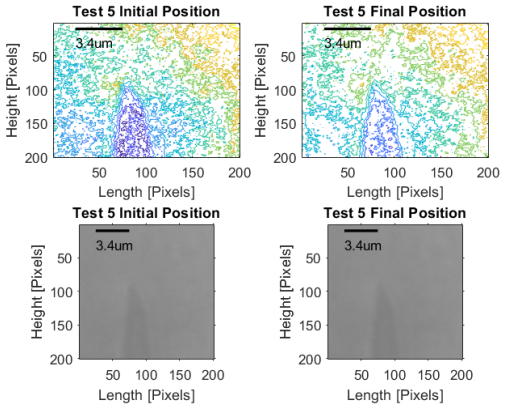

Figure 79: Repeatability Test 2 Trial 5

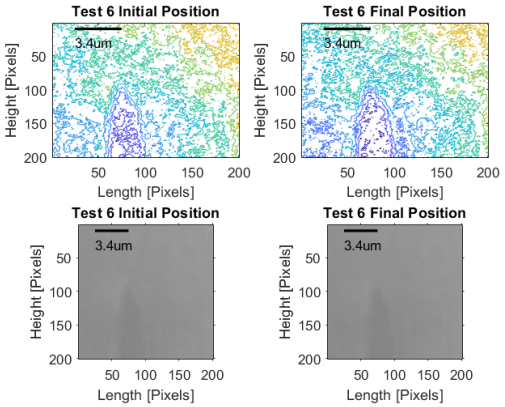

Figure 80: Repeatability Test 2 Trial 6

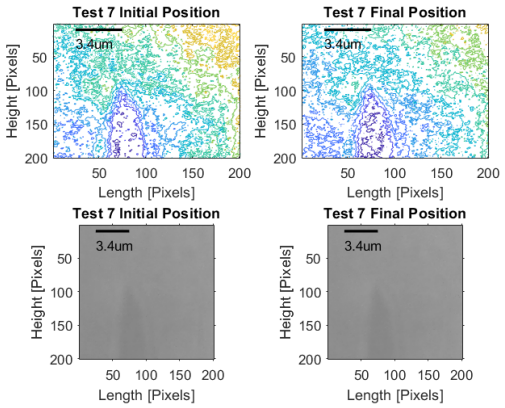

Figure 81: Repeatability Test 2 Trial 7

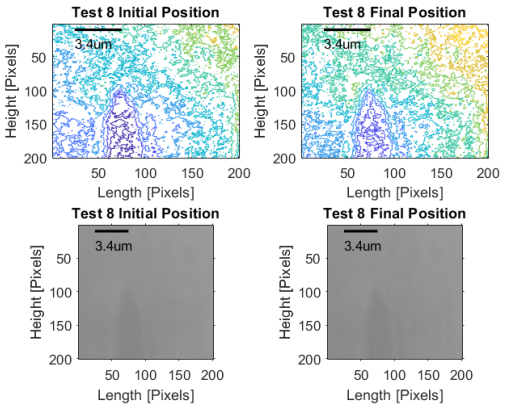

Figure 82: Repeatability Test 2 Trial 8

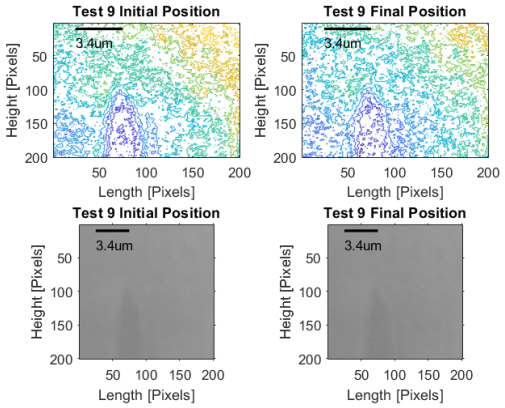

Figure 83: Repeatability Test 2 Trial 9

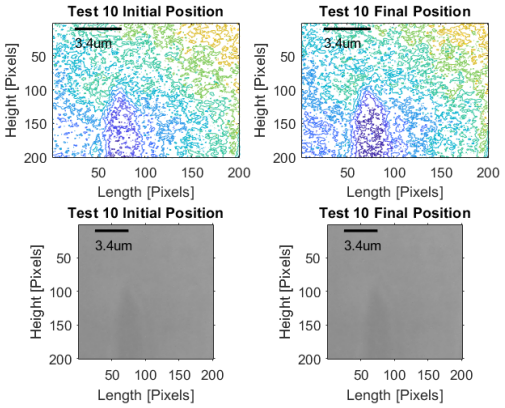

Figure 84: Repeatability Test 2 Trial 10

It becomes quite apparent that the improvement is substantial. Each of the images could easily overlap each other within a tolerance of 1μm.

With the effect of increasing the current to the motors validated with test 2, a test was conducted to validate the repeatability in the Y axis of the optics stage. The specific sub program to translate the Y axis a total of $75\mu m$ is presented below. The feed factor of 11 is to add $11\mu s$ to each microstep period resulting in a feed rate of approximately $0.1mm$ per second. Printing the step count is executed to validate that the appropriate number of steps have been counted.

```
else if (operation[0] == 6 && operation[1] == NULL) {
  Serial.print(optics_y_stepcount);
  feed_factor = 11;
  optics_y(5120, 1);
  Serial.print(optics_y_stepcount);
  optics_y(5120, -1);
  operation[0] = 2;
  Serial.print(optics_y_stepcount);
}
```

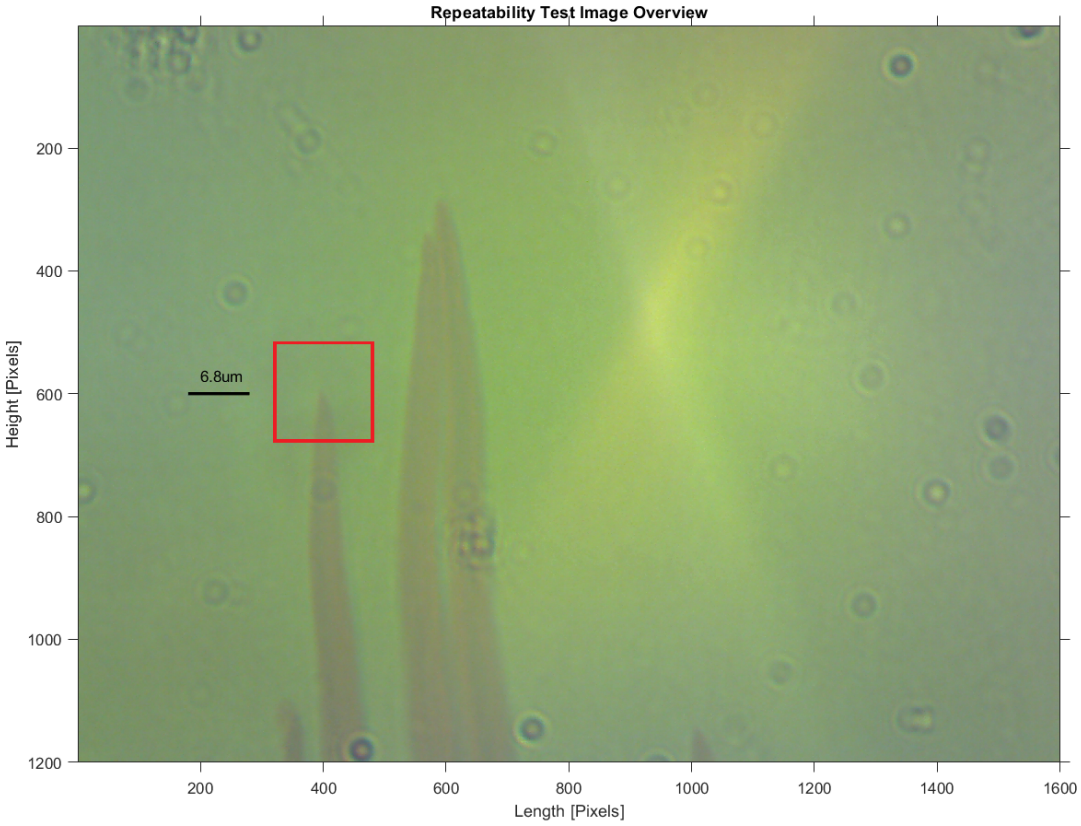

Figure 85: The setup for the second repeatability test in the Y axis over a total travel distance of 75μm. The box in the red indicates the area of interest for subsequent figures.

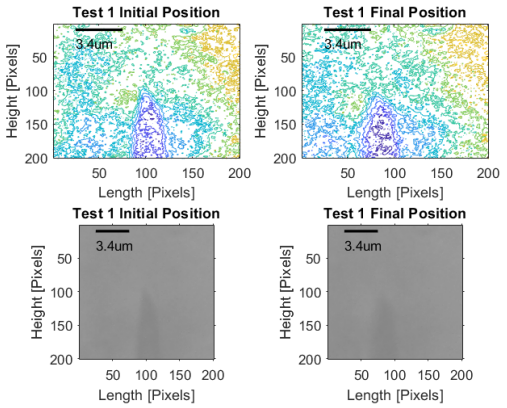

Figure 86: Repeatability Test 3 Trial 1

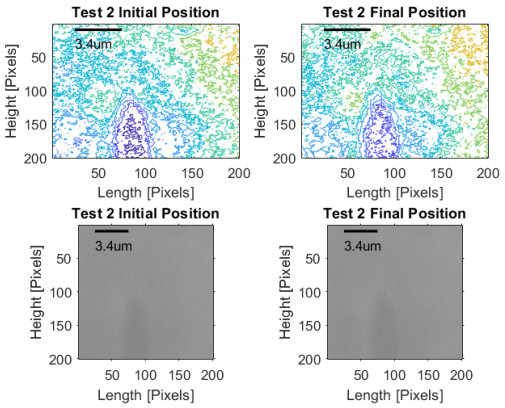

Figure 87: Repeatability Test 3 Trial 2

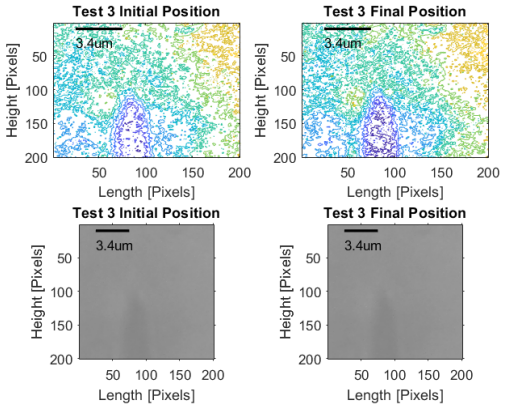

Figure 88: Repeatability Test 3 Trial 3

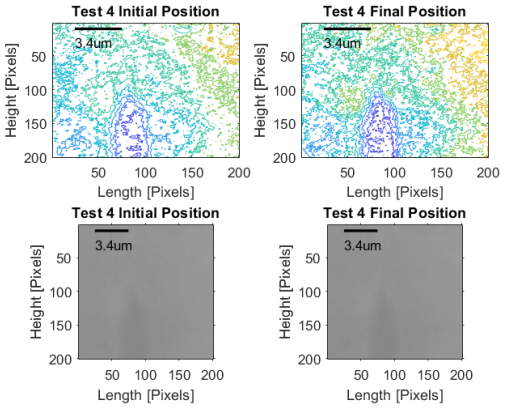

Figure 89: Repeatability Test 3 Trial 4

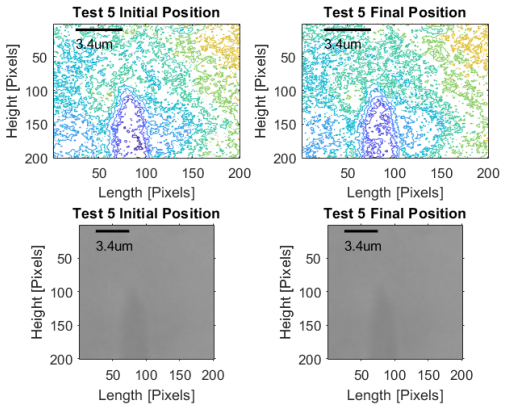

Figure 90: Repeatability Test 3 Trial 5

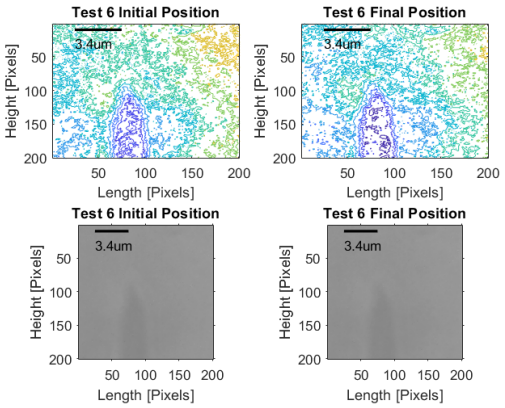

Figure 91: Repeatability Test 3 Trial 6

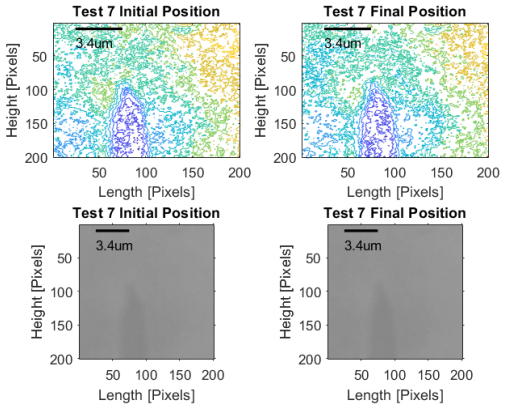

Figure 92: Repeatability Test 3 Trial 7

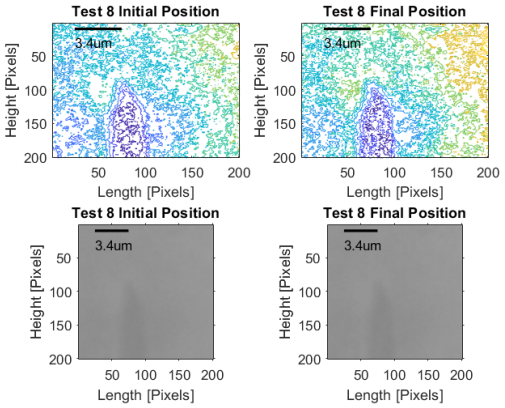

Figure 93: Repeatability Test 3 Trial 8

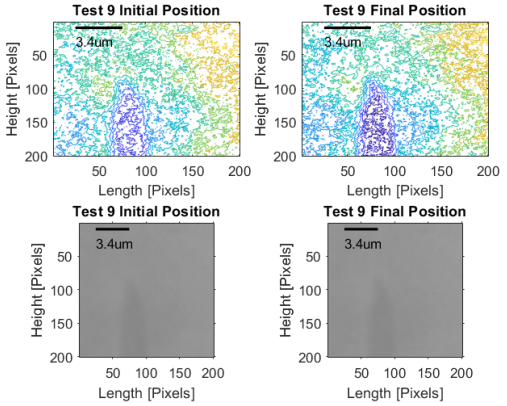

Figure 94: Repeatability Test 3 Trial 9

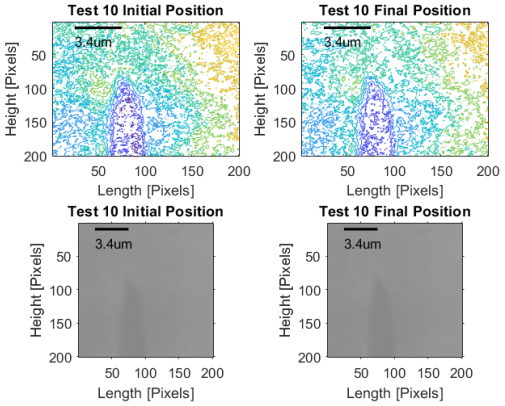

Figure 95: Repeatability Test 3 Trial 10

Again, it becomes quite apparent that the improvement is substantial. Each of the images could easily overlap each other within a tolerance of 1μm.

0.9.1.4 Linear Repeatability in Optics Stage X Axis

A more comprehensive test was then conducted to quantify the repeatability of the X and Y axis of the optics stage over a longer distance. Objective: To quantify the repeatability of translation in the X axis of the optics stage independently over a total travel distance of 200μm.

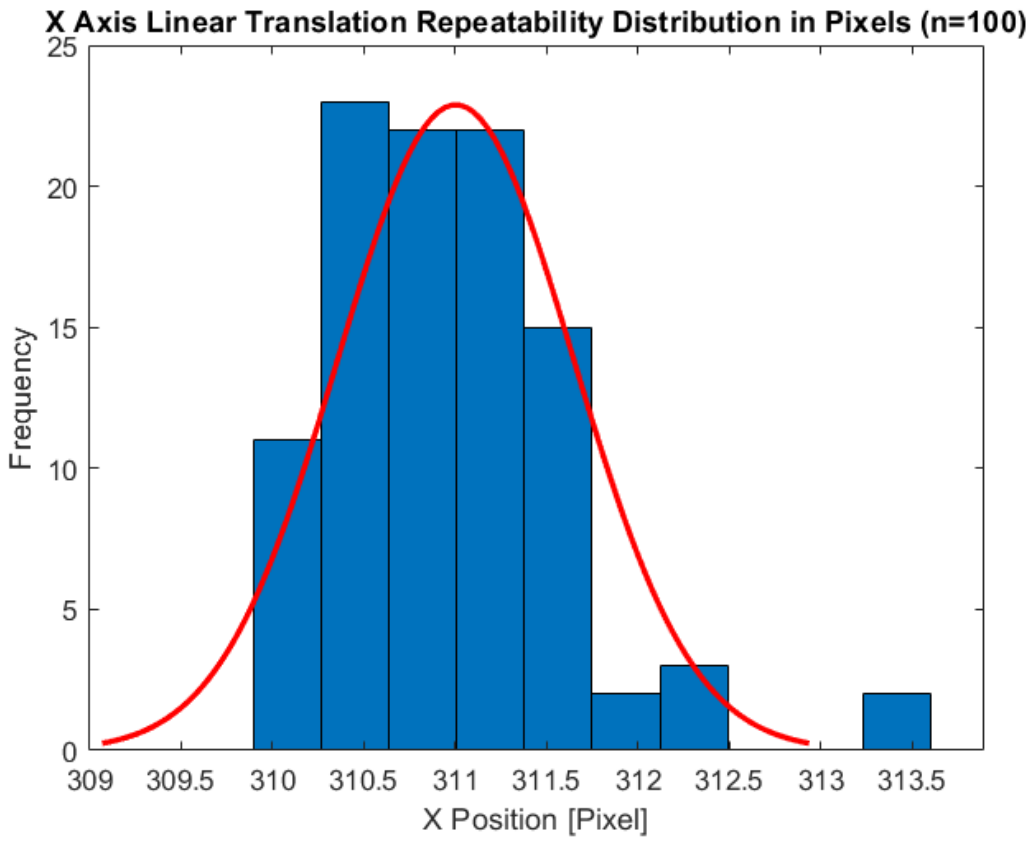

Figure 96: The position of the centroid of the feature in terms of pixel coordinates.

The pixel coordinates were then converted into micrometers based on the field of view of the 10x objective lens.

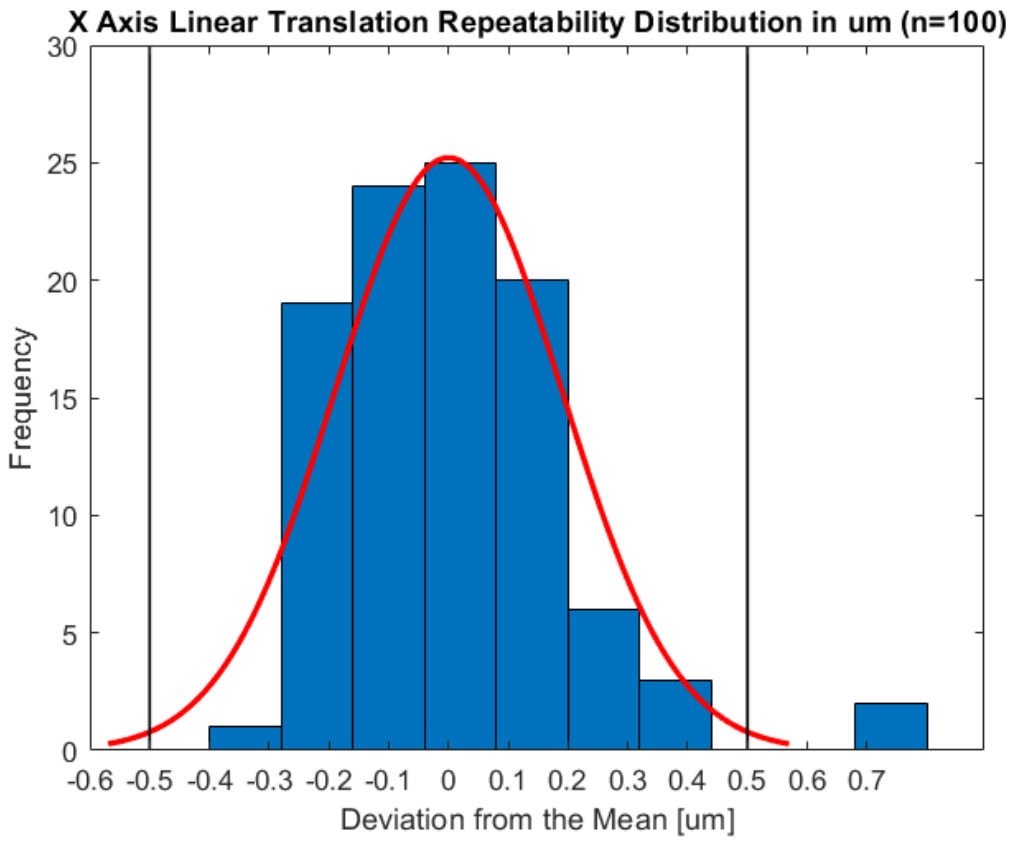

Figure 97: The position of the centroid of the feature in terms of um about the mean.

The distribution of the 100 samples were then plotted to determine how many samples fell within a micrometer.

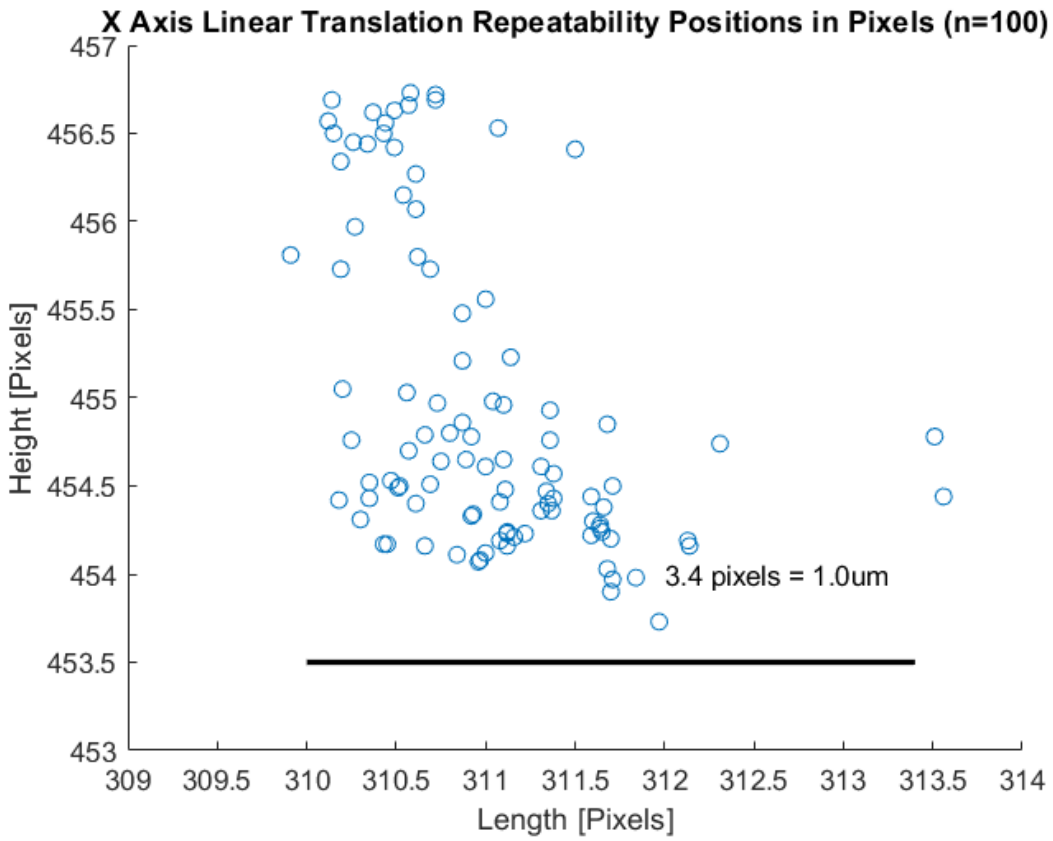

Figure 98: The distribution of the height coordinates in pixels for the centroid of each sampled feature.

The pixel coordinates were then converted into micrometers based on the field of view of the 10x objective lens.

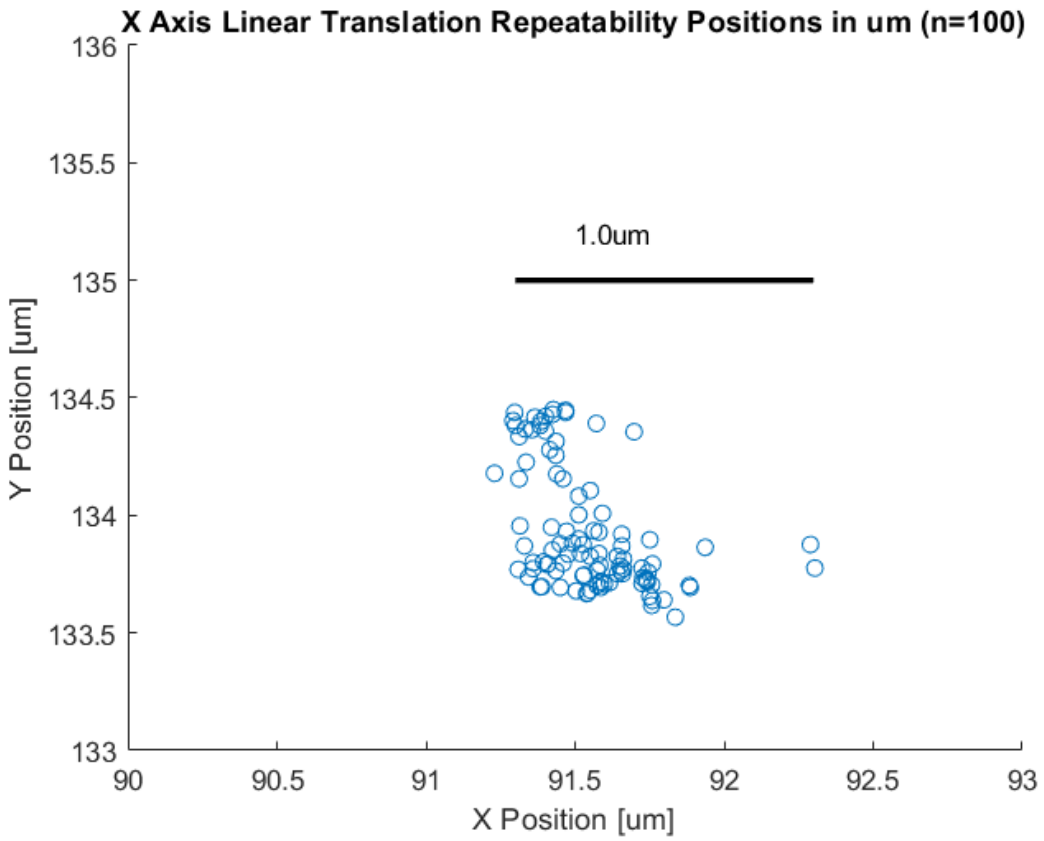

Figure 99: The distribution of the height coordinates in micrometers for the centroid of each sampled feature.

$$4\sigma = 0.76\mu m\,(+/-0.15\mu m)$$

$$6\sigma = 1.14\mu m\,(+/-0.15\mu m)$$

0.9.1.5 Linear Repeatability in Optics Stage Y Axis

Objective: To quantify the repeatability of translation in the Y axis of the optics stage independently over a total travel distance of $200\mu m$.

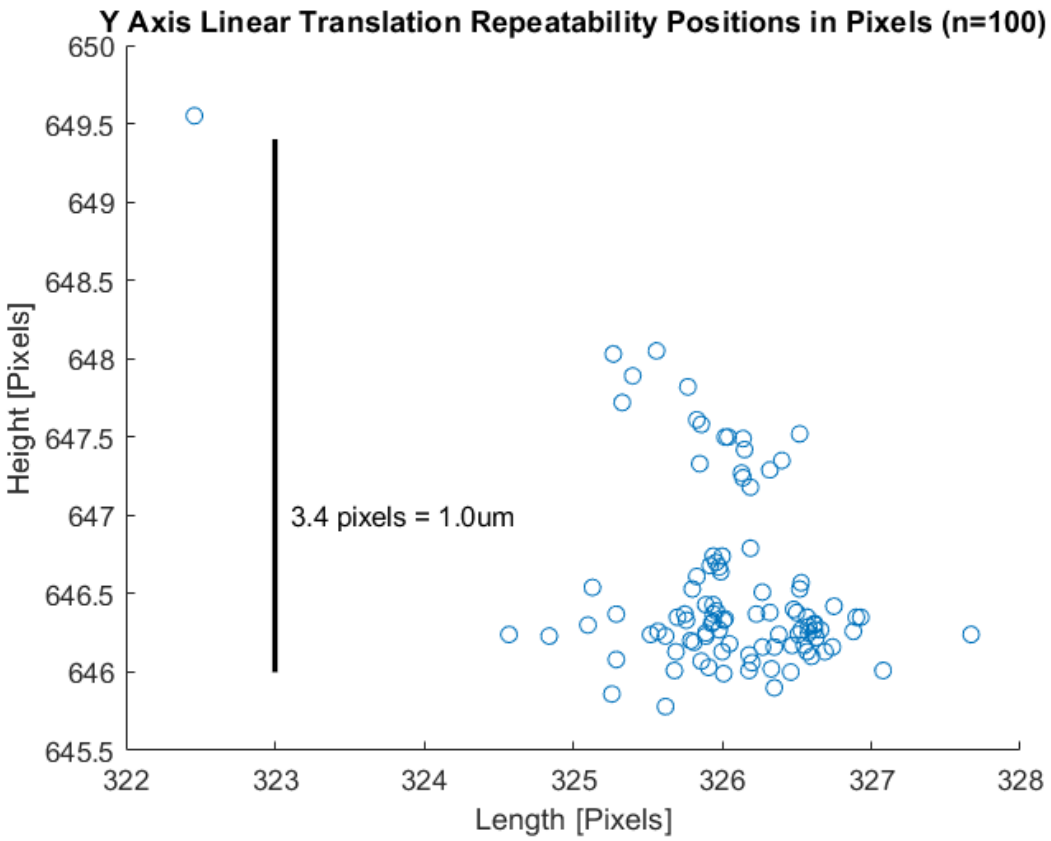

Figure 100: The position of the centroid of the feature in terms of pixel coordinates.

The pixel coordinates were then converted into micrometers based on the field of view of the 10x objective lens.

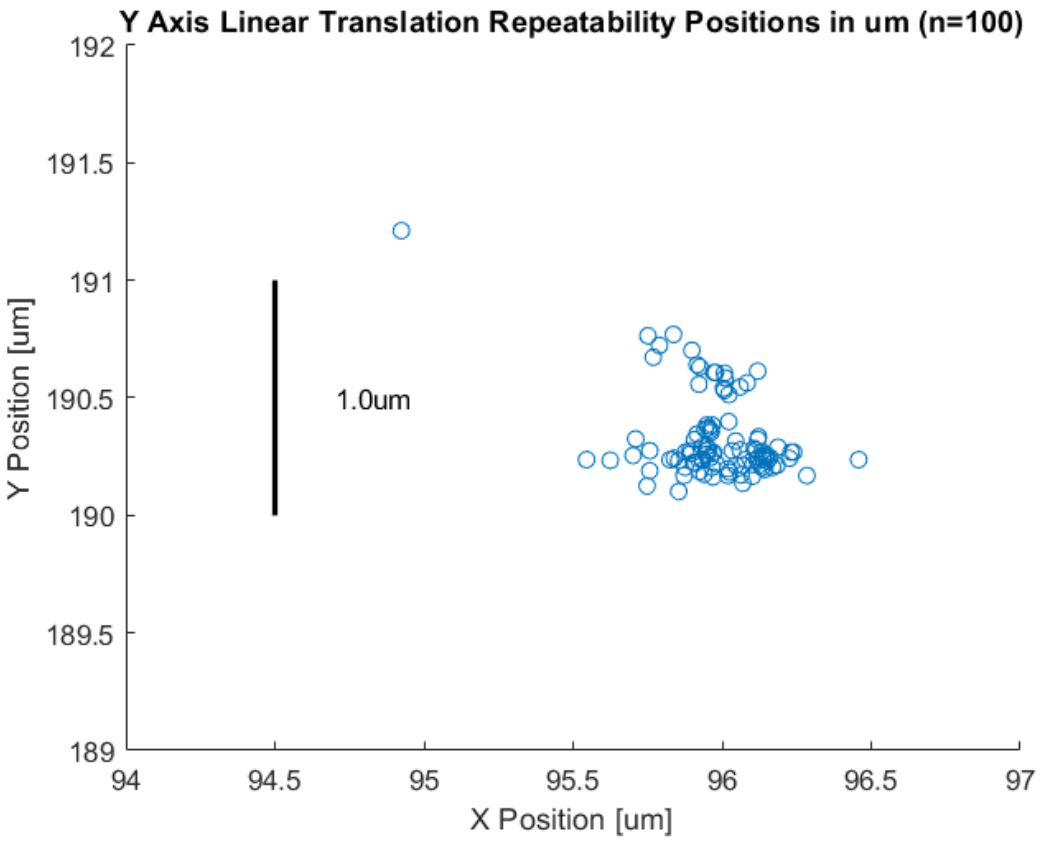

Figure 101: The position of the centroid of the feature in terms of um.

The distribution of the 100 samples were then plotted to determine how many samples fell within a micrometer.

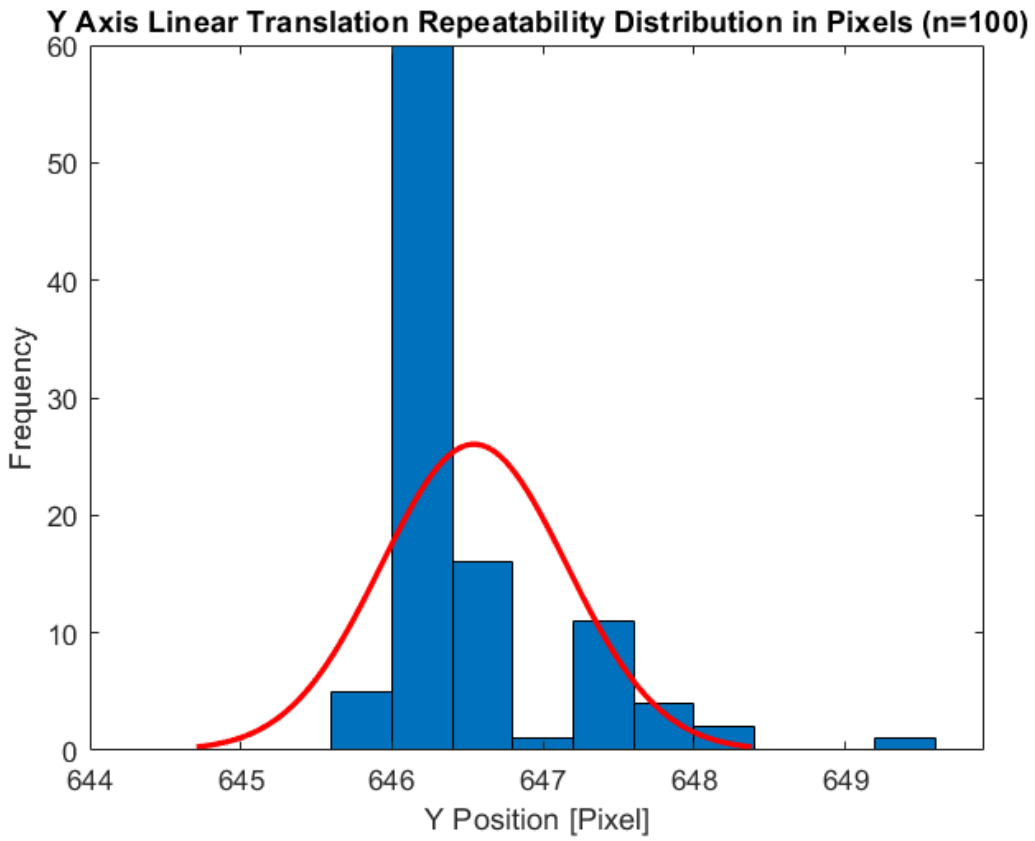

Figure 102: The distribution of the height coordinates in pixels for the centroid of each sampled feature.

The pixel coordinates were then converted into micrometers based on the field of view of the 10x objective lens.

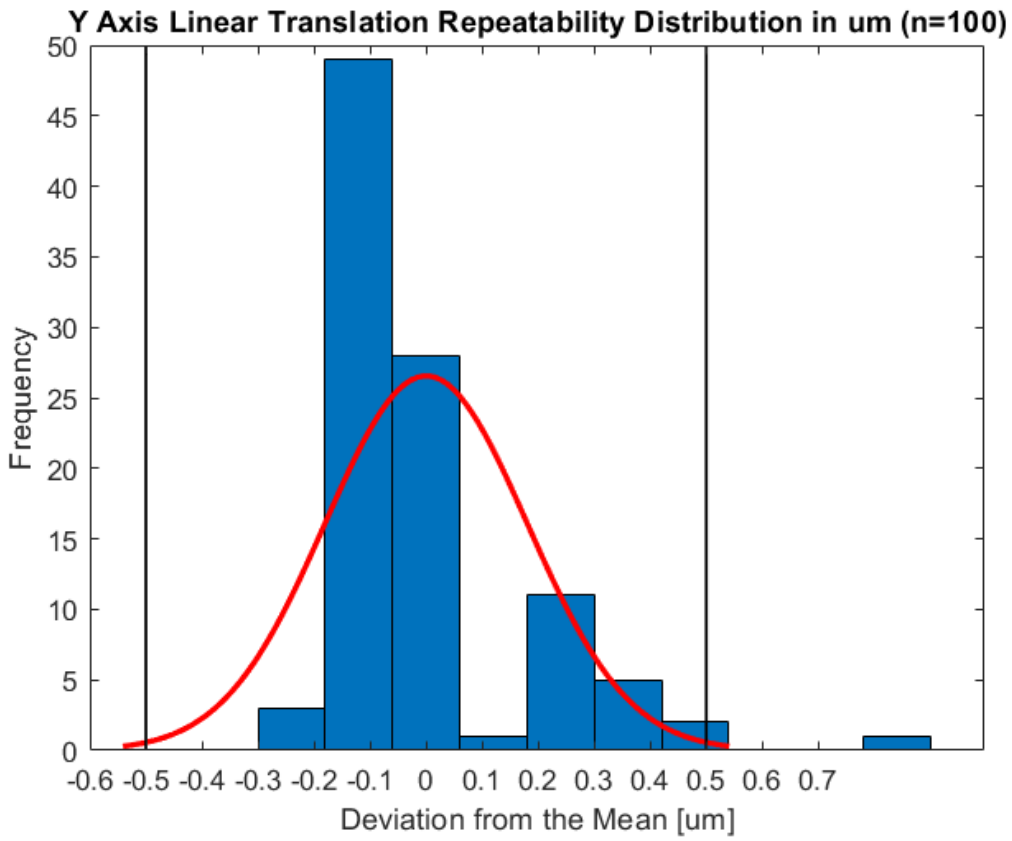

Figure 103: The distribution of the height coordinates in micrometers for the centroid of each sampled feature.

$$4\sigma = 0.72\mu m\,(+/-0.15\mu m)$$

$$6\sigma = 1.08\mu m\,(+/-0.15\mu m)$$

0.9.1.6 Emulated Ballbar Test

Objective: To quantify the repeatability of motion in both X and Y axis of the optics stage in an elliptical path.

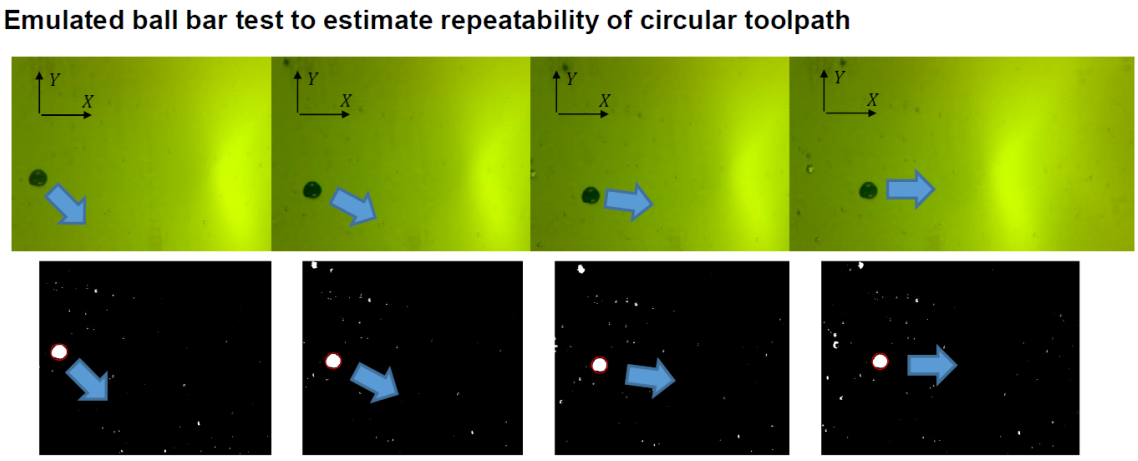

Figure 104: Repeatability after converting to binary image and detecting the large area object. The centroid is then calculated and the coordinates recorded as the position.

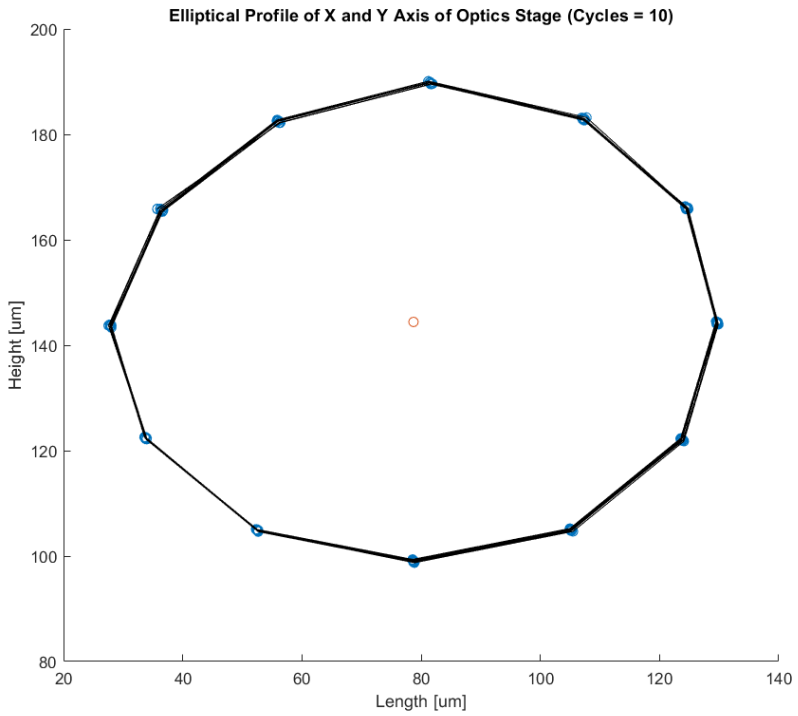

Figure 105: An emulated ballbar test was conducted to reveal the repeatability and accuracy of the optics stage.

$$\text{Max radius deviation} = 51.2\mu m\,(+/-0.15\mu m)$$
$$\text{Min radius deviation} = 43.9\mu m\,(+/-0.15\mu m)$$

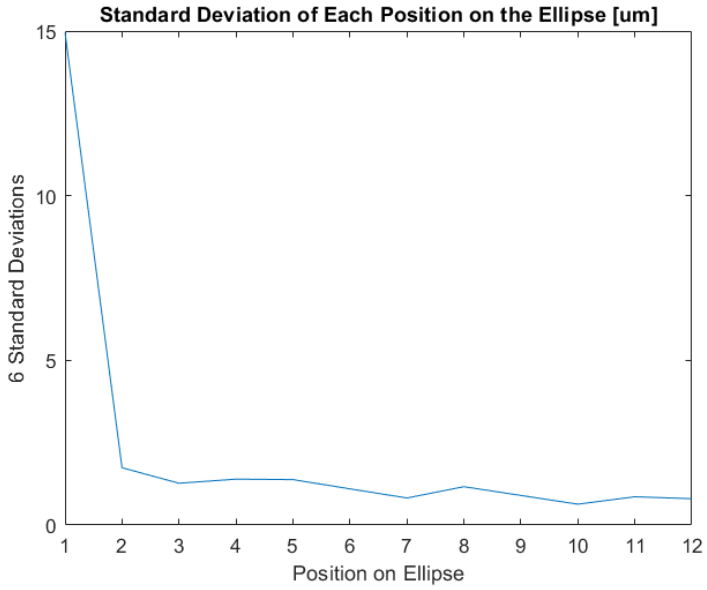

Figure 106: Standard deviation at each point on the ellipse.

$$1\sigma < 2\mu m$$

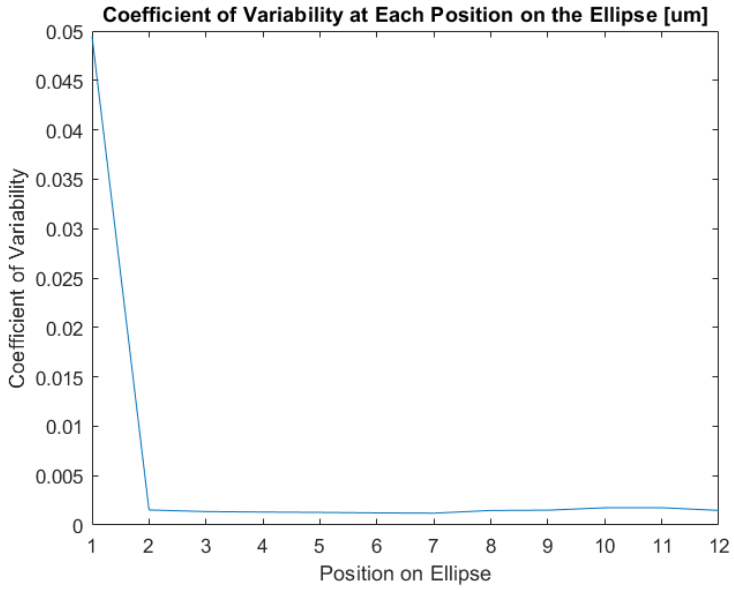

Figure 107: The coefficient of variability at each point. The variability remains constant after the first position validating the consistent repeatability as a function of distance over the travel range.

$$CV = \frac{\sigma}{\mu} \approx constant$$

$$CV \approx 0.2\, percent$$

The error in proportion to the mean travel distance is small.

0.9.2 Separation Process Characteristics

Cutting Beam Properties Objective: To determine how beam diameter varies as a function of Z position and laser duration. This is important since it will give insight on how thick a workpiece can be machined.

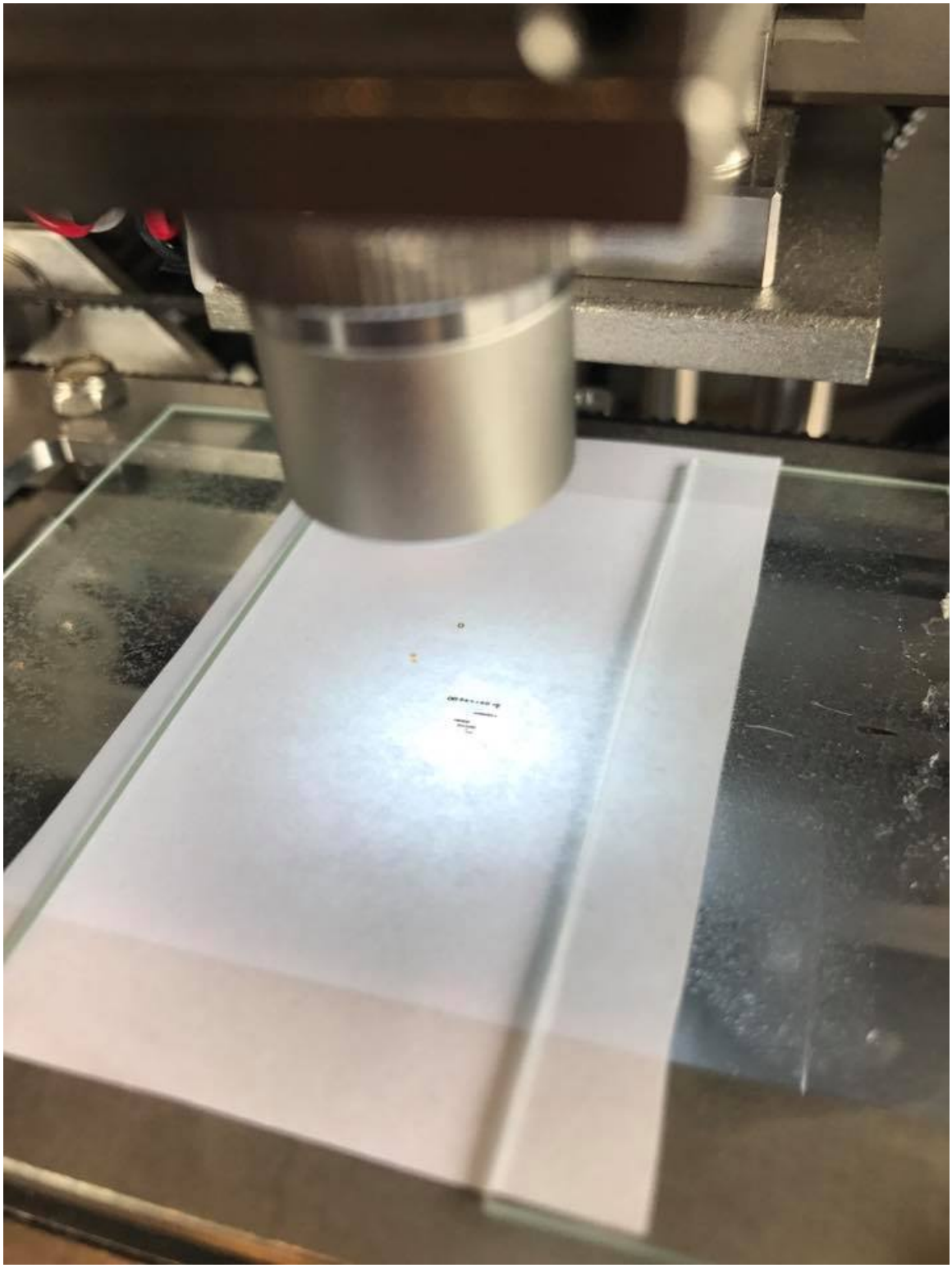

Figure 108: The setup for the beam diameter testing.

Figure 109: The cut holes varying in diameter as a function of Z position. The center hole with the smallest diameter represents the Z position most likely near the focal point of the objective lens.

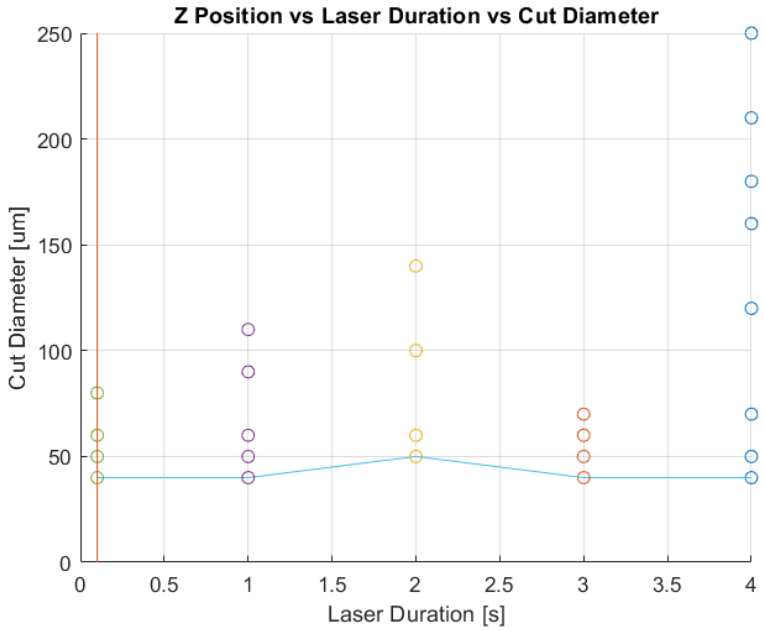

Figure 110: The laser duration versus the cut diameter. A minimum value can be observed.

For the material paper, there seems to be no effect of shortened laser duration on the minimum diameter of the cut.

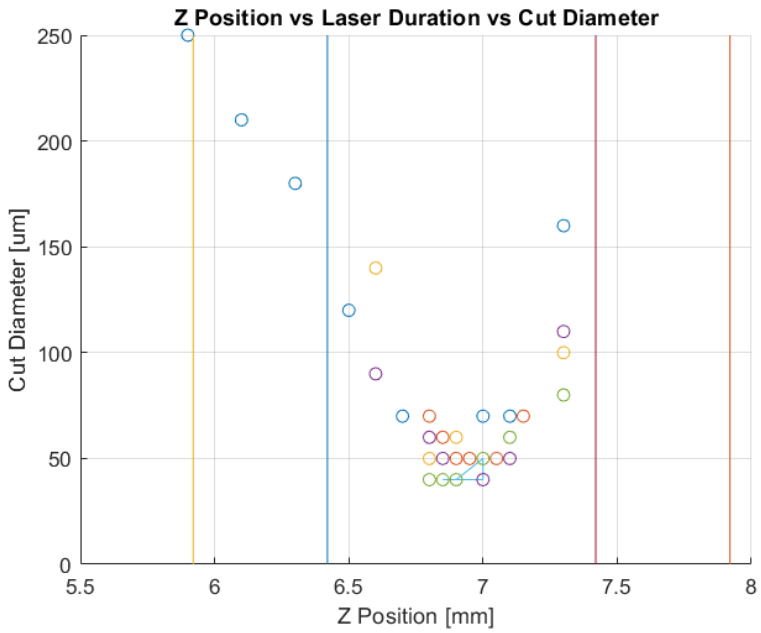

Figure 111: The Z position versus the cut diameter. A minimum cut diameter can be observed at just under a Z position of $7mm$. The profile of the laser can be observed by the increasing diameter. The vertical lines represent a material thickness of $1mm$ and $2mm$ with the center based on the mean of the Z positions that the minimum diameters occur at.

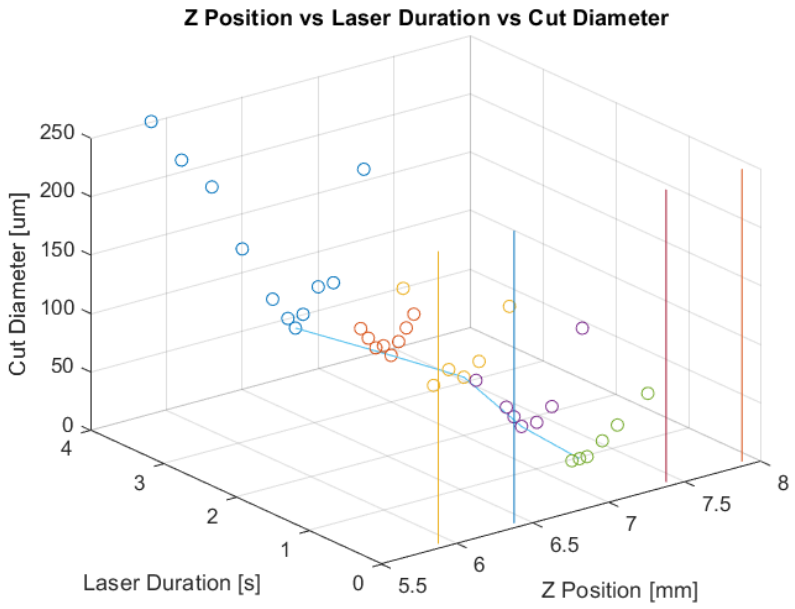

Figure 112: A 3D scatter plot of the 3 variables. A minimum cut diameter can be observed snaking just under $7mm$ in the Z position as well as the repeating shape of the change in diameter was a function of Z.

The conclusion of the cutting beam property experiment is that the focal length of the objective lens is likely not long enough to prevent a large valley from being cut into the work material. At 1mm thickness the largest kerf width (closest to the surface of the workpiece) is expected to be around 160μ m. At $2mm$ thickness the largest kerf width (closest to the surface of the workpiece) is expected to be at around $250\mu m$.

The conclusion is that a narrow kerf width on the order of that needed in the engineering requirements ($1\mu m$) may not be possible with the current optical configuration. Additional modifications to the cutting process or optical setup need to be implemented.

0.9.3 Autonomous Separation

Machining the agar workpiece presented many challenges. The main difficulty is in maintaining water retention within the agar sample. In initial tests with Jello, the sample was very large in volume and greater in opacity. The larger volume may have had an effect of acting as a greater heat buffer. The greater opacity may have contributed to greater absorbance within the local area resulting in a quicker cut. In addition, during initial cuts the full 2 watts of the laser output was utilized in comparison to the laser beam that is first filtered with the dichroic mirror and then the objective lens. In summary, there appears to be challenges with managing the heat transfer within the agar sample.

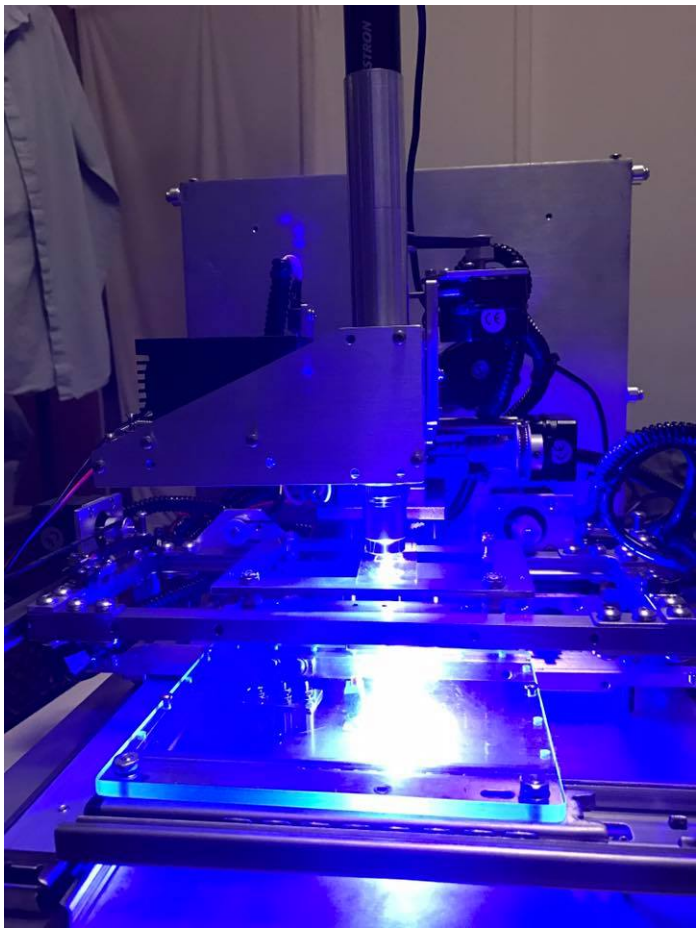

Figure 113: The setup for the autonomous separation tests.

The subsequent sample cuts can show the outcome of the machining process.

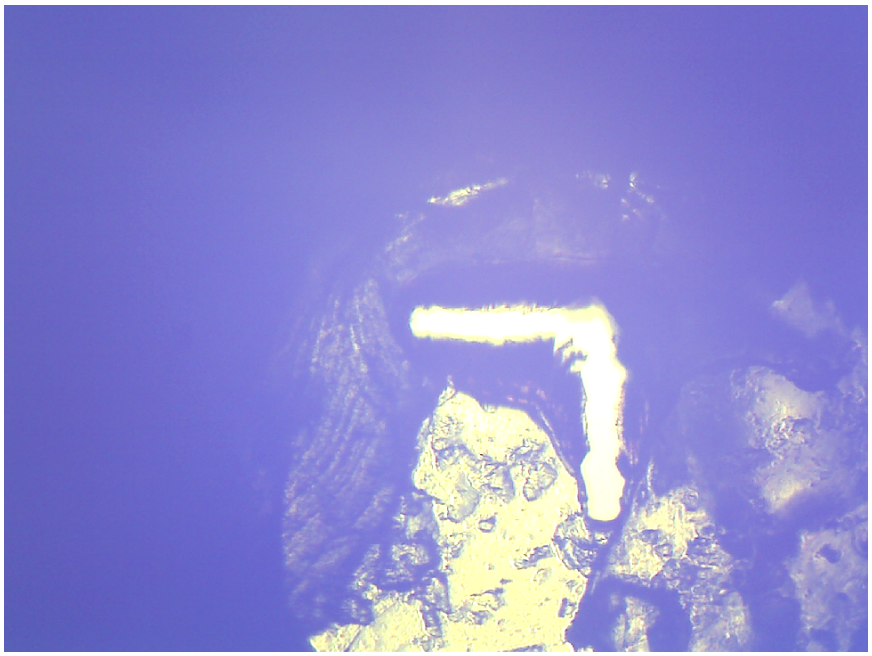

Figure 114: The first two cuts of a square profiled toolpath

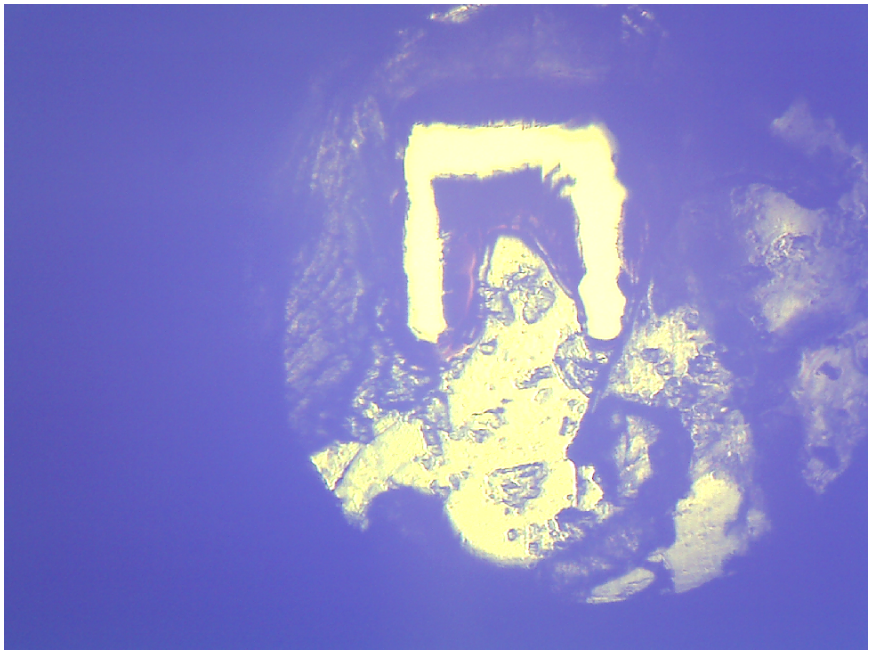

Figure 115: The first two cuts of a square profiled toolpath

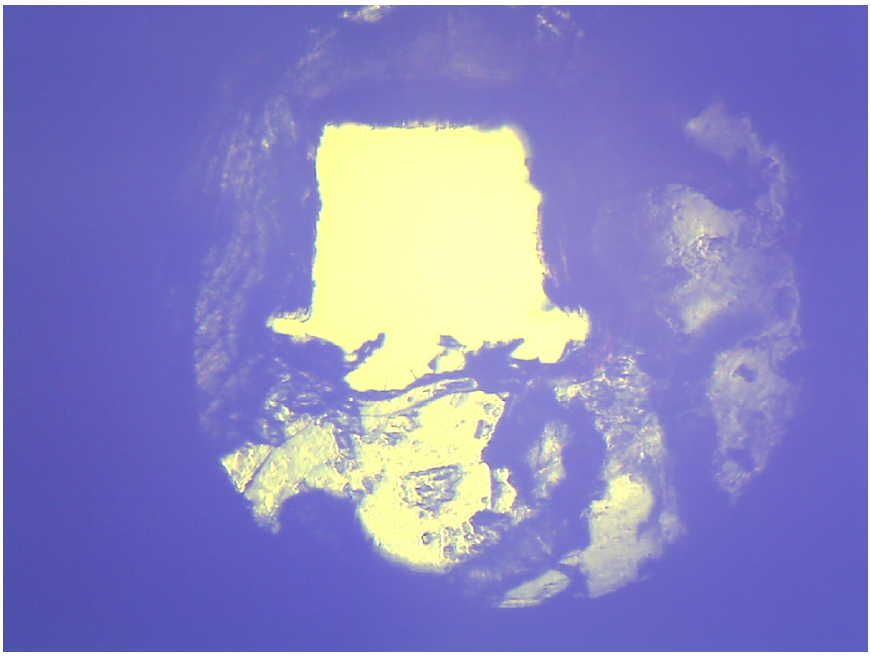

Figure 116: The finished cut.

The final cut is not very clean, but it does appear to have separated the sample. The kerf width however is very large.

Another test in agar clearly shows the sample contracting in size as water leaves the medium.

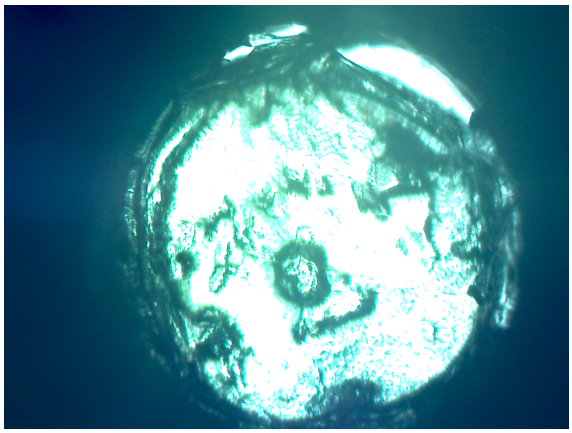

Figure 117: The sample before processing.

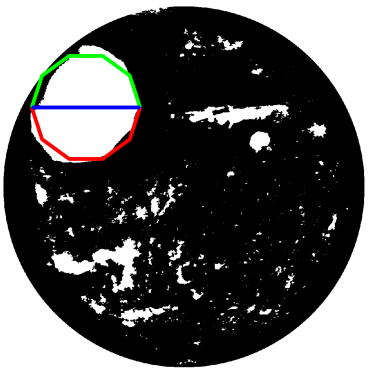

Figure 118: Generating the toolpath.

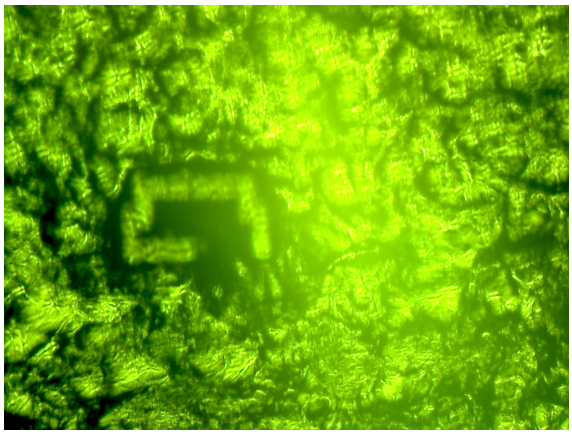

Figure 119: After the first toolpath. Already exterior contraction is visible and the cut width has expanded due to contraction.

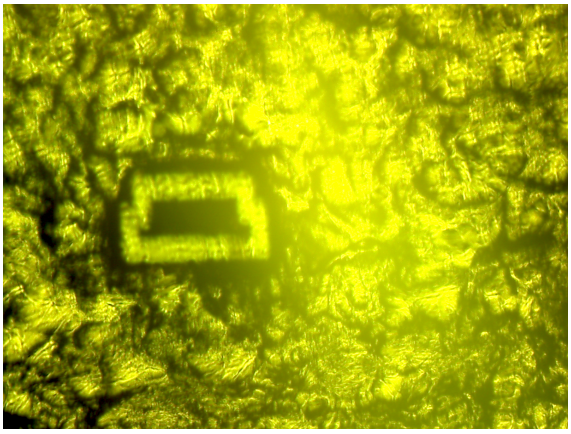

Figure 120: After the second pass of the first toolpath.

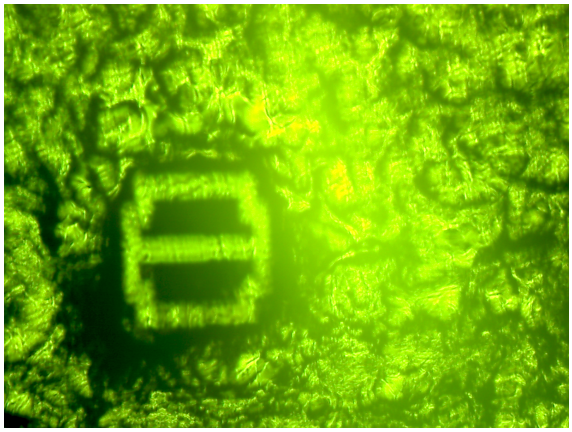

Figure 121: After the first pass of the second toolpath.

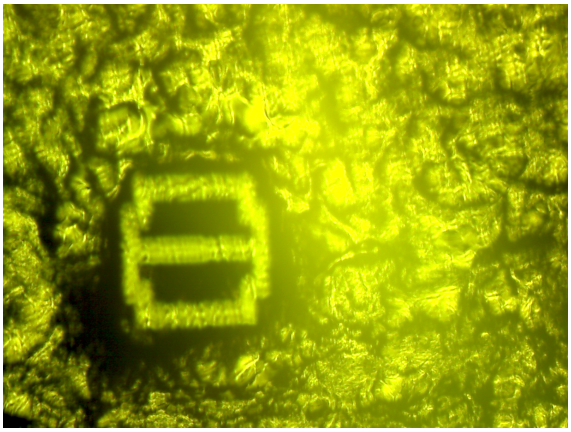

Figure 122: After the second pass of the second toolpath. The sample has greatly contracted.

To observe the toolpath in a medium other than agar housed in a diffusion chamber, a sample image of a diffusion chamber was processed to generate a toolpath. The cutting process was then performed on some dried agar that had formed a very thin layer on a glass slide.

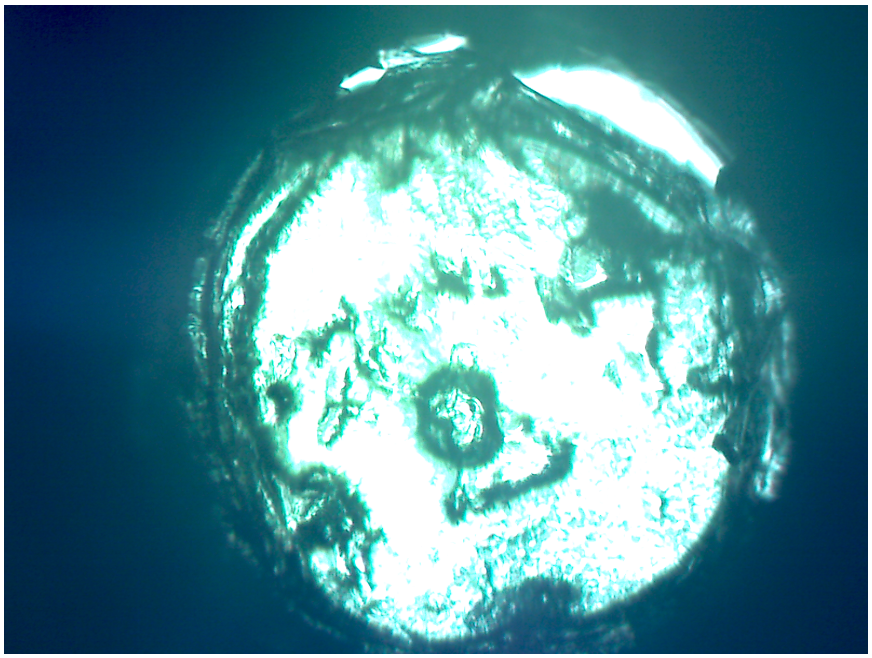

Figure 123: The initial workpiece before cutting.

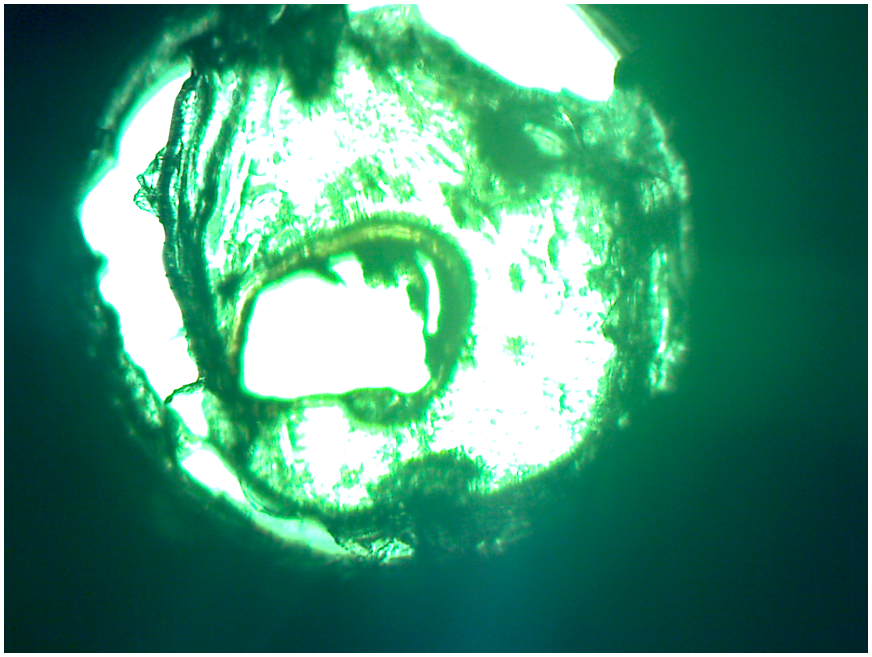

Figure 124: The workpiece mid cut.

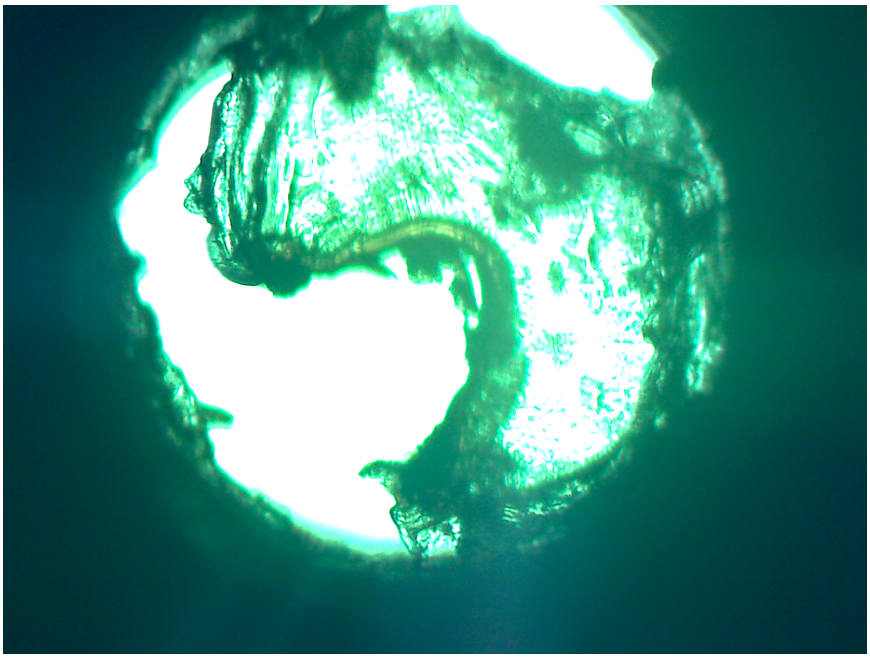

Figure 125: The finished cut.

With such a thin sample the medium directly under the laser beam is vaporized rapidly resulting in no medium to transmit heat to the surrounding material via conduction. What results is a much cleaner cut and a clear separation of two samples. This setup for cutting is similar to the proprietary slides that are utilized in the commercial laser microdissection units.

Finally, to observe the performance of the image processing and separation process of the system a simulated cut was performed in dry agar that was less than 1mm thick situated on a glass slide. A 4x objective lens was used.

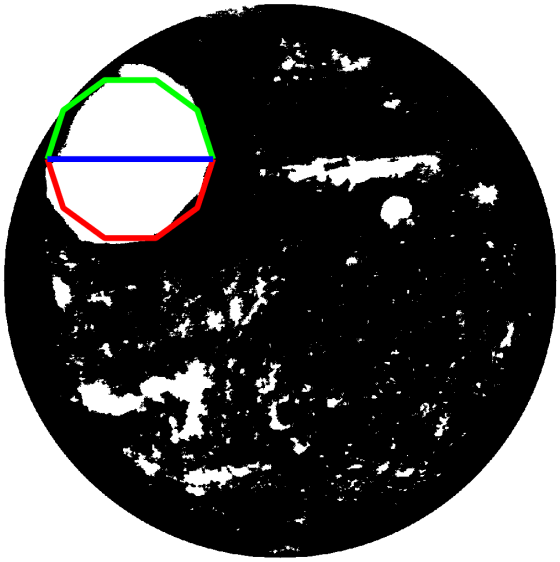

Figure 126: Toolpath generation on an example image

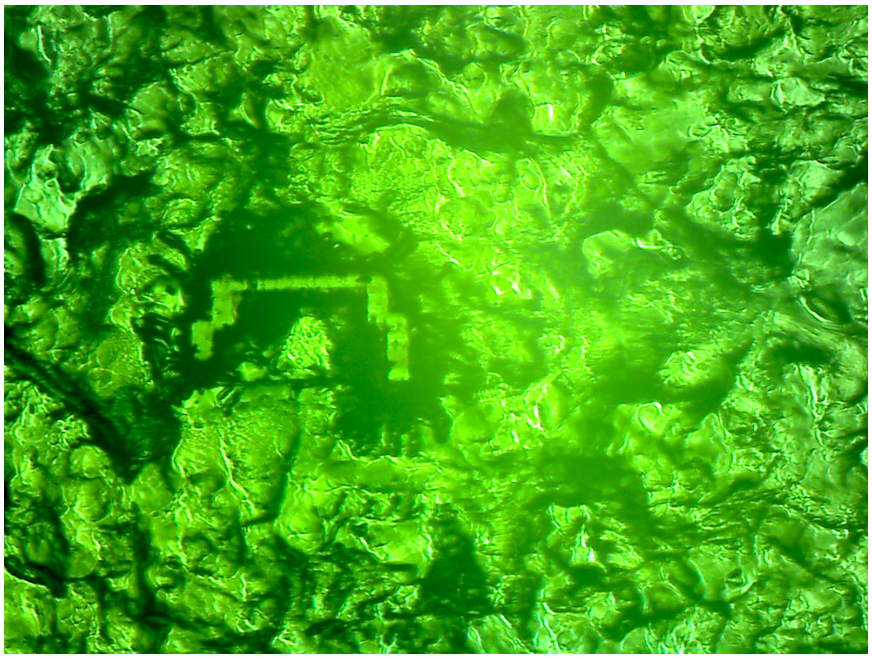

Figure 127: The first half of toolpath 1

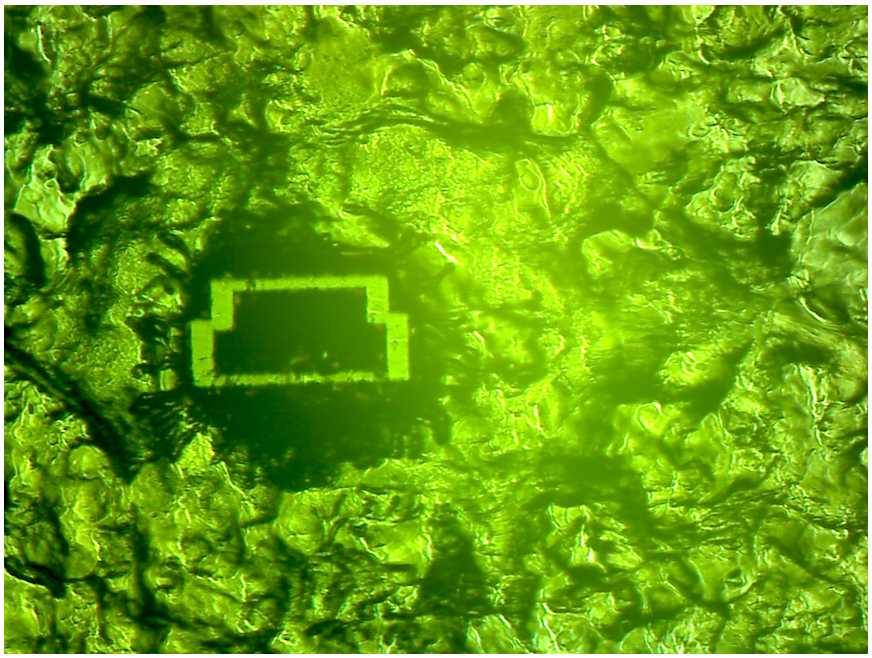

Figure 128: The second half of toolpath 1

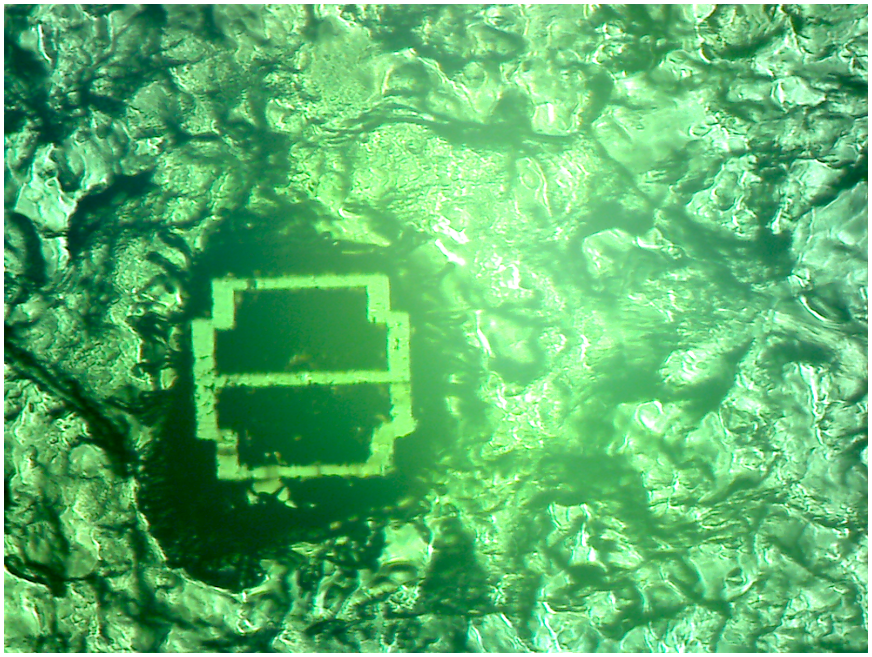

Figure 129: The first half of toolpath 2

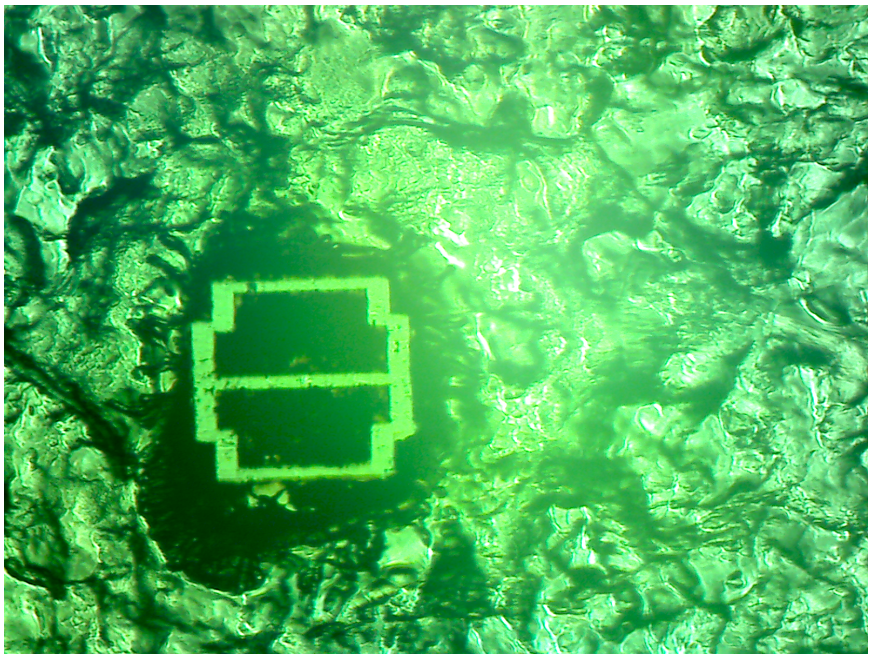

Figure 130: The second half of toolpath 2

The cut is situated on the lower left corner instead of the top left corner as a possible inversion when processed in Matlab.

In conclusion, the machine does successfully recognize an example sample and is capable of performing the required separation cut. Further work will be needed to calibrate the machine, develop the right cutting process (which involves finding the right machining process and improving the optics setup).

0.10 Conclusion

An inexpensive autonomous system with sub micrometer repeatability is realized in this thesis. The material cost to replicate the system is estimated at 4,000USD compared to 150,000USD commercial solutions. The actual material cost to produce the machine was lower by approximately 1,000USD since some components were sourced secondhand.

The engineering requirement of sub micrometer repeatability was validated through

two linear translation tests. Sub micrometer repeatability within the $100\mu m$ by $100\mu m$ work envelope was not accomplished however micrometer repeatability was achieved through the elliptical translation test. Size requirements were satisfied as well as the ability to easily reconfigure the machine to accommodate different size sample and capture vessels. Non destructive means of visualizing the samples was accomplished. Designing a machine to easily accommodate standard 22mm objective lenses were also accomplished.

Lastly the machine satisfied the requirement of autonomous processing of a sample in a diffusion chamber through identifying the best colony candidate with an image processing algorithm and generating a separation toolpath. Actual separation of samples was not achieved primarily due to time and monetary constraints.

Further work is needed to explore a low cost precision machining method to effectively separate colonies from the agar material.

0.11 Future Work

As mentioned in the conclusion, further work is needed to explore an effective machining method to separate bacteria colonies from the parent material. This could be achieved by designing an improved optics system perhaps utilizing a pulsed laser to reduce the amount of localized heat transfer within the parent material. A collimated beam is also likely to improve the cutting capabilities.

Lastly, lower cost stages could be substituted. In particular, the sample stage could be replaced with linear bearings reducing a majority of the 200 hours of machining as mentioned in the budget section. The stainless steel Newport stage could also be replaced with the more economical aluminum version as prior art did describe sub micrometer repeatability for a similar aluminum model. The system may need a few minutes upon start up to stabilize thermally due to heat generation from the actuators.

0.12 References

Bibliography

[1] *Nichols, D., Cahoon, N., Trakhtenberg, E. M., Pham, L., Mehta, A., Belanger, A., Epstein, S. S. (2010). Use of Ichip for High-Throughput In Situ Cultivation of "Uncultivable" Microbial Species. Applied and Environmental Microbiology, 76(8), 2445-2450. doi:10.1128/aem.01754-09*

[2] *Ling, L. L., Schneider, T., Peoples, A. J., Spoering, A. L., Engels, I., Conlon, B. P., . . . Lewis, K. (2015). A new antibiotic kills pathogens without detectable resistance. Nature, 517(7535), 455-459. doi:10.1038/nature14098*

[3] *Donofrio, A., Crawford, J. M., Stewart, E. J., Witt, K., Gavrish, E., Epstein, S., . . . Lewis, K. (2010). Siderophores from Neighboring Organisms Promote the Growth of Uncultured Bacteria. Chemistry & Biology, 17(3), 254-264. doi:10.1016/j.chembiol.2010.02.010*

[4] *Leica Microsystems Inc. (2018), Quotation for LMD6*

[5] *Schatz, A., Bugle, E., & Waksman, S. A. (1944). Streptomycin, a Substance Exhibiting Antibiotic Activity Against Gram-Positive and Gram-Negative Bacteria.* . Experimental Biology and Medicine, 55(1), 66-69. doi:10.3181/00379727-55-14461*

[6] *Epstein, A., 2016, Professor at Northeastern University, U.S., private communication*

[7] *Niyaz, Y., & Sägmüller, B. (2005). Non-contact laser microdissection and pressure catapulting: Automation via object-oriented image processing. Medical Laser Application, 20(3), 223-232. doi:10.1016/j.mla.2005.07.006*

[8] *Epstein, S. S. (2009). Microbial awakenings. Nature, 457(7233), 1083-1083. doi:10.1038/4571083a*

[9] *Staley, J. (1985). Measurement of In Situ Activities of Nonphotosynthetic Microorganisms in Aquatic and Terrestrial Habitats. Annual Review of Microbiology, 39(1), 321-346. doi:10.1146/annurev.micro.39.1.321*

[10] *Patel, R. (2005, August). Biofilms and antimicrobial resistance. Retrieved from https://www.ncbi.nlm.nih.gov/pubmed/16056024*

[11] *Uncultivated microorganisms. (2011). Place of publication not identified: Springer-Verlag Berlin An.*

[12] *Baltz, Richard. (2007). Antimicrobials from actinomycetes: Back to the future. Microbe. 2. 125-131.*

[13] *NovoBiotic Pharmaceuticals, LLC. (n.d.). Retrieved from https://www.novobiotic.com/*

[14] *Microdissection, I. L., Systems, M., Material, F. (n.d.). At the Forefront of Science. Retrieved from http://applications.zeiss.com/C125792900358A3F/0/A4C6E8C131538FD6C125790600482057*

[15] *US7035004B2 - Laser microdissection device. (n.d.). Retrieved from https://patents.google.com/patent/US7035004*

[16] *Campbell, R. A., Eifert, R. W., & Turner, G. C. (2014). Openstage: A Low-Cost Motorized Microscope Stage with Sub-Micron Positioning Accuracy. PLoS ONE, 9(2). doi:10.1371/journal.pone.0088977*

[17] *Sizova, M. V., Hohmann, T., Hazen, A., Paster, B. J., Halem, S. R., Murphy, C. M., . . . Epstein, S. S. (2011). New Approaches for Isolation of Previously Uncultivated Oral Bacteria. Applied and Environmental Microbiology, 78(1), 194-203. doi:10.1128/aem.06813-11*

[18] *National Research Council (US) Steering Group for the Workshop on Size Limits of Very Small Microorganisms. (1999, January 01). Bacteria, Their Smallest Representatives and Subcellular Structures, and the Purported Precambrian Fossil "Metallogenium". Retrieved from https://www.ncbi.nlm.nih.gov/books/NBK224752/*

[19] *Kim, S., Jonghe, J. D., Kulesa, A. B., Feldman, D., Vatanen, T., Bhattacharyya, R. P., . . . Blainey, P. C. (2017). High-throughput automated microfluidic sample preparation for accurate microbial genomics. Nature Communications, 8, 13919. doi:10.1038/ncomms13919*

[20] *Slocum, A. H. (1992). Precision machine design. Englewood Cliffs, N.J: Prentice Hall.*

[21] *Trimble, A., 2018, Professor at University of Hawaii at Manoa, U.S., private communication*

[22] *Bearing, A. R. (n.d.). Friction & Frequency Factors. Retrieved from https://www.amroll.com/friction-frequency-factors.html*

[23] Budimir, M. (2013, March 31). Microstepping myths. Retrieved from http://www.machinedesign.com/archive/microstepping-myths

[24] *Trimble, A. Z., Yammamoto, B., & Li, J. (2016). An Inexpensive, Portable Machine to Facilitate Testing and Characterization of the Friction Stir Blind Riveting Process. Journal of Manufacturing Science and Engineering, 138(9), 095001. doi:10.1115/1.4034158*

[25] *(n.d.). Retrieved from http://asm.matweb.com/search/SpecificMaterial.asp?bassnum=mq303h*

[26] *(n.d.). Retrieved from http://asm.matweb.com/search/SpecificMaterial.asp?bassnum=mq316a*

[27] *AZoM, W. B. (2013, June 11). Stainless Steel – Grade 440C (UNS S44004). Retrieved from https://www.azom.com/article.aspx?ArticleID=6846*

[28] *(n.d.). Retrieved from http://asm.matweb.com/search/SpecificMaterial.asp?bassnum=ma6061t6*

[29] *MatWeb - The Online Materials Information Resource. (n.d.). Retrieved from http://www.matweb.com/search/datasheet.aspx?matguid=e6f654c5f65f45339e672f1f6ce7008c&ckck=*

[30] *Chaplin, M., M. C. (n.d.). Water Absorption Spectrum. Retrieved from*

http://www1.lsbu.ac.uk/water/water_vibrational_spectrum.html

[31] Technical Note: Gaussian Beam Optics. (n.d.). Retrieved from https://www.newport.com/n/gaussian-beam-optics

[32] *Tsukamoto, P., 2018, Owner at Precision Machinery and Tooling LLC , U.S., private communication*

0.13 Appendix

0.13.1 Eagle PCB Schematics and Diagrams

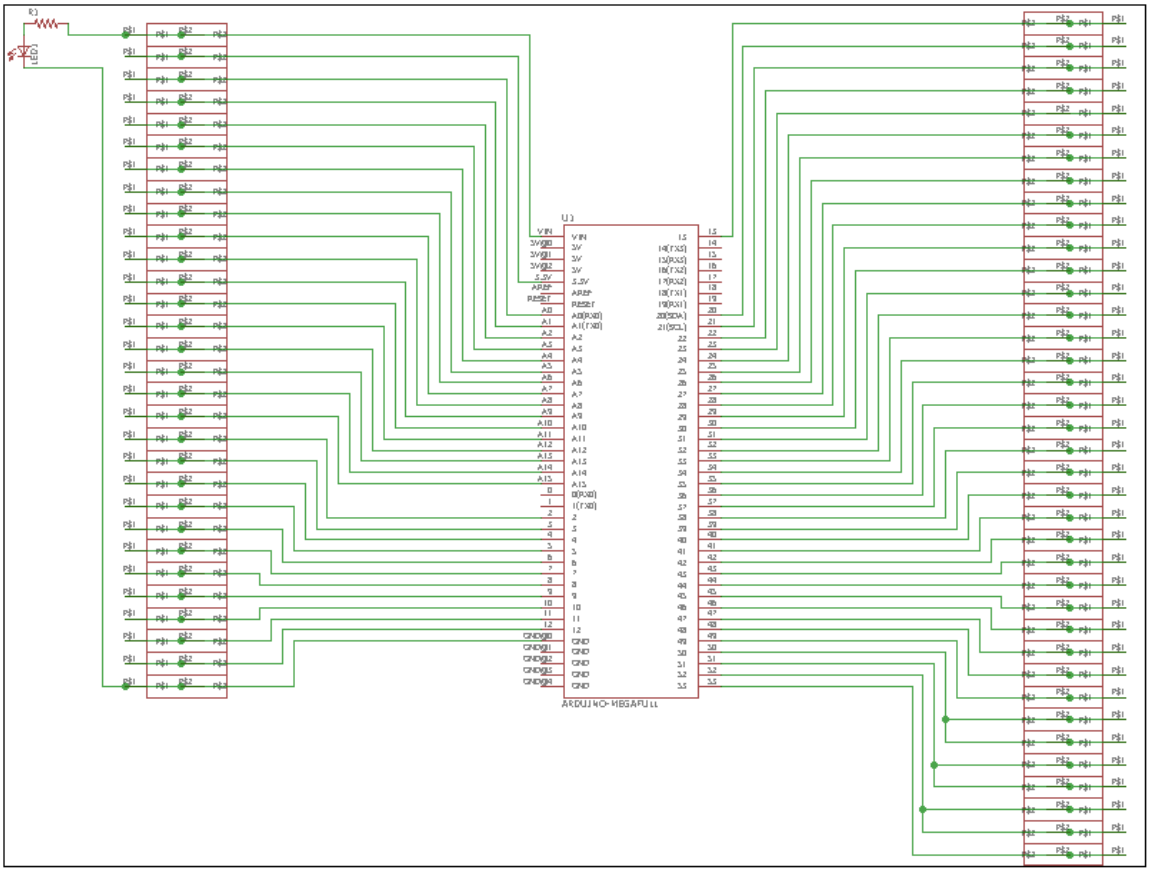

Figure 131: Eagle schematic of the main controller Arduino mega shield circuit board.

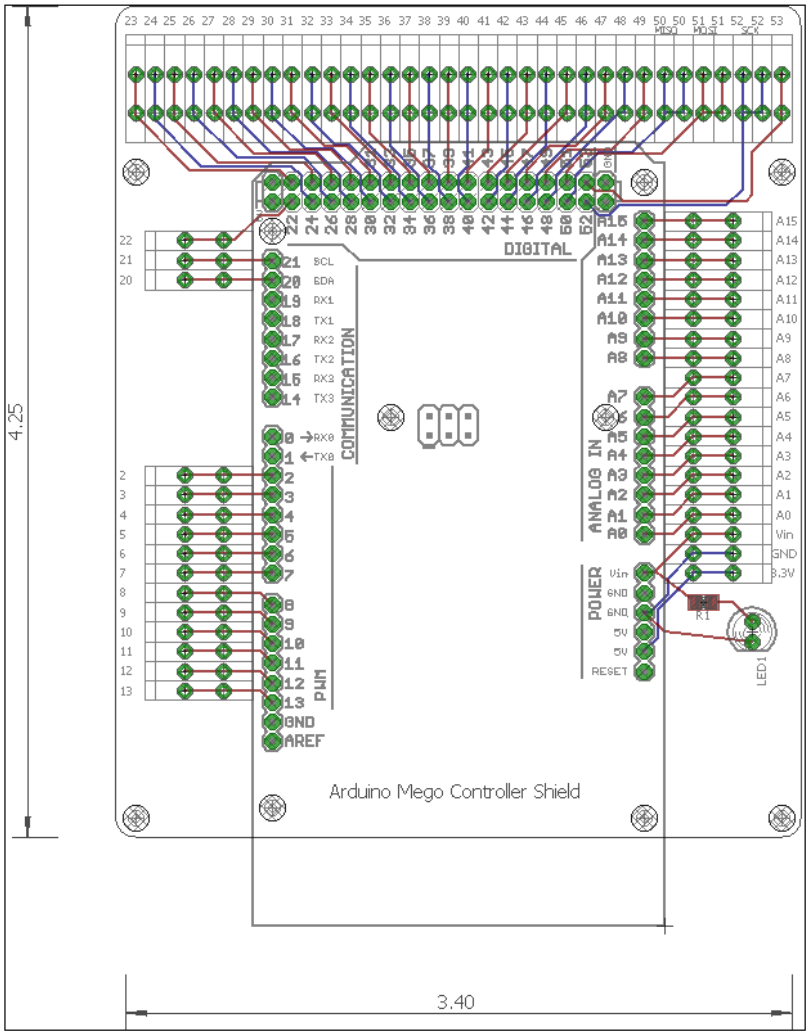

Figure 132: Eagle board diagram of the main controller Arduino mega shield circuit board.

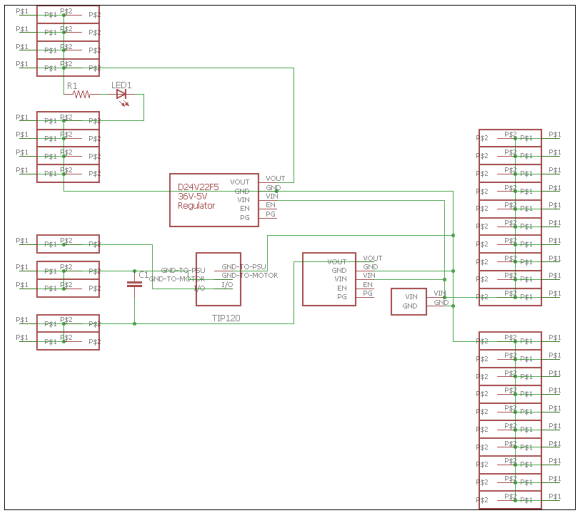

Figure 133: Eagle schematic of the power distribution board

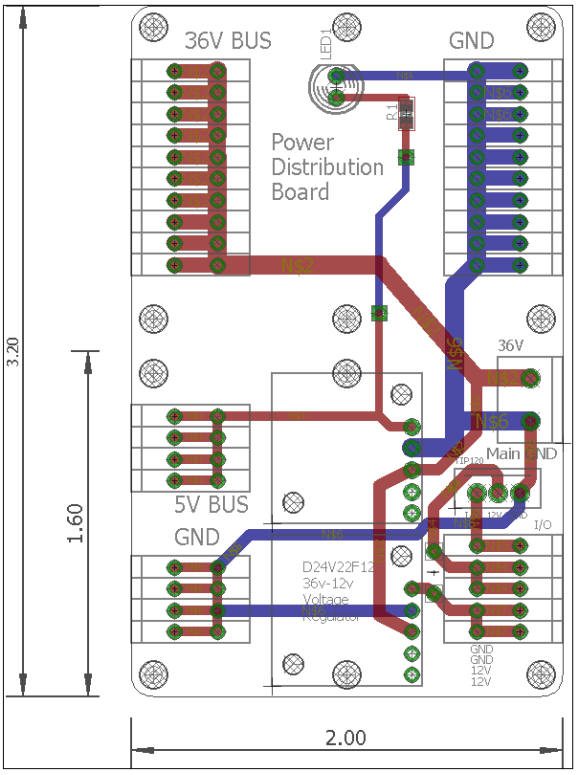

Figure 134: Eagle board diagram of the power distribution board

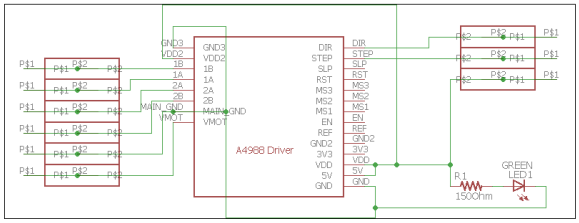

Figure 135: Eagle schematic diagram of the A4988 Motor Driver Shield. The Eagle board diagram is no longer available. This board was used for non precision applications.

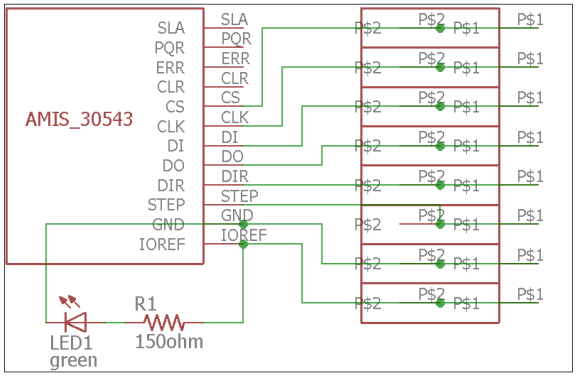

Figure 136: Eagle schematic diagram of the AMIS 30543 Motor Driver Shield. This board was used to drive the X and Y axis of the optics stage.

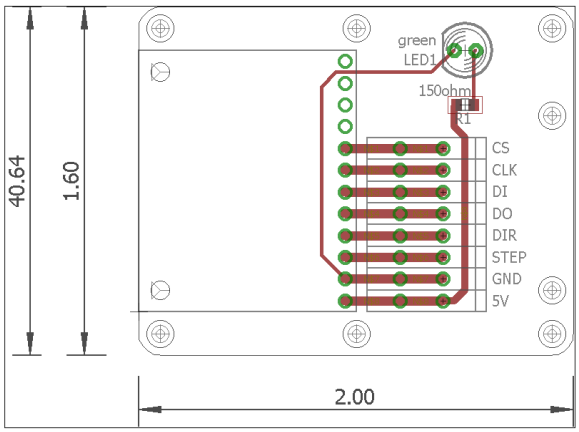

Figure 137: Eagle board diagram of the AMIS 30543 Motor Driver Shield.

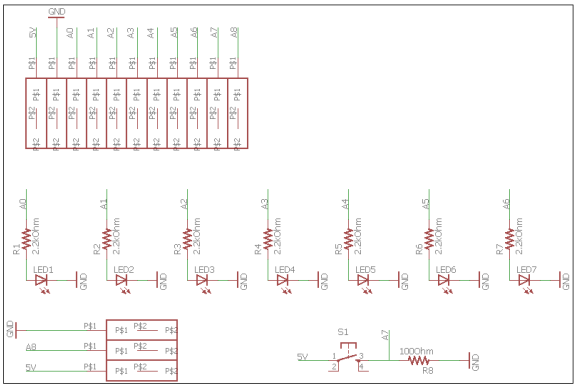

Figure 138: Eagle schematic diagram of the manual jog controller.

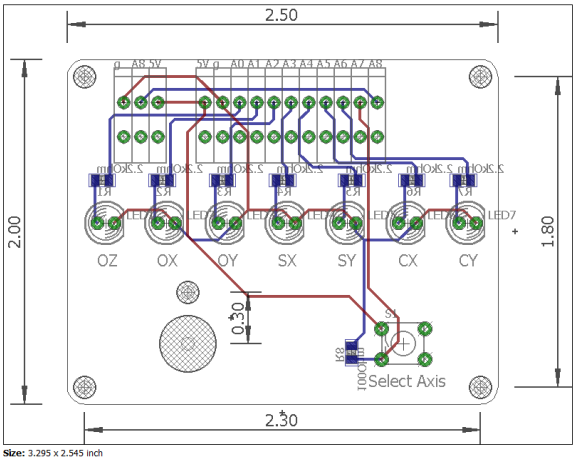

Figure 139: Eagle board diagram of the manual jog controller.

0.13.2 Arduino Controller Code

0.13.2.1 Main

```
//Autonomous Colony Separator Controller Code
//Grant Takara 12-29-17

#include <SPI.h>
#include <AMIS30543.h>
```

```
//HARDWARE VARIABLES
const uint8_t optics_x_DirPin = 2, optics_x_StepPin = 3,
    optics_x_SlaveSelect = 4; //Optics stage X axis stepper motor pins
const uint8_t optics_y_DirPin = 5, optics_y_StepPin = 6,
    optics_y_SlaveSelect = 7; //Optics stage Y axis stepper motor pins

const int laser = A14;   //laser output signal pin
const int backlight = A15; //backlight output signal pin
const int jog_input = 8, jog_output = 9;

const int optics_z_dirPin = 22, optics_z_stepPin = 23; //Optics Z axis
    stepper motor pins
const int sample_x_dirPin = 24, sample_x_stepPin = 25; //Sample X axis
    stepper motor pins
const int sample_y_dirPin = 26, sample_y_stepPin = 27; //Sample Y axis
    stepper motor pins
const int capture_x_dirPin = 28, capture_x_stepPin = 29; //Capture X axis
    stepper motor pins
const int capture_y_dirPin = 30, capture_y_stepPin = 31; //Capture Y axis
    stepper motor pins

const int optics_lim_neg_x = 32, optics_lim_pos_x = 33, optics_lim_neg_y =
    34, optics_lim_pos_y = 35, optics_lim_neg_z = 36, optics_lim_pos_z =
    37; //optics limit switches
const int sample_lim_neg_x = 38, sample_lim_pos_x = 39, sample_lim_neg_y =
    40, sample_lim_pos_y = 41; //sample stage limit switches
const int capture_lim_neg_x = 42, capture_lim_pos_x = 43, capture_lim_neg_y
     = 44, capture_lim_pos_y = 45; //sample stage limit switches
```

```
const long int optics_z_steps = 50500, optics_y_steps = 1400000,
    optics_x_steps = 1010000, sample_x_steps = 10500, sample_y_steps =
    12000, capture_x_steps = 12000, capture_y_steps = 6500;

long int optics_z_stepcount = 0, optics_x_stepcount = 0, optics_y_stepcount
     = 0, sample_x_stepcount = 0, sample_y_stepcount = 0,
    capture_x_stepcount = 0, capture_y_stepcount = 0;

///DATA PARSING VARIABLES
char receivedChars[100]; boolean newData = true; long int operation[100];

//Manual control pins
const int optics_z_jog = A0, optics_x_jog = A1, optics_y_jog = A2,
    sample_x_jog = A3, sample_y_jog = A4, capture_x_jog = A5, capture_y_jog
     = A6, select_axis_button = A7, pot = A8;

unsigned long int feed_factor = 0; //speed factor changes the manual jog
    feedrate using this quantity as the denominator and proportional to the
     potentiometer reading
int dir = 1, num_step = 0;
unsigned int selected_axis = 1;

AMIS30543 stepper_x; AMIS30543 stepper_y;

void setup()
{
  setup_machine();
}

void loop()
```

```
{
  MakeDataString(); delay(2000); showNewData();
  int i = 0;
  if (operation[0] == 1 && operation[1] == NULL) {
    home_machine();
  }
  else if (operation[0] == 2 && operation[1] == NULL) {
    Serial.println("Manual Jog Mode");
    manual_jog_mode();
  }
  else if (operation[0] == 3 && operation[1] == NULL) {
    analogWrite(backlight, 0);
  }
  else if (operation[0] == 4 && operation[1] == NULL) {
    analogWrite(backlight, 175);
  }
  else if (operation[0] == 5) {  //Subprogram for rapid positioning of the
      optics stage
    rapid_subprogram5();
  }
  else if (operation[0] == 6) {  //Subprogram for cutting positioning of the
       optics stage
    cutting_subprogram6();
  }
  else if (operation[0] == 7) {  //Subprogram for positioning the sample
      stage
    sample_subprogram7();
  }
  else if (operation[0] == 8) {  //Subprogram for positioning the capture
      stage
```

```
    capture_subprogram8();
  }
  else if (operation[0] == 9 && operation[1] == NULL) { //subprogram for
      turning off the laser
    digitalWrite(laser, LOW);
  }
  else if (operation[0] == 10 && operation[1] == NULL) { //subprogram for
      turning on the laser
    digitalWrite(laser, HIGH);
  }
}
```

0.13.2.2 Setup Machine Function

```
void setup_machine() {
  Serial.begin(250000); SPI.begin();
  stepper_x.init(optics_x_SlaveSelect); stepper_y.init(optics_y_SlaveSelect
      ); //initialize driver

  pinMode(optics_x_DirPin, OUTPUT); digitalWrite(optics_x_DirPin, LOW);
      pinMode(optics_x_StepPin, OUTPUT); digitalWrite(optics_x_StepPin, LOW)
      ; // Drive the NXT/STEP and DIR pins low initially.
  pinMode(optics_y_DirPin, OUTPUT); digitalWrite(optics_y_DirPin, LOW);
      pinMode(optics_y_StepPin, OUTPUT); digitalWrite(optics_y_StepPin, LOW)
      ; // Drive the NXT/STEP and DIR pins low initially.

  pinMode(laser, OUTPUT); pinMode(backlight, OUTPUT);

  delay(1);                        // Give the driver some time to power up.

  pinMode(jog_output, OUTPUT); pinMode(jog_input, INPUT);
```

```
pinMode(optics_z_dirPin, OUTPUT); digitalWrite(optics_z_dirPin, LOW);
    pinMode(optics_z_stepPin, OUTPUT); digitalWrite(optics_z_stepPin, LOW)
    ;
pinMode(sample_x_dirPin, OUTPUT); digitalWrite(sample_x_dirPin, LOW);
    pinMode(sample_x_stepPin, OUTPUT); digitalWrite(sample_x_stepPin, LOW)
    ;
pinMode(sample_y_dirPin, OUTPUT); digitalWrite(sample_y_dirPin, LOW);
    pinMode(sample_y_stepPin, OUTPUT); digitalWrite(sample_y_stepPin, LOW)
    ;
pinMode(capture_x_dirPin, OUTPUT); digitalWrite(capture_x_dirPin, LOW);
    pinMode(capture_x_stepPin, OUTPUT); digitalWrite(capture_x_stepPin,
    LOW);
pinMode(capture_y_dirPin, OUTPUT); digitalWrite(capture_y_dirPin, LOW);
    pinMode(capture_y_stepPin, OUTPUT); digitalWrite(capture_y_stepPin,
    LOW);

pinMode(optics_z_jog, OUTPUT);    analogWrite(optics_z_jog, LOW);
pinMode(optics_x_jog, OUTPUT);    analogWrite(optics_x_jog, LOW);
pinMode(optics_y_jog, OUTPUT);    analogWrite(optics_y_jog, LOW);
pinMode(sample_x_jog, OUTPUT);    analogWrite(sample_x_jog, LOW);
pinMode(sample_y_jog, OUTPUT);    analogWrite(sample_y_jog, LOW);
pinMode(capture_x_jog, OUTPUT);   analogWrite(capture_x_jog, LOW);
pinMode(capture_y_jog, OUTPUT);   analogWrite(capture_y_jog, LOW);

pinMode(select_axis_button, INPUT); pinMode(pot, INPUT);

stepper_x.resetSettings();       // Reset the driver to its default
    settings.
stepper_x.setCurrentMilliamps(500); // Set the current limit. You should
```

```
    change the number here to an appropriate value for your particular
    system.
  stepper_x.setStepMode(32);          // Set the number of microsteps that
    correspond to one full step.

  stepper_y.resetSettings();         // Reset the driver to its default
    settings.
  stepper_y.setCurrentMilliamps(500); // Set the current limit. You should
    change the number here to an appropriate value for your particular
    system.
  stepper_y.setStepMode(32);          // Set the number of microsteps that
    correspond to one full step. (run at 30us 100% duty cycle)
}
```

0.13.2.3 Make String Function

```
void MakeDataString() {
  static boolean recvInProgress = false;
  unsigned int index = 0;
  char startMarker = '<';
  char endMarker = '>';
  char input_char;

  while (Serial.available() > 0 && newData == true) { //check for new data
    in serial port if there is no new data
    input_char = Serial.read();                      //read the next input
      character

    if (input_char == startMarker) {                 //if the program has
      seen the start marker, start making the character array
      recvInProgress = true;
```

```
      //delete the old string
      int i = 0;
      while (operation[i] != NULL) {                  //Clear the character
          array
        operation[i] = (char)0;
        i++;
      }
    }
    if (recvInProgress == true) {
      if (input_char != endMarker) {                  //append the character
          array with the incoming characters
        receivedChars[index] = input_char;
        index++;
      }
      else {
        receivedChars[index] = input_char;
        newData = false;                              //no new data coming in
            , stop appending the character array
      }
    }
  }
}
```

0.13.2.4 Parse and Validate Input Data Function

```
void showNewData() {
  if (newData == false) {
    Serial.print("This just in ... ");
    Serial.println(receivedChars);                    //display the character
        array
```

```
    newData = true;

    int i = 0; char *delim = "<,>"; char *token;

    token = strtok(receivedChars, delim);       //get the first token
    operation[i] = (String(token)).toInt();     //convert the first token to
        an integer
    i++;                                        //increment the operation
       table cell
    //Serial.println(operation[0]);               //print the first cell,
       lets see what it saved

    while (token != NULL) {                     //continue getting tokens
       until the string is empty
      token = strtok(NULL, delim);
      operation[i] = (String(token)).toInt();
      i++;
      //Serial.println(operation[i]);
    }

    i = 0;
    while (receivedChars[i] != NULL) {        //Clear the character array
      receivedChars[i] = (char)0;
      i++;
    }
  }
}
```

0.13.2.5 Read Manual Jog Potentiometer Function

```
void read_pot() {
```

```
  int pot_value = analogRead(pot);
  if (pot_value >= 0 && pot_value < 200) { //negative full speed
    feed_factor = 0;    dir = -1;    num_step = 1;
  }
  else if (pot_value > 200 && pot_value < 400) {
    feed_factor = 3000;    dir = -1;    num_step = 1;
  }
  else if (pot_value > 400 && pot_value < 700) {
    num_step = -1;
  }
  else if (pot_value > 700 && pot_value < 900) {
    feed_factor = 3000;   dir = 1;   num_step = 1;
  }
  else if (pot_value > 900) {
    feed_factor = 0;    dir = 1;    num_step = 1;
  }
  else {//do nothing
    num_step = -1;
  }
}
```

0.13.2.6 Optics Stage Rapid Feedrate Function

```
void rapid_subprogram5() {
  while (operation[i] != NULL || operation[i] != '>') {
    i++;
    int sign = 1;
    if (operation[i] == 0 || operation[i] == '>') {
      operation[0] = 2;
      break;
    }
```

```
    if (operation[i] > 0) {          //Determine the direction of the steps
      sign = 1;
    }
    else {
      sign = -1;
    }
    if (i % 2 != 0) {                //this is an odd number, thus a command
        for x<
      optics_x(abs(operation[i]), sign);
    }
    else {
      optics_y(abs(operation[i]), sign); //this is an even number, thus a
          command for y
    }
    delay(200);
  }
}
```

0.13.2.7 Optics Cutting Feedrate Subprogram

```
void cutting_subprogram6() {
  while (operation[i] != NULL || operation[i] != '>') {
    i++;
    int sign = 1;
    if (operation[i] == 0 || operation[i] == '>') {
      operation[0] = 2;
      break;
    }
    if (operation[i] > 0) {          //Determine the direction of the steps
      sign = 1;
    }
```

```
    else {
      sign = -1;
    }
    if (i % 2 != 0) {               //this is an odd number, thus a command
        for x<
      optics_x(abs(operation[i]), sign);
    }
    else {
      optics_y(abs(operation[i]), sign); //this is an even number, thus a
          command for y
    }
    delay(200);
  }
  digitalWrite(laser, LOW); //turn off laser
}
```

0.13.2.8 Sample Stage Feedrate Function

```
void sample_subprogram7() {
  while (operation[i] != NULL || operation[i] != '>') {
    i++;
    int sign = 1;
    if (operation[i] == 0 || operation[i] == '>') {
      operation[0] = 2;
      break;
    }
    if (operation[i] > 0) {         //Determine the direction of the steps
      sign = 1;
    }
    else {
      sign = -1;
```

```
    }
    if (i % 2 != 0) {               //this is an odd number, thus a command
        for x<
      sample_x(abs(operation[i]), sign);
    }
    else {
      sample_y(abs(operation[i]), sign); //this is an even number, thus a
          command for y
    }
    delay(200);
  }
}
```

0.13.2.9 Capture Stage Feedrate Function

```
void capture_subprogram8(){
  while (operation[i] != NULL || operation[i] != '>') {
    i++;
    int sign = 1;
    if (operation[i] == 0 || operation[i] == '>') {
      operation[0] = 2;
      break;
    }
    if (operation[i] > 0) {         //Determine the direction of the steps
      sign = 1;
    }
    else {
      sign = -1;
    }
    if (i % 2 != 0) {               //this is an odd number, thus a command
        for x<
```

```
      capture_x(abs(operation[i]), sign);
    }
    else {
      capture_y(abs(operation[i]), sign); //this is an even number, thus a
          command for y
    }
    delay(200);
  }
}
```

0.13.2.10 Home Machine Function

```
void home_machine() {
  Serial.println("Homing optics X"); optics_z(1000000, 1);
  Serial.println("Homing Capture Y"); capture_y(10000000, -1);
  Serial.println("Homing Capture X"); capture_x(10000000, -1);
  Serial.println("Homing Sample Y"); sample_y(100000, -1);
  Serial.println("Homing Sample X"); sample_x(100000, -1);
  Serial.println("Homing Optics X"); optics_x(10000000, -1);
  Serial.println("Homing Optics Y"); optics_y(10000000, -1);
}
```

0.13.2.11 Driver Functions

```
//*************************************************************************//

//*******************************OPTICS STAGE
    *******************************//
//*************************************************************************//
```

```
void optics_x(long int steps, int dir) { // The NXT/STEP minimum high pulse
    width is 2 microseconds.

  stepper_x.enableDriver();          // Enable the motor outputs.

  int d = 240; //20um/s
  //int d = 370; //31um/s

  if (dir == 1) { //moves in positive X
    for (int i = 0; i < steps; i++) {
      if (i < 200 || i > (steps - 200)) {
        feed_factor = 100;
      }
      else {
        feed_factor = 40;
      }
      digitalWrite(optics_x_DirPin, 0); delayMicroseconds(1); digitalWrite(
          optics_x_StepPin, HIGH); delayMicroseconds(d); digitalWrite(
          optics_x_StepPin, LOW); delayMicroseconds(d); optics_x_stepcount
          ++; delayMicroseconds(feed_factor);
      if (digitalRead(optics_lim_pos_x) == 1) {
        digitalWrite(optics_x_DirPin, 1); delayMicroseconds(1); digitalWrite
            (optics_x_StepPin, HIGH); delayMicroseconds(d); digitalWrite(
            optics_x_StepPin, LOW); delayMicroseconds(d); optics_x_stepcount
            --; delayMicroseconds(feed_factor);
        break;
      }
    }
  }
  else {
```

```
    for (int i = 0; i < steps; i++) { //moves in negative X

      if (i < 200 || i > (steps - 200)) {
        feed_factor = 100;
      }
      else {
        feed_factor = 40;
      }
      digitalWrite(optics_x_DirPin, 1); delayMicroseconds(1); digitalWrite(
          optics_x_StepPin, HIGH); delayMicroseconds(d); digitalWrite(
          optics_x_StepPin, LOW); delayMicroseconds(d); optics_x_stepcount
          --; delayMicroseconds(feed_factor);
      if (digitalRead(optics_lim_neg_x) == 1) {
        digitalWrite(optics_x_DirPin, 0); delayMicroseconds(1); digitalWrite
            (optics_x_StepPin, HIGH); delayMicroseconds(d); digitalWrite(
            optics_x_StepPin, LOW); delayMicroseconds(d); optics_x_stepcount
            ++; delayMicroseconds(feed_factor);
        break;
      }
    }
  }
}

void optics_y(long int steps, int dir) { // The NXT/STEP minimum high pulse
     width is 2 microseconds.

  stepper_y.enableDriver();          // Enable the motor outputs.

  int d = 240; //20um/s
  //int d = 370;
```

```
if (dir == 1) { //moves in positive Y
  for (int i = 0; i < steps; i++) {
    if (i < 200 || i > (steps - 200)) {
      feed_factor = 100;
    }
    else {
      feed_factor = 40;
    }
    delayMicroseconds(1); digitalWrite(optics_y_DirPin, 1);
        delayMicroseconds(1); digitalWrite(optics_y_StepPin, HIGH);
        delayMicroseconds(d); digitalWrite(optics_y_StepPin, LOW);
        delayMicroseconds(d); optics_y_stepcount++; delayMicroseconds(
        feed_factor);
    if (digitalRead(optics_lim_pos_y) == 1) {
      delayMicroseconds(1); digitalWrite(optics_y_DirPin, 0);
          delayMicroseconds(1); digitalWrite(optics_y_StepPin, HIGH);
          delayMicroseconds(d); digitalWrite(optics_y_StepPin, LOW);
          delayMicroseconds(d); optics_y_stepcount--; delayMicroseconds(
          feed_factor);
      break;
    }
  }
}
else {
  for (int i = 0; i < steps; i++) { //moves in negative Y

    if (i < 200 || i > (steps - 200)) {
      feed_factor = 100;
    }
```

```
      else {
        feed_factor = 40;
      }

      delayMicroseconds(1); digitalWrite(optics_y_DirPin, 0);
          delayMicroseconds(1); digitalWrite(optics_y_StepPin, HIGH);
          delayMicroseconds(d); digitalWrite(optics_y_StepPin, LOW);
          delayMicroseconds(d); optics_y_stepcount--; delayMicroseconds(
          feed_factor);
      if (digitalRead(optics_lim_neg_y) == 1) {
        delayMicroseconds(1); digitalWrite(optics_y_DirPin, 1);
            delayMicroseconds(1); digitalWrite(optics_y_StepPin, HIGH);
            delayMicroseconds(d); digitalWrite(optics_y_StepPin, LOW);
            delayMicroseconds(d); optics_y_stepcount++; delayMicroseconds(
            feed_factor);
        break;
      }
    }
  }
}

void optics_z(long int steps, int dir) {
  if (dir == 1) { //moves in positive Z
    for (int i = 0; i < steps; i++) { //moves in negative z
      delayMicroseconds(1); digitalWrite(optics_z_dirPin, 1);
          delayMicroseconds(1); digitalWrite(optics_z_stepPin, HIGH);
          delayMicroseconds(10); digitalWrite(optics_z_stepPin, LOW);
          delayMicroseconds(10); optics_z_stepcount--; delayMicroseconds(
          feed_factor);
      if (digitalRead(optics_lim_neg_z) == 1) {
```

```
      delayMicroseconds(1); digitalWrite(optics_z_dirPin, 0);
          delayMicroseconds(1); digitalWrite(optics_z_stepPin, HIGH);
          delayMicroseconds(10); digitalWrite(optics_z_stepPin, LOW);
          delayMicroseconds(10); optics_z_stepcount++; delayMicroseconds(
          feed_factor);
      break;
    }
  }
 }
 else {
  for (int i = 0; i < steps; i++) { //moves in positive Z
    delayMicroseconds(1); digitalWrite(optics_z_dirPin, 0);
        delayMicroseconds(1); digitalWrite(optics_z_stepPin, HIGH);
        delayMicroseconds(10); digitalWrite(optics_z_stepPin, LOW);
        delayMicroseconds(10); optics_z_stepcount++; delayMicroseconds(
        feed_factor);
    if (digitalRead(optics_lim_pos_z) == 1) {
      delayMicroseconds(1); digitalWrite(optics_z_dirPin, 1);
          delayMicroseconds(1); digitalWrite(optics_z_stepPin, HIGH);
          delayMicroseconds(10); digitalWrite(optics_z_stepPin, LOW);
          delayMicroseconds(10); optics_z_stepcount--; delayMicroseconds(
          feed_factor);
      break;
    }
  }

 }
}

//*************************************************************************//
```

```
//*********************************SAMPLE STAGE
   *********************************//
//*****************************************************************************//


void sample_x(long int steps, int dir) {
  if (dir == 1) {
    for (int i = 0; i < steps; i++) {
      delayMicroseconds(1); digitalWrite(sample_x_dirPin, 0);
          delayMicroseconds(1); digitalWrite(sample_x_stepPin, HIGH);
          delayMicroseconds(200); digitalWrite(sample_x_stepPin, LOW);
          delayMicroseconds(200); sample_x_stepcount++; delayMicroseconds(
          feed_factor);
      if (digitalRead(sample_lim_pos_x) == 1) {
        delayMicroseconds(1); digitalWrite(sample_x_dirPin, 1);
            delayMicroseconds(1); digitalWrite(sample_x_stepPin, HIGH);
            delayMicroseconds(200); digitalWrite(sample_x_stepPin, LOW);
            delayMicroseconds(200); sample_x_stepcount--; delayMicroseconds(
            feed_factor);
        break;
      }
    }
  }
  else {
    for (int i = 0; i < steps; i++) {
      delayMicroseconds(1); digitalWrite(sample_x_dirPin, 1);
          delayMicroseconds(1); digitalWrite(sample_x_stepPin, HIGH);
          delayMicroseconds(200); digitalWrite(sample_x_stepPin, LOW);
          delayMicroseconds(200); sample_x_stepcount--; delayMicroseconds(
```

```
        feed_factor);
      if (digitalRead(sample_lim_neg_x) == 1) {
        delayMicroseconds(1); digitalWrite(sample_x_dirPin, 0);
            delayMicroseconds(1); digitalWrite(sample_x_stepPin, HIGH);
            delayMicroseconds(200); digitalWrite(sample_x_stepPin, LOW);
            delayMicroseconds(200); sample_x_stepcount++; delayMicroseconds(
            feed_factor);
        break;
      }
    }
  }
}

void sample_y(long int steps, int dir) {

  if (dir == 1) { //moves in positive Y
    for (int i = 0; i < steps; i++) {

      delayMicroseconds(1); digitalWrite(sample_y_dirPin, 0);
          delayMicroseconds(1); digitalWrite(sample_y_stepPin, HIGH);
          delayMicroseconds(300); digitalWrite(sample_y_stepPin, LOW);
          delayMicroseconds(300); sample_y_stepcount--; delayMicroseconds(
          feed_factor);
      if (digitalRead(sample_lim_pos_y) == 1) {
        delayMicroseconds(1); digitalWrite(sample_y_dirPin, 1);
            delayMicroseconds(1); digitalWrite(sample_y_stepPin, HIGH);
            delayMicroseconds(300); digitalWrite(sample_y_stepPin, LOW);
            delayMicroseconds(300); sample_y_stepcount++; delayMicroseconds(
            feed_factor);
        break;
```

```
      }
    }
  }
  else { //moves in positive Y
    for (int i = 0; i < steps; i++) {
      delayMicroseconds(1); digitalWrite(sample_y_dirPin, 1);
          delayMicroseconds(1); digitalWrite(sample_y_stepPin, HIGH);
          delayMicroseconds(300); digitalWrite(sample_y_stepPin, LOW);
          delayMicroseconds(300); sample_y_stepcount++; delayMicroseconds(
          feed_factor);
      if (digitalRead(sample_lim_neg_y) == 1) {
        delayMicroseconds(1); digitalWrite(sample_y_dirPin, 0);
            delayMicroseconds(1); digitalWrite(sample_y_stepPin, HIGH);
            delayMicroseconds(300); digitalWrite(sample_y_stepPin, LOW);
            delayMicroseconds(300); sample_y_stepcount--; delayMicroseconds(
            feed_factor);
        break;
      }
    }
  }
}

//*************************************************************************//

//*******************************CAPTURE STAGE
    *******************************//
//*************************************************************************//


void capture_x(long int steps, int dir) {
```

```
if (dir == 1) { //moves in positive X
  for (int i = 0; i < steps; i++) {
    delayMicroseconds(1); digitalWrite(capture_x_dirPin, 1);
       delayMicroseconds(1); digitalWrite(capture_x_stepPin, HIGH);
       delayMicroseconds(120); digitalWrite(capture_x_stepPin, LOW);
       delayMicroseconds(120); capture_x_stepcount++; delayMicroseconds(
       feed_factor);
    if (digitalRead(capture_lim_pos_x) == 1) {
      delayMicroseconds(1); digitalWrite(capture_x_dirPin, 0);
         delayMicroseconds(1); digitalWrite(capture_x_stepPin, HIGH);
         delayMicroseconds(120); digitalWrite(capture_x_stepPin, LOW);
         delayMicroseconds(120); capture_x_stepcount--; delayMicroseconds
         (feed_factor);
    }
  }
}
else { //moves in negative X
  for (int i = 0; i < steps; i++) {
    delayMicroseconds(1); digitalWrite(capture_x_dirPin, 0);
       delayMicroseconds(1); digitalWrite(capture_x_stepPin, HIGH);
       delayMicroseconds(120); digitalWrite(capture_x_stepPin, LOW);
       delayMicroseconds(120); capture_x_stepcount--; delayMicroseconds(
       feed_factor);
    if (digitalRead(capture_lim_neg_x) == 1) {
      delayMicroseconds(1); digitalWrite(capture_x_dirPin, 1);
         delayMicroseconds(1); digitalWrite(capture_x_stepPin, HIGH);
         delayMicroseconds(120); digitalWrite(capture_x_stepPin, LOW);
         delayMicroseconds(120); capture_x_stepcount++; delayMicroseconds
         (feed_factor);
    }
```

```
    }
  }
}

void capture_y(long int steps, int dir) {
  int x = 0;
  if (dir == 1) { //moves in positive Y
    for (int i = 0; i < steps; i++) {
      Serial.println(x);
      x++;
      delayMicroseconds(1); digitalWrite(capture_y_dirPin, 0);
          delayMicroseconds(1); digitalWrite(capture_y_stepPin, HIGH);
          delayMicroseconds(120); digitalWrite(capture_y_stepPin, LOW);
          delayMicroseconds(120); capture_y_stepcount--; delayMicroseconds(
          feed_factor);
      if (digitalRead(capture_lim_neg_y) == 1) {
        delayMicroseconds(1); digitalWrite(capture_y_dirPin, 1);
            delayMicroseconds(1); digitalWrite(capture_y_stepPin, HIGH);
            delayMicroseconds(120); digitalWrite(capture_y_stepPin, LOW);
            delayMicroseconds(120); capture_y_stepcount++; delayMicroseconds
            (feed_factor);
        break;
      }
    }
  }
  else { //moves in negative Y
    for (int i = 0; i < steps; i++) {
      delayMicroseconds(1); digitalWrite(capture_y_dirPin, 1);
          delayMicroseconds(1); digitalWrite(capture_y_stepPin, HIGH);
          delayMicroseconds(120); digitalWrite(capture_y_stepPin, LOW);
```

```
        delayMicroseconds(120); capture_y_stepcount++; delayMicroseconds(
        feed_factor);
    if (digitalRead(capture_lim_pos_y) == 1) {
      delayMicroseconds(1); digitalWrite(capture_y_dirPin, 0);
         delayMicroseconds(1); digitalWrite(capture_y_stepPin, HIGH);
         delayMicroseconds(120); digitalWrite(capture_y_stepPin, LOW);
         delayMicroseconds(120); capture_y_stepcount--; delayMicroseconds
         (feed_factor);
      break;
    }
   }
  }
}
```

0.13.3 Matlab Controller Code

```
clear all
clc

display('Welcome to the colony separator');
display('Below is a list of the selectable operations');
display('1 = Home machine');
display('2 = Manual jog mode');
display('3 = Turn off Backlight');
display('4 = Turn on Backlight');
display('5 = Separate Colonies');
display('6 = Cutting Subprogram');
display('7 = Sample Stage Positioning');
display('8 = Capture Stage Positioning');
display('9 = Turn off laser');
display('10 = Turn on laser');
```

```
output = input('input operation (1-10):');

serial_output(output);
disp('User Command Received');

function serial_output(x)
if ~isempty(instrfind)
    fclose(instrfind);
    delete(instrfind);
end
arduino=serial('COM3','BaudRate',250000);
fopen(arduino);
pause(2);
switch x
    case 1 %Home Machine
        fprintf(arduino,'%s\n','<1>');
    case 2 %Manual Jog Mode
        fprintf(arduino,'%s\n','<2>');
    case 3 %Turn off Backlight
        fprintf(arduino,'%s\n','<3>');
    case 4 %Turn on Backlight
        fprintf(arduino,'%s\n','<4>');
    case 5 %Begin Separation Process
        %Assumes the current position has the machined entirely zeroed
        %%
        %upload the ichip coordinates
        ichip = csvread('ichip_coord.txt');
        %upload the microplate coordinates
        capture_plate = csvread('24_well_microplate_coord.csv');
```

```
ichip_x = ichip(:,1);

%Z axis should already generally be zeroed
%Take an image (this is also the initial view)
disp('Beginning Separation Process');
fprintf(arduino,'%s\n','<5>');



%%%%%%%%%%%%%%%%%%%%%%%%%%%%%%%%%%%%%%%%%%%%%%%%
disp('Taking Pre Operation Photo');
webcamlist; cam = webcam(1); cam.Resolution = '1600x1200'; img =
   snapshot(cam);
fname = sprintf('001Separation_initial_photo.png'); save(fname);
   imwrite(img, fname);
pause(2);

%THIS LINE BELOW JUST FOR TESTING USING A PREVIOUS IMAGE
img = imread('example_chamber.png'); figure; imshow(img);

%%%%%%%%%%%%%%%%%%%%%%%%%%%%%%%%%%%%%%%%%%%%%%%%%%%%%%%%%%%%%%%%%%%%%%%%%

disp('Entered generate toolpath');

dc = [1200,1600]/2; %[px,px], center of the dish in pixel
   coordinates
dr = 1200/2; %[px], radius of the dish in pixel coordinates
th = 0.1;

I=img; %Store image into another variable
```

```
%Isololate only the the area of the dish
[Y,X] = meshgrid(1:1600,1:1200); %setting up 2D coordinates of the Y
     and X of the grid from 1: to value
X = X-dc(1); %X is equal to center of dish/2
Y = Y-dc(2); %Y is equal to center of dish/2
R = repmat(sqrt(X.^2+Y.^2),[1,1,3]); %make copies of the matrix
    hypotenuse of X^2+Y^2 in a 1by 1 by 3 block arrangement
Idish = I;
Idish(R>dr)=0; %if the pixel is at a distance greater than the
    radius, set it to 0, making the mask

%Grayscale the image
%figure;
Idish_g = rgb2gray(Idish);
%imshow(Idish_g);

%Convert image to a binary image
BW = imbinarize(Idish_g,'adaptive','ForegroundPolarity','dark','
    Sensitivity',0.6);
%imshow(BW);

%Find the inverse of the image
A = imcomplement(BW);
%imshow(A);

%Fill in any glare that may occur in an opaque region
figure;
I2 = imfill(A, 'holes');
imshow(I2);
```

```
%Find the centroid and size characterisitics of regions
stats = regionprops('table',I2,'Centroid',...
    'MajorAxisLength','MinorAxisLength');
centers = stats.Centroid;
diameters = mean([stats.MajorAxisLength stats.MinorAxisLength],2);

%Find the number of regions that are large but not larger than the
%diffusion chamber%
[row, col] = find(diameters > 200 & diameters < 1000); %find all
    instances which satisfy the diameter parameters

new_diameters = zeros(max(row)-1, 1); %create a vector to store the
    new diameters
new_centers = zeros(max(row)-1, 2); %create a vector to store the
    origin of each circlar object

%Find all diameters that satisfy the size parameters
k=1;
for n = 1:length(diameters)
    if diameters(n) > 200 & diameters(n) < 1000
        new_diameters(k) = diameters(n);
        new_centers(k, 1) = centers(n, 1);
        new_centers(k, 2) = centers(n, 2);
        k=k+1;
    end
end

%first find the range for x
r = new_diameters/2; %find the radius
```

```
if isempty(new_centers) == 0 %If there was a center detected

    x_o = new_centers(1, 1); %X coordinate for center of circle
    y_o = new_centers(1, 2); %Y coordinate for center of circle
    x_max = x_o+r; %find x max (right hand most side of circle)
    x_min = x_o-r; %find x min (lelft hand most side of circle)

    %get coordinates for top half of circle, toolpath 1
    theta = 0:pi/5:pi;
    x1 = x_o+(r(1)*cos(theta)); %convert from polar to cartesian
        coordinates
    y1 = y_o+(r(1)*sin(theta)); %convert from polar to cartesian
        coordinates

    %get coordinates for the bottom half of the circle, toolpath 2
    theta = pi:pi/5:2*pi;
    x2 = x_o+(r(1)*cos(theta)); %convert from polar to cartesian
        coordinates
    y2 = y_o+(r(1)*sin(theta)); %convert from polar to cartesian
        coordinates

    %viscircles(new_centers,new_diameters/2);
    hold on; plot(x1, y1, 'r', 'LineWidth',5); %validate the
        circular tool path
    hold on; plot(x2, y2, 'g', 'LineWidth',5); %validate the
        circular tool path
    hold on; plot([max(x_max) min(x_min)], [y_o y_o], 'b', '
        LineWidth',5); %validate the mid cut mark
    hold off;
    saveas(gcf,'toolpath.png')
```

```
%pixel to step conversion based on 4x objective lens and 2MP
%CMOS USB Camera
pixel_to_ustep = (1205/1600)*34.1;

%First find the rapid toolpath
%generate the rapid path to travel to the start of the toolpath
%start from the center
rapid_initial = [max(x_max)-800 600-y_o]; %800 and 600 is the
    midpoint in pixels

%rapid final is to recenter the machine
rapid_final = [800-max(x_max) y_o-600];

%get the coordinates from the top half to generate toolpath1
toolpath1_pixel = horzcat(x1.', y1.');
toolpath2_pixel = horzcat(x2.', y2.');
preview(cam);

midline = int32([max(x_max) y_o; min(x_min) y_o])

%convert toolpath to integers to reduce buffer size
toolpath1_pixel = int32(toolpath1_pixel);
toolpath1_pixel = int32(toolpath1_pixel);

%Convert pixel coordinates to ustep coordinates
toolpath1_ustep = toolpath1_pixel*pixel_to_ustep;
toolpath2_ustep = toolpath2_pixel*pixel_to_ustep;

%generate the rapid toolpath
```

```
rapid_i_s = {'<5,'};
delim = (',');
s1 = num2str(int32(rapid_initial(1,1)*pixel_to_ustep));
rapid_i_s = strcat(rapid_i_s, s1); rapid_i_s = strcat(rapid_i_s,
    delim);
s1 = num2str(int32(rapid_initial(1,2)*pixel_to_ustep));
rapid_i_s = strcat(rapid_i_s, s1); rapid_i_s = strcat(rapid_i_s,
    '>>');
rapid_i_string=string(rapid_i_s)

%Generate the first toolpath

%path 1 is cut the midline
x_step = pixel_to_ustep*int32((min(x_min)-max(x_max)));

toolpath1_s = {'<6,'}; %Begin the toolpath char array
s1 = num2str(x_step);
toolpath1_s = strcat(toolpath1_s, s1); toolpath1_s = strcat(
   toolpath1_s, delim);

%Now start cutting clockwise, going up first
y_step = toolpath1_ustep(5, 2)-toolpath1_ustep(6, 2);
x_step = toolpath1_ustep(5, 1)-toolpath1_ustep(6, 1);
s1 = num2str(y_step);
toolpath1_s = strcat(toolpath1_s, s1); toolpath1_s = strcat(
   toolpath1_s, delim);
s1 = num2str(x_step);
toolpath1_s = strcat(toolpath1_s, s1); toolpath1_s = strcat(
   toolpath1_s, delim);
```

```
y_step = toolpath1_ustep(4, 2)-toolpath1_ustep(5, 2);
x_step = toolpath1_ustep(2, 1)-toolpath1_ustep(5, 1);
s1 = num2str(y_step);
toolpath1_s = strcat(toolpath1_s, s1); toolpath1_s = strcat(
    toolpath1_s, delim);
s1 = num2str(x_step);
toolpath1_s = strcat(toolpath1_s, s1); toolpath1_s = strcat(
    toolpath1_s, delim);

toolpath1_s = strcat(toolpath1_s, '>>');
toolpath1_string = string(toolpath1_s)

%%%%%%%%%%%%%%%%%%%%%%%%%%%%%%%%%%%%%%%%%%%%%%%%%%%%%%%%%%%%%%%%%5
%Start the toolpath 2 string
toolpath2_s = {'<6,'}; %Begin the toolpath char array
x_step = 1;
s1 = num2str(x_step);
toolpath2_s = strcat(toolpath2_s, s1); toolpath2_s = strcat(
    toolpath2_s, delim);
y_step = toolpath1_ustep(2, 2)-toolpath1_ustep(3, 2);
s1 = num2str(y_step);
toolpath2_s = strcat(toolpath2_s, s1); toolpath2_s = strcat(
    toolpath2_s, delim);

x_step = toolpath1_ustep(1, 1)-toolpath1_ustep(2, 1);
y_step = toolpath1_ustep(1, 2)-toolpath1_ustep(2, 2);
s1 = num2str(x_step);
toolpath2_s = strcat(toolpath2_s, s1); toolpath2_s = strcat(
    toolpath2_s, delim);
s1 = num2str(y_step);
```

```
toolpath2_s = strcat(toolpath2_s, s1); toolpath2_s = strcat(
    toolpath2_s, delim);

toolpath2_s = strcat(toolpath2_s, '>>');
toolpath2_string = string(toolpath2_s)
%thats all that can fit in the serial buffer

%%%%%%%%%%%%%%%%%%%%%%%%%%%%%%%%%%%%%%%%%%%%%%%%%%%%%%%%%%%%%%%%%%%%5
%Start the toolpath 3 string
toolpath3_s = {'<6,'}; %Begin the toolpath char array
x_step = 1;
s1 = num2str(x_step);
toolpath3_s = strcat(toolpath3_s, s1); toolpath3_s = strcat(
    toolpath3_s, delim);
y_step = toolpath2_ustep(5, 2)-toolpath2_ustep(6, 2);
s1 = num2str(y_step);
toolpath3_s = strcat(toolpath3_s, s1); toolpath3_s = strcat(
    toolpath3_s, delim);

x_step = toolpath2_ustep(5, 1)-toolpath2_ustep(6, 1);
s1 = num2str(x_step);
toolpath3_s = strcat(toolpath3_s, s1); toolpath3_s = strcat(
    toolpath3_s, delim);
y_step = toolpath2_ustep(4, 2)-toolpath2_ustep(5, 2);
s1 = num2str(y_step);
toolpath3_s = strcat(toolpath3_s, s1); toolpath3_s = strcat(
    toolpath3_s, delim);

x_step = toolpath2_ustep(2, 1)-toolpath2_ustep(5, 1);
s1 = num2str(x_step);
```

```
toolpath3_s = strcat(toolpath3_s, s1); toolpath3_s = strcat(
    toolpath3_s, delim);
y_step = toolpath2_ustep(2, 2)-toolpath2_ustep(3, 2);
s1 = num2str(y_step);
toolpath3_s = strcat(toolpath3_s, s1); toolpath3_s = strcat(
    toolpath3_s, delim);

toolpath3_s = strcat(toolpath3_s, '>>');
toolpath3_string = string(toolpath3_s)
%thats all that can fit in the serial buffer

%%%%%%%%%%%%%%%%%%%%%%%%%%%%%%%%%%%%%%%%%%%%%%%%%%%%%%%%%%%%%%%%%%%%5
%Start the toolpath 4 string
toolpath4_s = {'<6,'}; %Begin the toolpath char array
x_step = toolpath2_ustep(1, 1)-toolpath2_ustep(2, 1);
s1 = num2str(x_step);
toolpath4_s = strcat(toolpath4_s, s1); toolpath4_s = strcat(
    toolpath4_s, delim);
y_step = toolpath2_ustep(1, 2)-toolpath2_ustep(2, 2);
s1 = num2str(y_step);
toolpath4_s = strcat(toolpath4_s, s1); toolpath4_s = strcat(
    toolpath4_s, delim);
%Now go back to the first position

x_step = toolpath2_ustep(6, 1)-toolpath2_ustep(1, 1);
s1 = num2str(x_step);
toolpath4_s = strcat(toolpath4_s, s1); toolpath4_s = strcat(
    toolpath4_s, delim);
toolpath4_s = strcat(toolpath4_s, '>>');
toolpath4_string = string(toolpath4_s)
```

```
    %thats all that can fit in the serial buffer

    %generate the final rapid toolpath to go back to the center
    rapid_f_s = {'<5,'};
    delim = (',');
    s1 = num2str(int32(rapid_final(1,1)*pixel_to_ustep));
    rapid_f_s = strcat(rapid_f_s, s1); rapid_f_s = strcat(rapid_f_s,
        delim);
    s1 = num2str(int32(rapid_final(1,2)*pixel_to_ustep));
    rapid_f_s = strcat(rapid_f_s, s1); rapid_f_s = strcat(rapid_f_s,
        '>>');
    rapid_f_string=string(rapid_f_s)

else
    toolpath1_s = '<>';
    disp('No Colony Detected, No Toolpath Generated');
    %No toolpath generated, move on
end

img = snapshot(cam);
fname = sprintf('002Separation.png'); save(fname); imwrite(img,
    fname);
pause(2);

fclose(arduino);
arduino=serial('COM3','BaudRate',250000);
fopen(arduino);
pause(2);
%Send out the Rapid toolpath
fprintf(arduino,'%s\n',rapid_i_string); disp('Rapid string sent');
```

```
   pause(20);
%Send out the first toolpath
fprintf(arduino,'%s\n', toolpath1_string); disp('Toolpath 1 string
   sent'); pause(30);
%Send out the first toolpath
fprintf(arduino,'%s\n', toolpath2_string); disp('Toolpath 2 string
   sent'); pause(30);

%Take mid separation photo to see if a second toolpath is needed
fprintf(arduino,'%s\n','<5>'); %This turns on the backlight
pause(5);

img = snapshot(cam);
fname = sprintf('003Separation.png'); save(fname); imwrite(img,
   fname);
pause(2);

%Second cutting pass
%Send out the second toolpath
fprintf(arduino,'%s\n', toolpath1_string); disp('Toolpath 1 string
   sent'); pause(30);
%Send out the second toolpath
fprintf(arduino,'%s\n', toolpath2_string); disp('Toolpath 2 string
   sent'); pause(30);

img = snapshot(cam);
fname = sprintf('004Separation.png'); save(fname); imwrite(img,
   fname);
pause(2);
%%%%%%%%%%%%%%%%%%%%%%%%%%%%%%%%%%%%%%%%%%%%%%%%%%%%%%%%%%%%%%%%%%%%%%%%%%%%%%%
```

```
%Index capture stage

%Send out the third toolpath
fprintf(arduino,'%s\n', toolpath3_string); disp('Toolpath 3 string
    sent'); pause(30);
%Send out the third toolpath
fprintf(arduino,'%s\n', toolpath4_string); disp('Toolpath 4 string
    sent'); pause(30);

%Send out the final Rapid toolpath
fprintf(arduino,'%s\n',rapid_f_string); disp('Final Rapid string
    sent'); pause(20);

fprintf(arduino,'%s\n','<5>'); %This turns on the backlight
pause(5);

img = snapshot(cam);
fname = sprintf('005Separation.png'); save(fname); imwrite(img,
    fname);
pause(5);

%Second cutting pass
%Send out the third toolpath
fprintf(arduino,'%s\n', toolpath3_string); disp('Toolpath 3 string
    sent'); pause(30);
%Send out the third toolpath
fprintf(arduino,'%s\n', toolpath4_string); disp('Toolpath 4 string
    sent'); pause(30);
```

```
        img = snapshot(cam);
        fname = sprintf('006Separation.png'); save(fname); imwrite(img,
            fname);
        pause(2);

        disp('Finished sending toolpath to Arduino');
        preview(cam);
        pause(10);
        pause(100000);
        %export toolpath string
        %confirm that toolpath is complete

        %Close the port so we don't tie it up

        %Index next diffusion chamber
        %Index next capture chamber

    case 6 %Cutting Subprogram
        fprintf(arduino,'%s\n','<6>');
    case 7 %Sample Stage Positioning
        fprintf(arduino,'%s\n','<7>');
    case 8 %Capture Stage Positioning
        fprintf(arduino,'%s\n','<8>');
    case 9 %Turn off laser
        fprintf(arduino,'%s\n','<9>');
    case 10 %Turn on laser
        fprintf(arduino,'%s\n','<10>');
    otherwise
end
```

```
display('Finished sending command to home machine');
fprintf(arduino,'%s\n','<1>'); %This turns on the backlight
pause(1);
fclose(arduino);
delete(arduino);
end
```

0.13.4 Error Budget: Homogenous Transformation Matrices Matlab Code

For any future reader that wishes to utilize Matlab or any programming language to calculate error budgets using HTMs here is my code.

```
clc
clear

real_values = 0; %change to 1 to compute real values

%Coefficients of linear thermal expansion
syms cte6061 cte303 cte440 cte316 ctebk602pom

%theta = 100e-6; %units are urad, use for accuracy
syms theta

%translational lengths [m]
%X axis
syms L1415x L1617x L1819x

%Y axis
syms L12y L56y L1415y L1617y L1819y L1920y L2021y
```

```
%Z axis
%L01z = -0.02286 if using 4x objective lens
%L01z = -0.0381 if using 10x objecgive lens
syms L01z L12z L56z L910z L1314z L1415z L1516z L1718z

%change in temperature [K[
syms delT

if real_values == 1
    cte6061 = 23.6e-6; cte303 = 17.2e-6; cte440 = 10.2e-6; cte316 = 16e-6;
        ctebk602pom = 110e-6; %units are um/mK
    theta = 100e-6; %units are urad, use for repeatability
    L1415x = 0.0254; L1617x = 0.1016; L1819x = -0.127;
    L12y = 0.0254; L56y = 0.04318; L1415y = 0.0381; L1617y = -0.01524;
        L1819y = -0.17272; L1920y = 0.03048; L2021y = 0.0508;
    L01z = -0.02286; L12z = -0.02921; L56z = 0.02159; L910z = 0.01524;
        L1314z = 0.01524; L1415z = 0.00635; L1516z = 0.09144; L1718z =
        -0.08128-.0165;
    delT = 0.1;
    %delT = 0;
    %check the summation of each axis
    display("summation of X axis"); sum_x = L1415x+L1617x+L1819x
    display("summation of Y axis"); sum_y = L12y+L56y+L1415y+L1617y+L1819y+
        L1920y+L2021y
    display("summation of Z axis"); sum_z = L01z+L12z+L56z+L910z+L1314z+
        L1415z+L1516z+L1718z
end


dL01z = cte6061*L01z*delT; %error due to thermal expansion from 0 to 1
```

```
%Below is the HTM from 0 to 1
t01 = [1 0 0 0;
    0 1 0 0;
    0 0 1 L01z-dL01z;
    0 0 0 1];

dL12y = cte303*L12y*delT; dL12z = cte303*L12z*delT;

t12 = [1 0 0 0;
    0 1 0 L12y+dL12y;
    0 0 1 L12z-dL12z;
    0 0 0 1];

t23 = [1 0 0 0;
    0 cos(theta) sin(theta) 0;
    0 -sin(theta) cos(theta) 0;
    0 0 0 1];

t34 = [cos(theta) 0 -sin(theta) 0;
    0 1 0 0;
    sin(theta) 0 cos(theta) 0;
    0 0 0 1];

t45 = [cos(theta) sin(theta) 0 0;
    -sin(theta) cos(theta) 0 0;
    0 0 1 0;
    0 0 0 1];

dL56y = cte440*L56y*delT; dL56z = cte440*L56z*delT;
```

```
t56 = [1 0 0 0;
    0 1 0 L56y+dL56y;
    0 0 1 L56z+dL56z;
    0 0 0 1];

t67 = [1 0 0 0;
    0 cos(theta) sin(theta) 0;
    0 -sin(theta) cos(theta) 0;
    0 0 0 1];

t78 = [cos(theta) 0 -sin(theta) 0;
    0 1 0 0;
    sin(theta) 0 cos(theta) 0;
    0 0 0 1];

t89 = [cos(theta) sin(theta) 0 0;
    -sin(theta) cos(theta) 0 0;
    0 0 1 0;
    0 0 0 1];

dL910z = cte440*L910z*delT;

t910 = [1 0 0 0;
    0 1 0 0;
    0 0 1 L910z+dL910z;
    0 0 0 1];

t1011 = [1 0 0 0;
    0 cos(theta) sin(theta) 0;
```

```
    0 -sin(theta) cos(theta) 0;
    0 0 0 1];

t1112 = [cos(theta) 0 -sin(theta) 0;
    0 1 0 0;
    sin(theta) 0 cos(theta) 0;
    0 0 0 1];

t1213 = [cos(theta) sin(theta) 0 0;
    -sin(theta) cos(theta) 0 0;
    0 0 1 0;
    0 0 0 1];

dL1314z = cte440*L1314z*delT;

t1314 = [1 0 0 0;
    0 1 0 0;
    0 0 1 L1314z+dL1314z;
    0 0 0 1];

dL1415x = cte303*L1415x*delT; dL1415y = cte303*L1415y*delT; dL1415z =
    cte303*L1415z*delT;

t1415 = [1 0 0 L1415x+dL1415x;
    0 1 0 L1415y+dL1415y;
    0 0 1 L1415z+dL1415z;
    0 0 0 1];

dL1516z = cte316*L1516z*delT;
```

```
t1516 = [1 0 0 0;
    0 1 0 0;
    0 0 1 L1516z+dL1516z;
    0 0 0 1];

dL1617x = cte6061*L1617x*delT; dL1617y = cte6061*L1617y*L1617y*delT;

t1617 = [1 0 0 L1617x+dL1617x;
    0 1 0 L1617y-dL1617y;
    0 0 1 0;
    0 0 0 1];

dL1718z = cte303*L1718z*delT;

t1718 = [1 0 0 0;
    0 1 0 0;
    0 0 1 L1718z-dL1718z;
    0 0 0 1];

dL1819x = cte303*L1819x*delT; dL1819y = cte303*L1819y*delT;

t1819 = [1 0 0 L1819x-dL1819x;
    0 1 0 L1819y-dL1819y;
    0 0 1 0;
    0 0 0 1];

dL1920y = cte303*L1920y*delT;

t1920 = [1 0 0 0;
    0 1 0 L1920y+dL1920y;
```

```
    0 0 1 0;
    0 0 0 1];

%dL2021y = ctebk602pom*L2021y*delT;
dL2021y = 0;

t2021 = [1 0 0 0;
    0 1 0 L2021y+dL2021y;
    0 0 1 0;
    0 0 0 1];

%The product of all the HTMs
t021 = t01*t12*t23*t34*t45*t56*t67*t78*t89*t910*t1011*t1112*t1213*t1314*
    t1415*t1516*t1617*t1718*t1819*t1920*t2021;

%Converting so that 3 sig figs of the result are displayed
t021 = vpa(t021, 3)

%A vector to hold translations and errors in the translation axis
syms x y z
r = [x;
    y;
    z;
    1];

%r021 = t021*r;

%Small angle approximation substitution
if real_values == 0
    t021_1 = subs(t021, [sin(theta), cos(theta)], [0, 1]);
```

```
    t021_2 = subs(t021_1, [theta^2, theta^3], [0, 0]);
    t021_2
    t = t021_2*r
end

%r021 = vpa(r021, 3);
```

0.13.5 Centers of Action: Matlab Code

I personally could not find much detailed material on centers of action and struggled with it conceptually for a few weeks. Below is my code to aid in any future readers who wish to utilize Matlab or other programming language to calculate the center of friction and center of stiffness of their design. Many of the commented out vectors correspond to the different stages that I ran an analysis on previously described in this document.

```
%The purpose of this script is to calculate the center of stiffness
%by solving a system of equations

clear all
clc

%For a 1DOF stage (5 constraints)
syms Fb1 Fb2 Fb3 Fb4 Fb5 vx; %The unknown bearing reaction forces

u=0.005;
%u = 0.57;
m = 2;
g = -9.81;
FT=0.6;
Fnest_upper = 0;
```

```
Fnest_lower = 0;
Fmg = m*g;
Fn1 = 15;
Fn2 = 15;
Fn3 = 15;
Fn4 = 15;
Fn5 = 15;
Fk = 0;
%vx = 0.005; %m/s

%Declare the positions in XYZ of each feature
%{
Pb1 = [0 -0.003 -0.27/2];
Pb2 = [0 0.003 -0.27/2];
Pb3 = [0.05 -0.003 -0.27/2];
Pb4 = [0.05 0.003 -0.27/2];
Pb5 = [0.025 0.003 0.27/2];
PT = [-0.14,0.05,0.006];
Pmg = [0.025 0 0];
Pnest = [0.025, 0, 0.135];
%}

%Position vectors for capture stage X axis
%{
Pb1 = [0 -0.003 0.04];Pb2 = [0 -0.003 0.06];Pb3 = [0.075 -0.003 0.06];Pb4 =
     [0.15 -0.003 0.06];
Pb5 = [0.15 -0.003 0.04];Pnest_upper = [0.05, 0.005, 0.1];Pnest_lower =
    [0.05, -0.005, 0.1];
PT = [0.075 0.005 -0.07];Pmg = [0.075 0 0];
%}
```

```
%Position vectors for capture stage Y axis
%{
Pb1 = [0 -0.003 -0.14]; Pb2 = [0.12 -0.003 -0.14]; Pb3 = [0.24 -0.003
    -0.14]; Pb4 = [0 -0.02 0.14];
Pb5 = [0.24 -0.02 0.14]; Pnest_upper = [0.05, 0.005, 0.1]; Pnest_lower =
    [0.05, -0.005, 0.1];
PT = [0.12 0.005 -0.15];Pmg = [0.12 0 0];
%}

%Position vectors for sample stage X axis
%{
Pb1 = [0 0.003 0.045]; Pb2 = [0 -0.003 0.045]; Pb3 = [0.12 0.003 0.045];
    Pb4 = [0.12 -0.003 0.045];
Pb5 = [0.06 -0.003 0.06]; Pnest_upper = [0.05, 0.005, 0.1]; Pnest_lower =
    [0.05, -0.005, 0.1];
PT = [0.06 0.005 -0.05];Pmg = [0.06 0 0];
%}

%Position vectors for sample stage Y axis
%{
Pb1 = [0 0.003 -0.14]; Pb2 = [0 -0.003 -0.14]; Pb3 = [0.12 0.003 -0.14];
    Pb4 = [0.12 -0.003 -0.14];
Pb5 = [0.06 0.003 0.14]; Pnest_upper = [0.06, -0.003, -0.14]; Pnest_lower =
     [0.06, -0.003, -0.14];
PT = [0.06 0.005 -0.15];Pmg = [0.06 0 0];
%}

%Position vectors for optics stage X axis
```

```
Pb1 = [0 0.001 -0.02]; Pb2 = [0 -0.001 -0.02]; Pb3 = [0.04 0.001 -0.02];
    Pb4 = [0.04 -0.001 -0.02];
Pb5 = [0.02 -0.001 0.02]; Pnest_upper = [0.06, -0.003, -0.14]; Pnest_lower
    = [0.06, -0.003, -0.14];
PT = [0.04 0 0];Pmg = [0.02 0 0];
Pk = [0 0 0];
Pn1 = [0 0.001 -0.02];
Pn2 = [0 -0.001 -0.02];
Pn3 = [0.04 0.001 -0.02];
Pn4 = [0.04 -0.001 -0.02];
Pn5 = [0.02 -0.001 0.02];

%Declare direction cosine vectors
%{
theta1 = [0; -1/sqrt(2); 1/sqrt(2)];
theta2 = [0; 1/sqrt(2); 1/sqrt(2)];
theta3 = [0; -1/sqrt(2); 1/sqrt(2)];
theta4 = [0; 1/sqrt(2); 1/sqrt(2)];
theta5 = [0; 1/sqrt(2); -1/sqrt(2)];
thetamg = [0; -1; 0];
thetaT = [1;0;0];
thetanest_upper = [0; 1/sqrt(2); -1/sqrt(2)];
thetanest_lower = [0;-1/sqrt(2);-1/sqrt(2)];
%}

%Direction cosines for Capture Stage X Axis
%{
theta1 = [0; 1; 0];theta2 = [0; 0; -1];theta3 = [0; 1; 0];theta4 = [0; 0;
    -1];theta5 = [0; 1; 0];
```

```
thetamg = [0; -1; 0];thetaT = [1;0;0];thetanest_upper = [0; 1/sqrt(2); -1/
    sqrt(2)];thetanest_lower = [0;-1/sqrt(2);-1/sqrt(2)];
%}

%Direction cosines for Capture Stage Y Axis
%{
theta1 = [0; 1; 0];theta2 = [0; 0; 1];theta3 = [0; 0; 1];theta4 = [0; 1;
    0];theta5 = [0; 1; 0];
thetamg = [0; -1; 0];thetaT = [1;0;0];thetanest_upper = [0; 1/sqrt(2); -1/
    sqrt(2)];thetanest_lower = [0;-1/sqrt(2);-1/sqrt(2)];
%}

%Direction cosines for Sample Stage X Axis
%{
theta1 = [0; 1/sqrt(2); -1/sqrt(2)];theta2 = [0; -1/sqrt(2); -1/sqrt(2)];
    theta3 = [0; 1/sqrt(2); -1/sqrt(2)];
theta4 = [0; -1/sqrt(2); -1/sqrt(2)];theta5 = [0; -1/sqrt(2); 1/sqrt(2)];
    thetamg = [0; -1; 0];thetaT = [1;0;0];
thetanest_upper = [0; 1/sqrt(2); -1/sqrt(2)];thetanest_lower = [0;-1/sqrt
    (2);-1/sqrt(2)];
%}

%Direction cosines for Sample Stage Y Axis
%{
theta1 = [0; 1/sqrt(2); 1/sqrt(2)];theta2 = [0; -1/sqrt(2); 1/sqrt(2)];
    theta3 = [0; 1/sqrt(2); 1/sqrt(2)];
theta4 = [0; -1/sqrt(2); 1/sqrt(2)];theta5 = [0; 1/sqrt(2); -1/sqrt(2)];
    thetamg = [0; -1; 0];thetaT = [1;0;0];
thetanest_upper = [0; -1/sqrt(2); -1/sqrt(2)];thetanest_lower = [0;1/sqrt
    (2);-1/sqrt(2)];
```

```
%}

%Direction cosines for Optics Stage X axis
theta1 = [0; 1/sqrt(2); 1/sqrt(2)];theta2 = [0; -1/sqrt(2); 1/sqrt(2)];
    theta3 = [0; 1/sqrt(2); 1/sqrt(2)];
theta4 = [0; -1/sqrt(2); 1/sqrt(2)];theta5 = [0; -1/sqrt(2); -1/sqrt(2)];
    thetamg = [0; -1; 0];thetaT = [1;0;0];
thetak = [-1;0;0]; thetanest_upper = [0; -1/sqrt(2); -1/sqrt(2)];
    thetanest_lower = [0;1/sqrt(2);-1/sqrt(2)];
thetaPn1 = [0; 1/sqrt(2); 1/sqrt(2)];
thetaPn2 = [0; -1/sqrt(2); 1/sqrt(2)];
thetaPn3 = [0; 1/sqrt(2); 1/sqrt(2)];
thetaPn4 = [0; -1/sqrt(2); 1/sqrt(2)];
thetaPn5 = [0; -1/sqrt(2); -1/sqrt(2)];

sum_Fx = -5*u*vx+...
    Fmg*thetamg(1)+...
    FT*thetaT(1)+...
    Fnest_upper*thetanest_upper(1)+...
    Fnest_lower*thetanest_lower(1)+...
    Fk*thetak(1)+...
    Fn1*thetaPn1(1)+...
    Fn2*thetaPn2(1)+...
    Fn3*thetaPn3(1)+...
    Fn4*thetaPn4(1)+...
    Fn5*thetaPn5(1)==0;

sum_Fy = Fb1*theta1(2)+...
    Fb2*theta2(2)+...
    Fb3*theta3(2)+...
```

```
    Fb4*theta4(2)+...
    Fb5*theta5(2)+...
    Fmg*thetamg(2)+...
    FT*thetaT(2)+...
    Fnest_upper*thetanest_upper(2)+...
    Fnest_lower*thetanest_lower(2)+...
    Fk*thetak(2)+...
    Fn1*thetaPn1(2)+...
    Fn2*thetaPn2(2)+...
    Fn3*thetaPn3(2)+...
    Fn4*thetaPn4(2)+...
    Fn5*thetaPn5(2)==0;

sum_Fz = Fb1*theta1(3)+...
    Fb2*theta2(3)+...
    Fb3*theta3(3)+...
    Fb4*theta4(3)+...
    Fb5*theta5(3)+...
    Fmg*thetamg(3)+...
    FT*thetaT(3)+...
    Fnest_upper*thetanest_upper(3)+...
    Fnest_lower*thetanest_lower(3)+...
    Fk*thetak(3)+...
    Fn1*thetaPn1(3)+...
    Fn2*thetaPn2(3)+...
    Fn3*thetaPn3(3)+...
    Fn4*thetaPn4(3)+...
    Fn5*thetaPn5(3)==0;

sum_Mx = Fb1*(-Pb1(3)*theta1(2)+Pb1(2)*theta1(3))+...
```

```
    Fb2*(-Pb2(3)*theta2(2)+Pb2(2)*theta2(3))+...
    Fb3*(-Pb3(3)*theta3(2)+Pb3(2)*theta3(3))+...
    Fb4*(-Pb4(3)*theta4(2)+Pb4(2)*theta4(3))+...
    Fb5*(-Pb5(3)*theta5(2)+Pb5(2)*theta5(3))+...
    Fmg*(-Pmg(3)*thetamg(2)+Pmg(2)*thetamg(3))+....
    FT*(-PT(3)*thetaT(2)+PT(2)*thetaT(3))+...
    Fnest_upper*(-Pnest_upper(3)*thetanest_upper(2)+Pnest_upper(2)*
        thetanest_upper(3))+...
    Fnest_lower*(-Pnest_lower(3)*thetanest_lower(2)+Pnest_lower(2)*
        thetanest_lower(3))+...
    Fk*(-Pk(3)*thetak(2)+Pk(2)*thetak(3))+...
    Fn1*(-Pn1(3)*thetaPn1(2)+Pn1(2)*thetaPn1(3))+...
    Fn2*(-Pn2(3)*thetaPn2(2)+Pn2(2)*thetaPn2(3))+...
    Fn3*(-Pn3(3)*thetaPn3(2)+Pn3(2)*thetaPn3(3))+...
    Fn4*(-Pn4(3)*thetaPn4(2)+Pn4(2)*thetaPn4(3))+...
    Fn5*(-Pn5(3)*thetaPn5(2)+Pn5(2)*thetaPn5(3))==0;

sum_My = u*vx*Pb1(3)+...
    u*vx*Pb2(3)+...
    u*vx*Pb3(3)+...
    u*vx*Pb4(3)+...
    u*vx*Pb5(3)+...
    Fb1*(Pb1(3)*theta1(1)-Pb1(1)*theta1(3))+...
    Fb2*(Pb2(3)*theta2(1)-Pb2(1)*theta2(3))+...
    Fb3*(Pb3(3)*theta3(1)-Pb3(1)*theta3(3))+...
    Fb4*(Pb4(3)*theta4(1)-Pb4(1)*theta4(3))+...
    Fb5*(Pb5(3)*theta5(1)-Pb5(1)*theta5(3))+...
    Fmg*(Pmg(3)*thetamg(1)-Pmg(1)*thetamg(3))+...
    FT*(PT(3)*thetaT(1)-PT(1)*thetamg(3))+...
```

```
    Fnest_upper*(Pnest_upper(3)*thetanest_upper(1)-Pnest_upper(1)*
        thetanest_upper(3))+...
    Fnest_lower*(Pnest_lower(3)*thetanest_lower(1)-Pnest_lower(1)*
        thetanest_lower(3))+...
    Fk*(Pk(3)*thetak(1)+Pk(1)*thetak(3))+...
    Fn1*(Pn1(3)*thetaPn1(1)+Pn1(1)*thetaPn1(3))+...
    Fn2*(Pn2(3)*thetaPn2(1)+Pn2(1)*thetaPn2(3))+...
    Fn3*(Pn3(3)*thetaPn3(1)+Pn3(1)*thetaPn3(3))+...
    Fn4*(Pn4(3)*thetaPn4(1)+Pn4(1)*thetaPn4(3))+...
    Fn5*(Pn5(3)*thetaPn5(1)+Pn5(1)*thetaPn5(3))==0;



sum_Mz = u*vx*Pb1(2)+...
    u*vx*Pb2(2)+...
    u*vx*Pb3(2)+...
    u*vx*Pb4(2)+...
    u*vx*Pb5(2)+...
    Fb1*(-Pb1(2)*theta1(1)+Pb1(1)*theta1(2))+...
    Fb2*(-Pb2(2)*theta2(1)+Pb2(1)*theta2(2))+...
    Fb3*(-Pb3(2)*theta3(1)+Pb3(1)*theta3(2))+...
    Fb4*(-Pb4(2)*theta4(1)+Pb4(1)*theta4(2))+...
    Fb5*(-Pb5(2)*theta5(1)+Pb5(1)*theta5(2))+...
    Fmg*(-Pmg(2)*thetamg(1)+Pmg(1)*thetamg(2))+...
    FT*(-PT(2)*thetaT(1)+PT(1)*thetaT(2))+...
    Fnest_upper*(-Pnest_upper(2)*thetanest_upper(1)+Pnest_upper(1)*
        thetanest_upper(2))+...
    Fnest_lower*(-Pnest_lower(2)*thetanest_lower(1)+Pnest_lower(1)*
        thetanest_lower(2))+...
    Fk*(-Pk(2)*thetak(1)+Pk(1)*thetak(2))+...
    Fn1*(-Pn1(2)*thetaPn1(1)+Pn1(1)*thetaPn1(2))+...
```

```
    Fn2*(-Pn2(2)*thetaPn2(1)+Pn2(1)*thetaPn2(2))+...
    Fn3*(-Pn3(2)*thetaPn3(1)+Pn3(1)*thetaPn3(2))+...
    Fn4*(-Pn4(2)*thetaPn4(1)+Pn4(1)*thetaPn4(2))+...
    Fn5*(-Pn5(2)*thetaPn5(1)+Pn5(1)*thetaPn5(2))==0;



[A,B] = equationsToMatrix([sum_Fx, sum_Fy, sum_Fz, sum_Mx, sum_My, sum_Mz],
     [Fb1 Fb2 Fb3 Fb4 Fb5 vx]);
X = linsolve(A,B);

eval(X)

cof_x = (u*(Fb1*theta1(2)*Pb1(1)+...
    Fb2*theta2(2)*Pb2(1)+...
    Fb3*theta3(2)*Pb3(1)+...
    Fb4*theta4(2)*Pb4(1)+...
    Fb5*theta5(2)*Pb5(1)))/+...
    (u*(Fb1*theta1(2)+...
    Fb2*theta2(2)+...
    Fb3*theta3(2)+...
    Fb4*theta4(2)+...
    Fb5*theta5(2)));

cof_y = (u*Fb1*theta1(3)*Pb1(2)+...
    u*Fb2*theta2(3)*Pb2(2)+...
    u*Fb3*theta3(3)*Pb3(2)+...
    u*Fb4*theta4(3)*Pb4(2)+...
    u*Fb5*theta5(3)*Pb5(2))/(+...
    Fb1*theta1(3)+...
    Fb2*theta2(3)+...
```

```
    Fb3*theta3(3)+...
    Fb4*theta4(3)+...
    Fb5*theta5(3));

cof_z = (u*(Fb1*theta1(2)*Pb1(3))+...
    u*Fb2*theta2(2)*Pb2(3)+...
    u*Fb3*theta3(2)*Pb3(3)+...
    u*Fb4*theta4(2)*Pb4(3)+...
    u*Fb5*theta5(2)*Pb5(3))/(+...
    u*Fb1*theta1(2)+...
    u*Fb2*theta2(2)+...
    u*Fb3*theta3(2)+...
    u*Fb4*theta4(2)+...
    u*Fb5*theta5(2));

cof_x = subs(cof_x, [Fb1, Fb2, Fb3, Fb4, Fb5], [X(1), X(2), X(3), X(4), X
    (5)]);
cof_y = subs(cof_y, [Fb1, Fb2, Fb3, Fb4, Fb5], [X(1), X(2), X(3), X(4), X
    (5)]);
cof_z = subs(cof_z, [Fb1, Fb2, Fb3, Fb4, Fb5], [X(1), X(2), X(3), X(4), X
    (5)]);

disp('Center of friction');
disp('Center of friction in x');
eval(cof_x)
disp('Center of friction in y');
eval(cof_y)
disp('Center of friction in z');
eval(cof_z)
```

```
K1 = 1.0e7;
K2 = 1.0e7;
K3 = 9.8e6;
K4 = 9.9e6;
K5 = 9.4e6;

COS_x = (K1*theta1(2)*Pb1(1)+...
    K2*theta2(2)*Pb2(1)+...
    K3*theta3(2)*Pb3(1)+...
    K4*theta4(2)*Pb4(1)+...
    K5*theta5(2)*Pb5(1))/+...
    (K1*theta1(2)+...
    K2*theta2(2)+...
    K3*theta3(2)+...
    K4*theta4(2)+...
    K5*theta5(2))

COS_y = (K1*theta1(3)*Pb1(2)+...
    K2*theta2(3)*Pb2(2)+...
    K3*theta3(3)*Pb3(2)+...
    K4*theta4(3)*Pb4(2)+...
    K5*theta5(3)*Pb5(2))/(+...
    K1*theta1(3)+...
    K2*theta2(3)+...
    K3*theta3(3)+...
    K4*theta4(3)+...
    K5*theta5(3))

COS_z = (K1*theta1(2)*Pb1(3)+...
    K2*theta2(2)*Pb2(3)+...
```

```
K3*theta3(2)*Pb3(3)+...
K4*theta4(2)*Pb4(3)+...
K5*theta5(2)*Pb5(3))/(+...
K1*theta1(2)+...
K2*theta2(2)+...
K3*theta3(2)+...
K4*theta4(2)+...
K5*theta5(2))
```